ESTUARINE DEPOSITS IN THE KOOTENAI FORMATION AS EVIDENCE OF AN EARLY CRETACEOUS (PRE-ALBIAN) MARINE ADVANCE INTO WESTERN MONTANA AND RELATIONSHIP TO CORDILLERAN FORELAND BASIN EVOLUTION

R.K. Schwartz[1] and Susan M. Vuke[2]

[1]*Department of Geology, Allegheny College, Meadville, Pennsylvania*

[2]*Montana Bureau of Mines and Geology, Montana Technological University, Butte, Montana*

MBMG

Montana Bureau of Mines and Geology

Cover photo: Great Falls member estuary mudstone facies with subtidal flat and bar sandstones exposed in a cliff along Belt Creek near its confluence with the Missouri River (background). On June 17, 1805, the Lewis and Clark expedition, which was traveling up the Missouri, entered Belt Creek to begin its 18-mile, 15-day overland portage around the great falls of the Missouri River. The Great Falls member of the Kootenai Formation is well exposed in the river gorge they portaged around. Photo by Robert K. Schwartz.

ESTUARINE DEPOSITS IN THE KOOTENAI FORMATION AS EVIDENCE OF AN EARLY CRETACEOUS (PRE-ALBIAN) MARINE ADVANCE INTO WESTERN MONTANA AND RELATIONSHIP TO CORDILLERAN FORELAND BASIN EVOLUTION

R.K. Schwartz[1] and Susan M. Vuke[2]

[1]*Department of Geology, Allegheny College, Meadville, Pennsylvania*

[2]*Montana Bureau of Mines and Geology, Montana Technological University, Butte, Montana*

Montana Bureau of Mines and Geology

CONTENTS

FIGURES

Supplementary figures 1–4 available for download from our website.

Supplementary figure 1. Gigapan panorama of stacked Great Falls member tide-dominated shoreface units (FAm2) and incised valley fill (FAv2-6) along the Missouri River near Morony Dam (sites MD1 and MD3). Inset rectangle marks the location of figure 16A.

Supplementary figure 2. Gigapan panorama of the lower Kootenai Formation at the juncture of Box Elder Creek and the Missouri River gorge (site BEe). At this location Kk2 is absent and the Great Falls inner-

estuary basin facies association (FAm4) disconformably overlies the basal Cutbank Member. At some locations along the gorge, thin remnant patches of Kk2 red mudstone disconformably underlie the estuary basin mudstone-dominated complex. A ravinement surface at the base of the estuary mouth bar marks a second local disconformity with the inner-estuary deposits. Great Falls member ~12 m thick. Inset rectangle marks the location of figure 24D.

Supplementary figure 3. Photo panorama of the mudstone-dominated inner-estuary facies association (FAm4) near the eastern basin margin (Belt Creek- BC). Inset rectangle marks the location of figure 29A.

Supplementary figure 4. Gigapan panorama of the lower Kootenai Formation along the Missouri River gorge at Box Elder west (Bew). The stratigraphic succession is the same as in Supplementary figure 2 with the exception of a large incised valley with fluvial sandstone fill that descends from the Fourth Kootenai member, truncating the entire Great Falls member as well as the top of the Cutbank Member.

x

ABSTRACT

The Lower Cretaceous Great Falls member (informally designated herein) of the Kootenai Formation near Great Falls, Montana, was deposited within the northern Rocky Mountain sector of the North American Cordilleran foreland basin. The deposits mark the southern terminus of the pre-Albian Boreal Sea that temporarily advanced into the alluvial-dominated foreland of western Montana. Tide-dominated estuarine facies define a lobate, northward-opening, basin-longitudinal complex representing inundation along pre-Kootenai paleovalley tracts axial to the Sweetgrass Arch, and ultimately across the southern Sweetgrass Arch (South Arch) area.

The Great Falls member was deposited within different scale paleogeographic spaces, including a relatively large highstand area, or main estuary basin, and small, isolated, estuarine valleys encompassed within the antecedent highstand area. The main estuary basin is marked by a central area that includes facies assemblages defining an estuary mouth bar, inner estuary basin, and estuary axis channel system. Tide-dominated shoreface facies lie adjacent to the estuary mouth bar, and thin tidal flat and channel deposits, locally interbedded with paleosol units, typically mark basin margins near the zero edge of deposition. The stratigraphic succession makes up a tide-dominated, transgressive to highstand system tract documenting: (1) pre-Great Falls member erosion along the central basin axis (preexisting topographic low); (2) estuary flooding and entrapment of mud, in addition to tidal flat and bar development; (3) headward encroachment of the estuary mouth bar system; and (4) subsequent regression capped by axial estuary channel and tidal flat facies followed by nonmarine delta plain facies of the overlying Kootenai member.

A small incised valley, nested within the upper part of the Great Falls member, contains tidally reworked lithic-rich fluvial deposits along the valley thalweg overlain by transgressive quartzose sandstone, basin-center mudstone, lake/pond carbonate, lithic-rich fluvial and paleosol deposits. Valley incision and the vertical facies succession indicates a short cycle of lowstand erosion and transgressive to highstand deposition, under wave-dominated estuarine conditions, during withdrawal of the Boreal Sea. Overall, the Great Falls member stratal succession makes up the marine/estuarine part of one of several higher frequency, and otherwise nonmarine, sequences within the lower Kootenai Formation.

The Great Falls member was deposited in a forebulge depozone that included the low-relief Sweetgrass Arch and adjacent, axial, incised valleys and trunk-fluvial systems. Coeval coastal/alluvial plain/lacustrine settings toward the foredeep and backbulge depozones and the sub-Kootenai incised valley pattern document that a topographically low longitudinal zone was located atop the flexural forebulge. This resulted in maximized and repeated fluvial incision along axial systems during times of lower sea level, with the paleovalley tracts serving as conduits for marine invasion during eustatic rise. Two alternative explanations are proposed for evolution of the topographically low forebulge depozone. Both involve interactive static flexure and dynamic subsidence for an overfilled-basin setting. One model involves orogenic loading followed by orogenic (erosional) unloading as the primary control upon the topographic profile. In this case, the overfilled foreland profile does not follow the shape of the underlying flexural profile and the top of foredeep becomes more elevated than the forebulge depozone. The other model calls upon continued orogenic loading with maximized differential erosion in strata above the flexural forebulge.

INTRODUCTION

Background and Purpose

Upper Jurassic through Upper Cretaceous strata between western Alberta and southern Utah make up most of the sedimentary fill within the Cordilleran foreland basin (fig. 1A; DeCelles, 2004). Throughout the Western Interior of the U.S., the Kootenai Formation and equivalent sedimentary rocks have historically been interpreted as nonmarine, primarily of fluvial, alluvial plain, and lacustrine origin (McGookey and others, 1972; Walker, 1974; Holm and others, 1977; Suttner and others, 1981; Condon, 2000; DeCelles, 2004; Miall and others, 2008). The Albian Flood Member of the Blackleaf Formation, which overlies the Kootenai Formation in western Montana, is widely accepted as representing the initial incursion of the Boreal Sea from Canada into the Western Interior of the United States (McGookey and others, 1972; Williams and Stelck, 1975; Schwartz and DeCelles, 1988). Further transgression placed marine over nonmarine deposits throughout the Western Interior (fig. 1B; Kauffman, 1977). With the exception of the quartzose Great Falls member described in this study, Kootenai Formation conglomerate and sandstone in western Montana are coarse- to fine-grained, lithic-rich deposits that reflect derivation from the fold-and-thrust belt to the west and southwest, and from intraforeland uplifts to the south (Walker, 1974; Berkhouse, 1985; DeCelles, 1986; Miall and others, 2008).
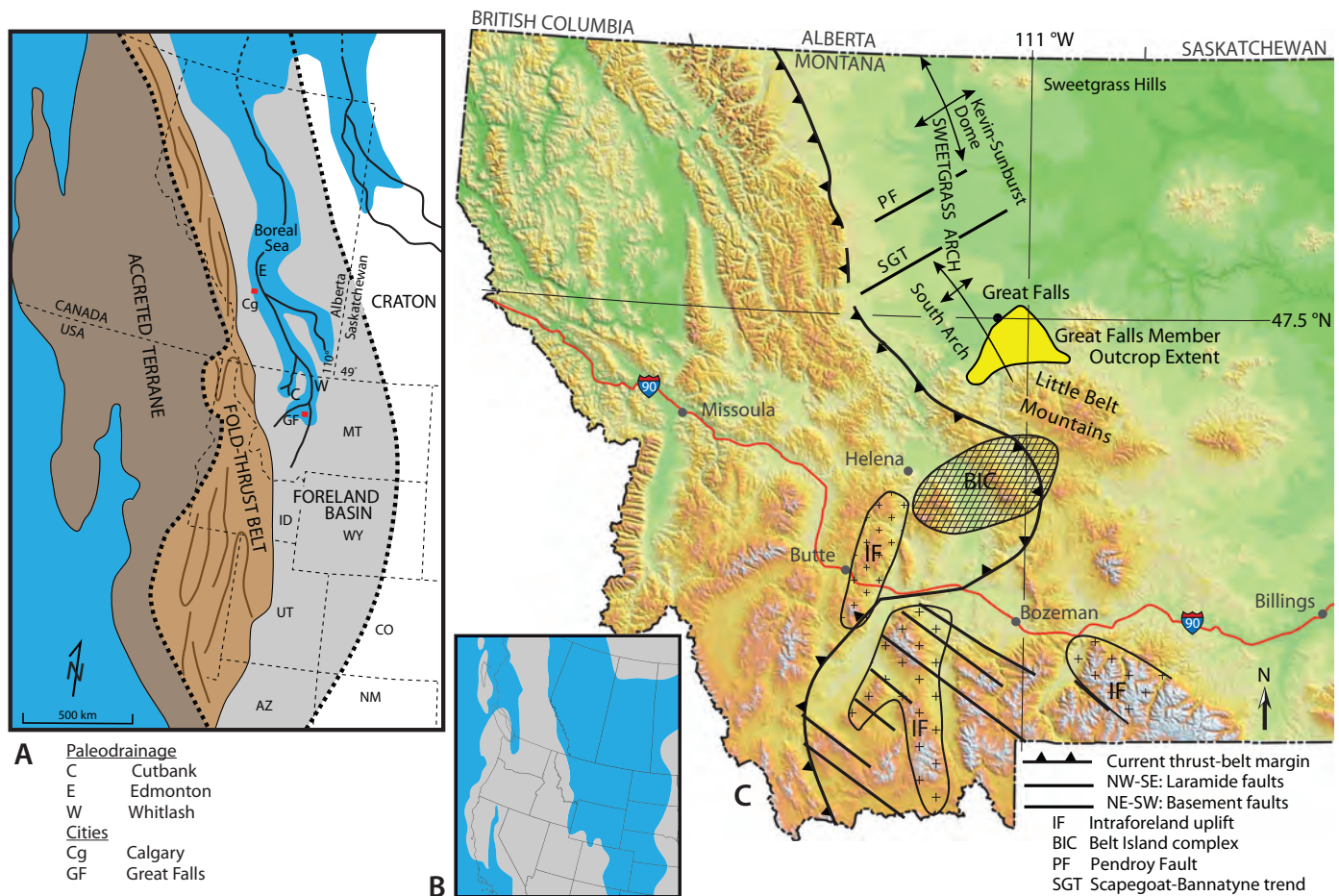
Figure 1. (A) Simplified tectonic map of the Aptian Cordilleran orogenic system showing southward extent of the Boreal Sea and valleys established prior to Kootenai and Mannville deposition, along which marine inundation occurred. Map features adapted from Ranger and Pemberton (1988), Dolson and Piombino (1994), Blakey and Umhoefer (2003), DeCelles (2004), Fuentes and others (2011), Blakey (2014), and Durkin and others (2017). (B) Simplified map showing extent of Albian Western Interior sea, traditionally considered the initial Early Cretaceous marine advance into Montana. This second Early Cretaceous advance of the sea into Montana followed an intervening episode of nonmarine deposition. Map from Slattery and others (2015). (C) Study area (yellow). Also shown are structural and paleogeographic features, including Laramide faults of Precambrian ancestry and interpreted positive features of the Late Jurassic Belt Island complex, Early Cretaceous intraforeland uplifts, and Sweetgrass Arch.

The lower Kootenai Formation in the subsurface of northern Montana and the correlative lower Mannville Group in the subsurface of southern Alberta (fig. 2A) contain billions of barrels of oil (Leckie, 2000). Consequently, this part of the section has been studied extensively and in much detail in the subsurface, primarily in Alberta (e.g., Dolson and Piombino, 1994; Arnott and others, 2000; Ardies and others, 2002; Arnott and others, 2002; Lukie and others, 2002; Leckie and others, 2004; Ratcliffe and others, 2004; Hildred and others, 2010). Despite abundant subsurface research, the following features complicate stratigraphic correlations in the subsurface: (1) multiple, stacked, incised valley sequences (Zaitlin and others, 2002) that may extend through the entire Mannville Group (Leckie and others, 2004); (2) homotaxial lithostratigraphic units (Hildred and others, 2010); (3) missing lower parts of the section; and (4) paucity of reliable geochronology. The Great Falls outcrop area provides clear stratigraphic relationships for this part of the section and a unique opportunity to study Great Falls member estuarine deposits, which are replaced by nonmarine Kootenai Formation to the south in Montana.

In southern Alberta, the Mannville Group, equivalent to the Kootenai Formation, consists of both marine and nonmarine sedimentary strata that record several southward advances and northward withdrawals of the Boreal Sea within the foreland of southern Canada (Farshori and Hopkins, 1989). Several investigations of the Great Falls member in the Great Falls area suggested possible deposition in brackish to marine environments, representing an Early Cretaceous invasion of the Boreal Sea into northern Montana (Burden, 1984; Vuke, 1987, Farshori and Hopkins, 1989; Schwartz and Vuke, 2006; Reid, 2015).

This study provides details of the sedimentary properties and facies architecture of the Great Falls member of the Kootenai Formation near Great Falls, Montana, and documents Early Cretaceous incursion of a tide-dominated sea into northern Montana. In addition, a direct relationship between inundation pathway, paleolandscape, facies distribution, and tectonic setting is demonstrated and used to interpret flexural, dynamic, and sea level controls upon foreland accommodation.

Geologic Background

Tectonic Setting

Middle Jurassic to Upper Cretaceous strata demonstrate that foredeep, forebulge, and backbulge depozones of a foreland basin system developed across western Montana in association with Sevier deformation (DeCelles and Giles, 1996; DeCelles, 2004; Fuentes and others, 2011). However, the foreland basin was structurally complex compared to that portrayed by the standard foredeep–forebulge–backbulge depozone model (DeCelles and Giles, 1996; DeCelles, 2004) due to the presence and syndepositional reactivation of large-scale basement-related structures (Peterson, 1966, 1981; Schwartz, 1982; DeCelles, 1986, 2004; Schwartz and DeCelles, 1988). Basement-related features within the foreland basin include: (1) well-developed intraforeland uplifts and intervening intraforeland basins where the foredeep overlaps with the Laramide structural province in southwestern Montana; (2) more subdued "Belt Island" positive elements at the northwestern terminus of the Laramide intraforeland structural province; and (3) in the study area, the subdued Sweetgrass Arch complex (fig. 1C).

Although tectonically much less complex than the Early Cretaceous foreland basin of southwestern Montana (Schwartz, 1982; DeCelles, 1986; Schwartz and DeCelles, 1988; DeCelles, 2004), each of the basement-related structures in the northwestern Montana part of the basin also influenced sedimentation prior to and during the Early Cretaceous. The NNW-elongate Sweetgrass Arch complex, including the South Arch near Great Falls and the Kevin–Sunburst Dome to the north, lies approximately 115 km east of the current position of the thrust belt. Following initial Precambrian development, the arch complex underwent a protracted, but irregular history of reactivation through the Paleozoic and Mesozoic, including basement fault reactivation and lithospheric flexure (Lorenz, 1982). Stratigraphic studies document that the Sweetgrass Arch was intermittently exposed and covered by sediments during Paleozoic and Mesozoic time and exhibited minor to strong control on deposition (Peterson, 1966; Lorenz, 1982; Meyers and Schwartz, 1994; Fuentes and others, 2011). At least some of the Sweetgrass Arch–Belt Island features underwent intermittent reactivation during the Middle Jurassic to Late Cretaceous, most likely in association with
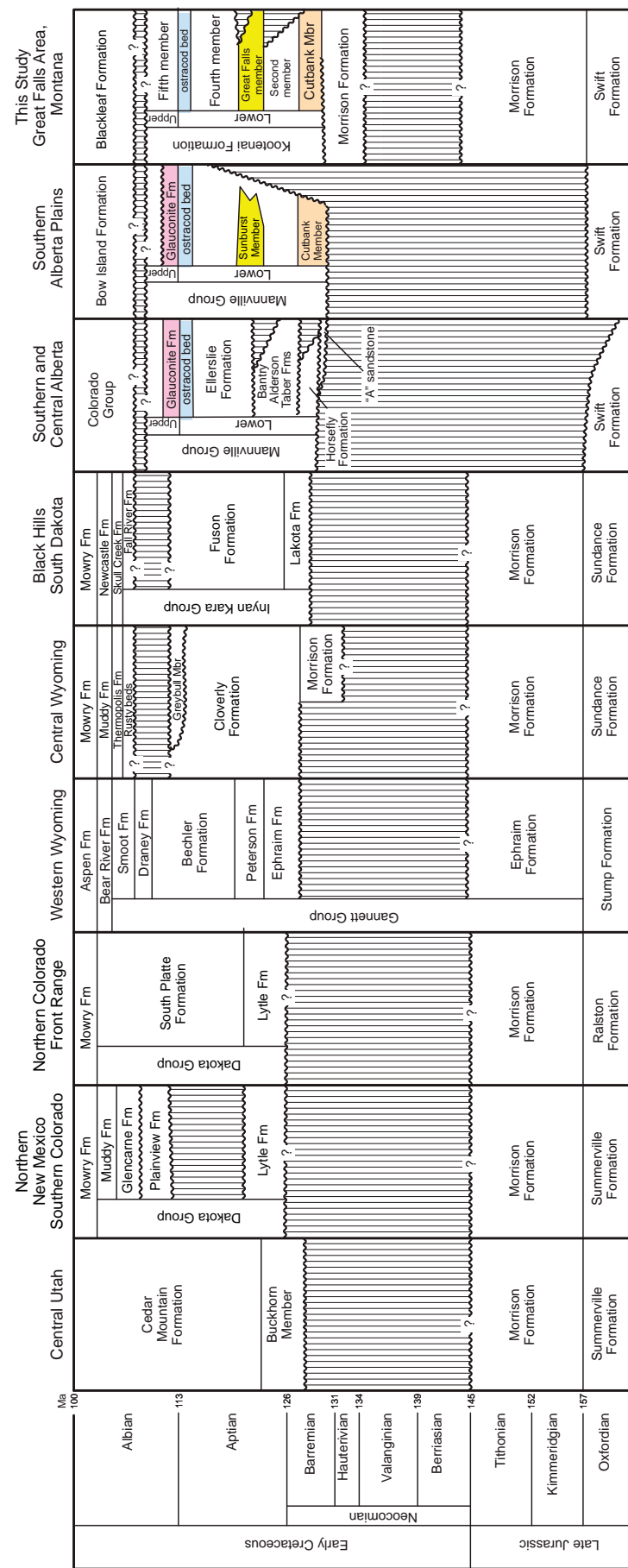
B

Walker, 1974	Farshori and Hopkins, 1989	Mapped units (Vuke, 2000, 2002a, 2002b)		This Study
Upper red mudstone unit		Fifth member (Kk5)	Upper Kootenai	Fifth member (Kk5)
Lignitic unit	Sunburst Sandstone			
Fossiliferous limestone unit		Fourth member (Kk4)		Fourth member (Kk4)
Red sandstone unit				
Quartzose sandstone unit (author correlated with Sunburst)		Sunburst member (Kks)		Great Falls member (Kkgf)
Red mudstone unit		Second member (Kk2)	Lower Kootenai	Second member (Kk2)
Basal sandstone unit (author correlated with Cutbank)		Cutbank Member (Kkc)		Cutbank Member (Kkc)

Figure 2. (A) Generalized correlation of Late Jurassic and Early Cretaceous units in the Great Falls outcrop area with those in the Western Interior Basin of Alberta and elsewhere in the western United States. Modified from Tschudy and others, 1984; Mateer, 1987; Winslow and Heller, 1987; Heller and Paola, 1989; Molenaar and Cobban 1991; Hayes and others, 1994; and Zaitlin and others, 2002. Cretaceous age for the upper Morrison Formation in the Great Falls study area is from Engelhardt, 1999, and Reynolds and Brandt, 2005. (B) Comparison of Kootenai Formation stratigraphic units used in the Great Falls area.

the reactivation of Laramide structures at the northern end of the Rocky Mountain foreland (Laramide structural province; Peterson, 1966, 1981; Herbaly, 1974; Schwartz and DeCelles, 1988; Meyers and Schwartz, 1994). The ancestral Sweetgrass Arch and aligned intraforeland structures in southwestern Montana were interpreted to at least partially control the location of the Cordilleran forebulge during Early Cretaceous Kootenai deposition (DeCelles, 2004; Fuentes and others, 2011). Erosion (i.e., paleovalley incision) and deposition were also controlled during Paleozoic and Mesozoic time by northeast-oriented basement faults and lineaments that cross-cut the Sweetgrass Arch (fig. 1C; McMannis, 1965; Oakes, 1966; O'Neill and Lopez, 1985; Meyers and Schwartz, 1994; Dolson and Piombino, 1994).

Paleolandscape Setting

The pre-Kootenai landscape provided the setting for marine incursion from the north. Two large-scale, parallel valley systems were incised into the sub-Kootenai unconformity surface (Dolson and Piombino, 1994) and axially drained the foreland basin of northwestern Montana toward Canada (fig. 3). The Kevin–Sunburst Dome and a positive feature to its southwest (the South Arch), bound by the northeast-trending Pendroy fault zone and Scapegoat–Bannatyne trend, served as the drainage divide between the two paleovalley systems (fig. 3). The two axial systems (the Whitlash Valley tract, within and directly north of the study area on the east side of the Sweetgrass Arch, and the Cutbank Valley tract northwest of the study area on the west side) extended into southern Canada where the name *Taber–Cutbank* is applied to the latter. In Alberta, the two systems are separated by the northeast-curving extension of the Sweetgrass Arch (Bow Island Arch) and are similarly incised into Jurassic and Mississippian strata at the sub-Cretaceous unconformity (Ardies and others, 2002; Hildred and others, 2010; Zaitlin and others, 2002). In Montana, the Whitlash system also extended axially south of this study area, with clast derivation from intraforeland uplifts in southwestern Montana and the thrust belt far to the southwest (DeCelles, 1986; Schwartz and DeCelles, 1988; Schwartz and Schwartz, 2013; Walker, 1974; Quinn and others, 2018).

Regional Stratigraphy of the Sunburst Sandstone and Great Falls Member

The name *Sunburst sandstone* has been applied to a distinctive quartzose sandstone that crops out in the Great Falls area and is the subject of this report. Owing to inconsistent correlations in the subsurface, and uncertain correlation between the subsurface type section and the outcrop area, the name *Great Falls member* is herein applied to the unit exposed in the Great Falls area.

Sunburst sandstone was first applied to a specific subsurface unit at the base of the Kootenai Formation in the Kevin–Sunburst oil field (Hager, 1923). Subsequently, the name was used in the subsurface throughout the Sweetgrass Arch area of Montana (Collier, 1929; Bartram and Erdmann, 1935; Cobban, 1955; Gussow, 1955; Leskela, 1955; Lynn, 1955; Reid, 1955; Rhodes, 1955; Oakes, 1966; Schulte, 1966; Thompson, 1966), and to the north in Alberta by oilfield workers (Hayes, 1990; Hopkins and others, 1987; Farshori and Hopkins, 1989; Hayes and others, 1994; Karavas and others, 1998).

Oakes (1966) noted that the name Sunburst was applied to the subsurface Lander member in the Cutbank field on the west side of the Sweetgrass Arch but to the stratigraphically higher Moulton member in the Kevin–Sunburst field on the east side. Although the Lander and Moulton both include quartzose sandstones, they are stratigraphically separated by a limestone marker bed. Rice (1976) specified a subsurface Sunburst type section at the base of the Kootenai Formation in the Kevin–Sunburst field, although he did not meet the criteria for establishing a formal stratigraphic unit.

Glaister (1959) applied the name Sunburst to a quartzose sandstone (the subject of this report) that crops out along the Missouri River near Great Falls, Montana. Others subsequently referred to this distinctive sandstone at the Missouri River section and throughout its outcrop extent as Sunburst (Walker, 1974; Burden, 1984; Farshori and Hopkins, 1989; Vuke, 2000; Vuke and others, 2002a,b; Quinn and others, 2018). The name Sunburst was also applied to Kootenai sandstone outcrops in the thrust belt west of the Sweetgrass Arch (Cobban, 1955; Mudge, 1972; Mudge and Rice, 1982), but this sandstone is above
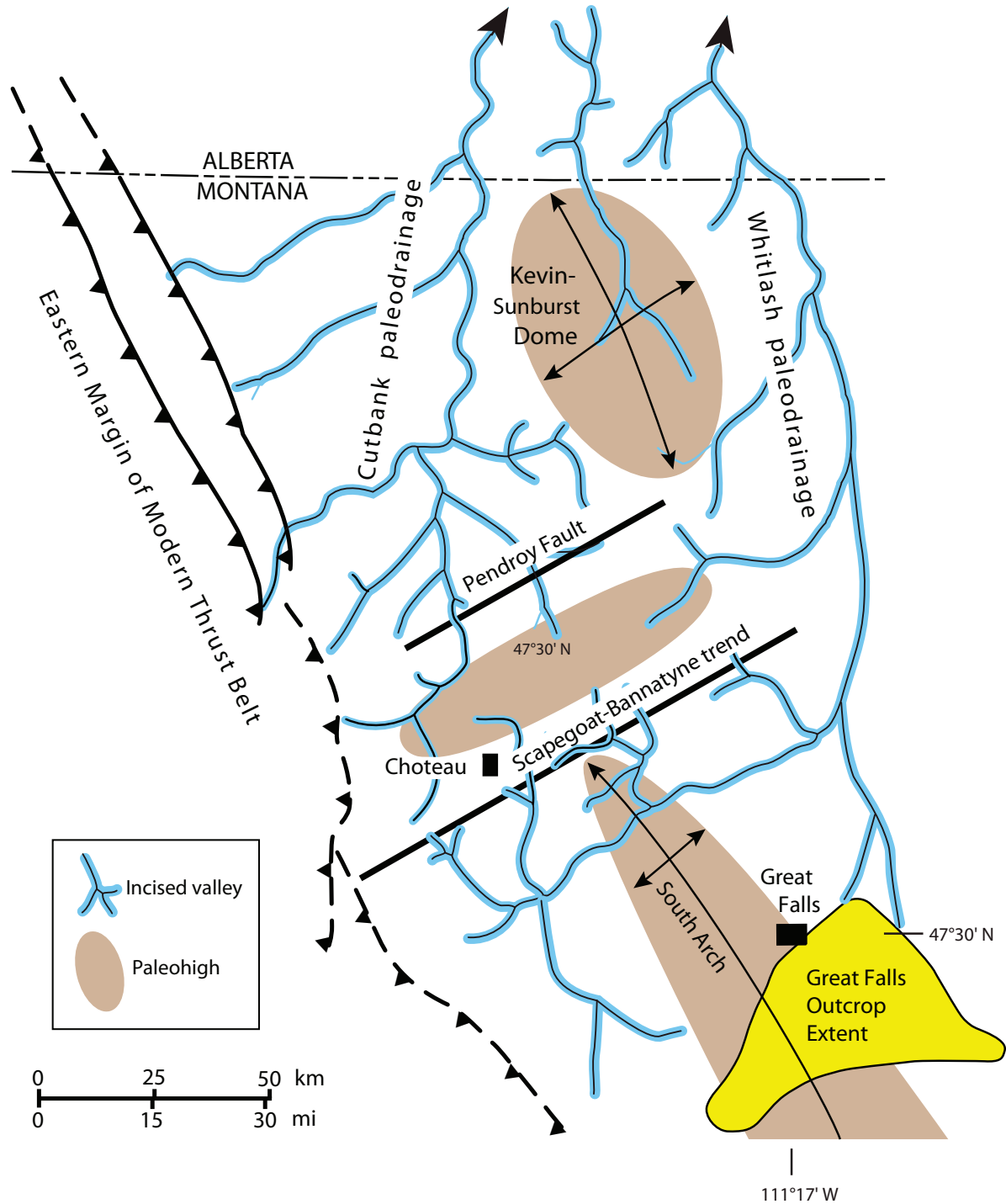
Figure 3. Paleotopography of the sub-Kootenai unconformity surface. Modified from Dolson and Piombino (1994).

the limestone marker bed and therefore likely does not correlate with the Great Falls member. The Sunburst sandstone was also recognized in the Sweet Grass Hills east of the Sweetgrass Arch (Lopez, 1995), but its relationship to the Great Falls member was not determined.

Hayes (1986, 1990) noted the Sunburst correlation discrepancies even over relatively short distances,

the lack of original authorship for the name, and the lack of useful description and basis for assignment at the type section. He cautioned against using the term Sunburst except where a direct correlation could be made with the Sunburst unit in the Kevin–Sunburst field near the crest of the Kevin Dome of the Sweetgrass Arch. The quartzose sandstone in the Great Falls outcrop area probably correlates with the Lander sandstone in the Cutbank field (W. Cobban, oral
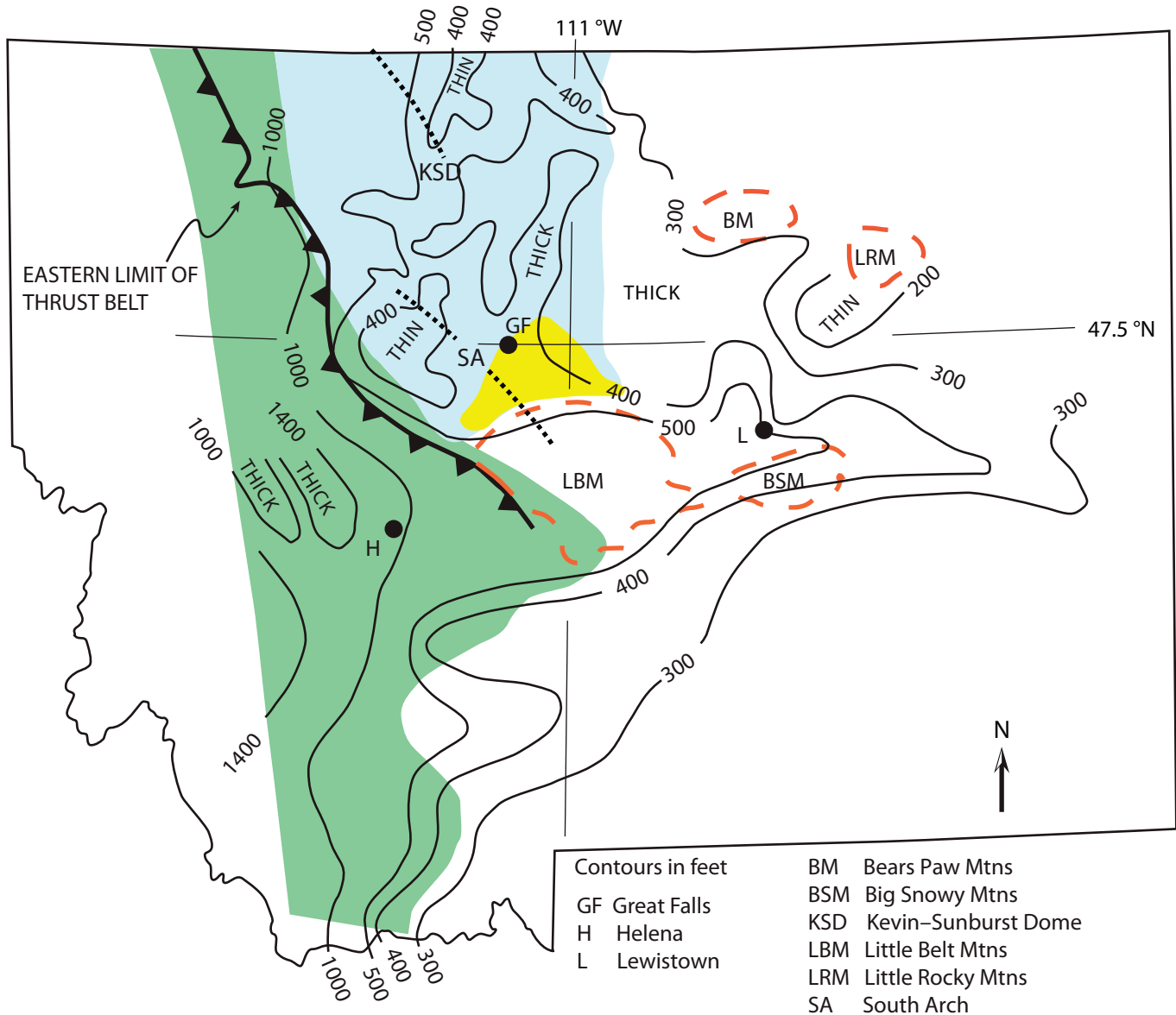
Figure 4. Isopach map of the Kootenai Formation and distribution of the Great Falls member (blue, subsurface; yellow, area of surface exposures; green, area where freshwater limestone is laterally equivalent to the Great Falls member). Isopach data from Walker (1974).

commun., 1987), which was also commonly referred to as Sunburst. However, based on the subsurface correlations of Oakes (1966), the basal sandstone in the Kevin–Sunburst field to the east (type Sunburst of Rice, 1976) is higher in the section, and the Lander equivalent is not present there. Therefore, the quartzose sandstone that crops out in the Great Falls area likely does not correlate with the type Sunburst of Rice (1976). For these reasons, we are applying the informal name (indicated by lower case "m") *Great Falls member*, rather than *Sunburst member*, to the Lower Kootenai Formation quartzose sandstone that crops out in the Great Falls, Montana area.

Walker (1974, his fig. 19) shows Sunburst sandstone (Great Falls member of this study) extending in a lobate pattern that widens from its terminus in the outcrop area of this study into the subsurface to the north (fig. 4). Many reports, primarily from Montana oil and gas fields, collectively indicate the subsurface presence of the Sunburst sandstone in this pattern; however, irregular unconformities and the stratigraphic complexities of the name Sunburst applied to quartzose sandstones at different stratigraphic horizons were not taken into account.

Based on its stratigraphic position, the Great Falls member has been approximately correlated with the Aptian Ellerslie Formation of the Mannville Group to the north (Farshori and Hopkins, 1989; Hayes, 1990; Hayes and others, 1994), which also contains quartzose sandstone beds (Zaitlin and others, 2002) (fig. 2A). Detrital zircon data from fluvial sandstones above and below this unit constrain its age. In the Great Falls area, the maximum age for the lower part of a unit that overlies the Great Falls member is reported to be 112.9 ± 1.5 Ma (latest Aptian–earliest Albian; Quinn and others, 2018), suggesting that the conformable Great Falls member is also Aptian. However, Burden (1984) interpreted a Barremian age for this unit based on palynomorphs. Approximately 36 km west of Great Falls, the maximum age for the Cutbank Member is reported as 131 ± 4.5 Ma and 133 ± 1.8 Ma (Hauterivian; Fuentes and others, 2012). In this paper, the Great Falls member is considered pre-Albian based on these data.

Walker (1974) first described the surface exposures of the Kootenai Formation in the Great Falls area in detail, and recognized seven stratigraphic units. Subsequently, the Kootenai Formation was divided and mapped as five members (fig. 2B; Vuke, 2000; Vuke and others, 2002a,b). The mapped Kootenai units include: (1) the Cutbank Member, equivalent to Walker's basal sandstone; (2) the second member, equivalent to Walker's limestone concretion unit; (3) the Sunburst member, equivalent to Walker's quartzose sandstone unit; (4) the fourth member, equivalent to Walker's fossiliferous limestone and red sandstone units; and (5) the fifth member (upper Kootenai Formation), equivalent to Walker's lignitic and upper red mudstone units (fig. 2B). In this paper, map symbols Kk2, Kk4, and Kk5 refer to the second, fourth and fifth members of the Kootenai Formation, and *Sunburst member* has been replaced with *Great Falls member*.

Distribution and Lithostratigraphic Context of the Great Falls Member in the Study Area

The quartzose Great Falls member is well exposed in the Great Falls area, but is only present in the subsurface north of Great Falls (figs. 2, 4). The main outcrop area lies along and atop the central part of South Arch. The Great Falls member pinches out to the east, south, and west of the study area, and is vertically

and laterally bound by lithic-rich, nonmarine members of the Kootenai Formation (fig. 5; Walker, 1974; Berkhouse, 1985; Farshori and Hopkins, 1989; Vuke, 2000; Vuke and others, 2002b). It is not present in the fold–thrust belt to the west. Within the study area, the thickness of the Great Falls member decreases toward its southern limit from about 30 m in the Missouri River gorge near Great Falls, Montana (Walker, 1974) to where it pinches out near Raynesford, Montana and near Hound Creek (fig. 5).

A disconformity with considerable local relief (up to 24 m) is present at the base of the Great Falls member (Walker, 1974). It is marked by an abrupt change in lithology, the presence of an oxidized and/or silicified mudstone zone at the top of the underlying Kk2 member, or direct contact with the Cutbank Member. The upper contact of the Great Falls member is gradational with overlying coastal plain mudstones and interbedded lithic-rich, fluvial sandstones (Walker, 1974).

Sequence Stratigraphic Context of the Great Falls Member

Although details of the Kootenai sequence stratigraphy in western Montana are not established, sequence stratigraphic interpretations of the correlative Mannville Group in southern Alberta (Cant, 1996, 1998; Banerjee and Kalkreuth, 2002) and southwestern Saskatchewan (Leckie and others, 1997) provide some context. The Mannville Group is internally complex with abundant unconformities, weathered horizons, and repeated, discontinuous facies associations due to frequent base-level oscillation in a longitudinally oriented, low accommodation, foreland deposystem (Cant, 1996, 1998), often making system tract and subsequence correlations difficult to impossible. The same stratigraphic complexity is typical of the Kootenai in the Great Falls area.

The Mannville Group is bound by major unconformities (Cant, 1996, 1998; Banerjee and Kalkreuth, 2002), both of which extend into the Western Interior of the U.S. and similarly bound the Kootenai Formation (fig. 2A; Hayes and others, 1994). The sub-Mannville and sub-Kootenai unconformity in both regions represents a time span of about 15–25 Ma (Cant, 1996; Banerjee and Kalkreuth, 2002; Fuentes and others, 2011), whereas duration of the upper unconformity is less certain but generally
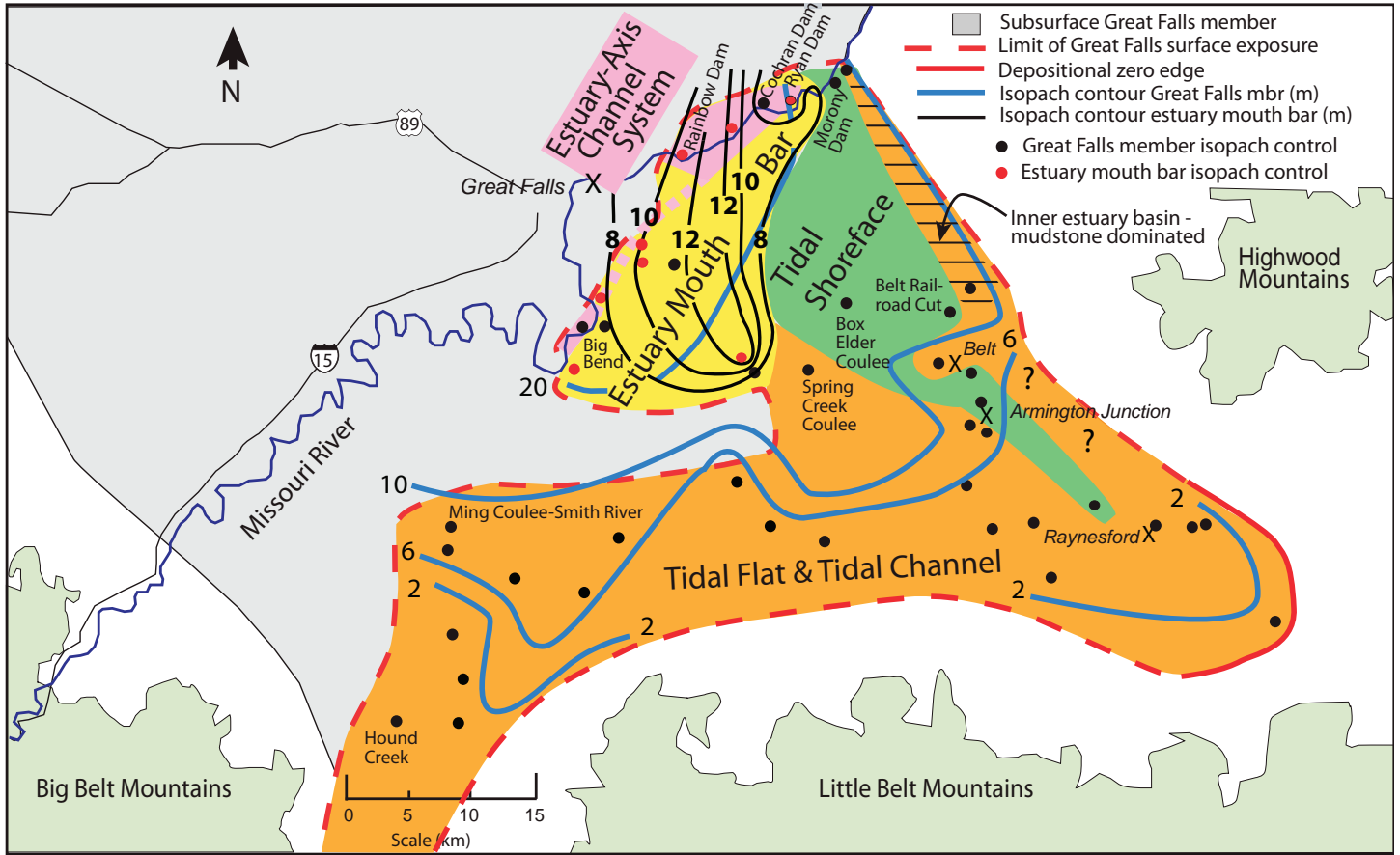
Figure 5. Facies associations making up the main estuary basin, and isopach map of the Great Falls member (variable contour interval) with estuary mouth bar facies (yellow) isopach in more detail (contour interval 2 m). The estuary axis channel facies (blue) overlies the estuary mouth bar facies and lies along a NE–SW transect indicated by the dashed blue line. The inner estuary basin facies underlies the estuary mouth bar facies in the basin interior and underlies tidal flat facies along the northeast margin of the study area (parallel line pattern). Selective outcrops discussed in the text are labeled.

accepted as shorter and reported to be about 10 Ma in Alberta (Banerjee and Kalkreuth, 2002). Cant (1998) designated the Mannville Group as a third-order sequence, with the lower Mannville Group representing a transgressive systems tract and the upper Mannville Group a highstand systems tract. However, based on the nature and time span of the Mannville-bounding unconformities, time span of the Mannville Group (~18 Ma), and internal stratal patterns, Banerjee and Kalkreuth (2002) designated the Mannville Group as a second-order sequence and the lower Mannville Group as a third-order sequence. Due to shared bounding unconformities and similar age relationships, we judge the Kootenai Formation in western Montana to also represent a second-order sequence and the lower Kootenai a third-order sequence. Similar to the basal part of the lower Mannville Group, coarse-grained fluvial sediments of the basal Kootenai (Cutbank Member) were deposited in valleys cut into Paleozoic and older

Mesozoic rocks. The sub-Kootenai unconformity and the upward succession into the Great Falls member constitutes a transgressive systems tract (after Cant, 1998; Banerjee and Kalkreuth, 2002). The third-order highstand systems tract (after Cant, 1998; Banerjee and Kalkreuth, 2002) is marked by an upward transition into lacustrine, floodplain, and fluvial facies representing a progradational delta plain setting (lower-middle part of Kk4; red sandstone unit of Walker, 1974). The upper boundary of the third-order sequence lies below a horizon of deeply incised fluvial sandstone bodies (upper part of Kk4) that are conformably overlain by fossiliferous lacustrine limestone (Walker, 1974), both of which mark the beginning of a subsequent nonmarine lowstand-to-highstand systems tract. Multiple disconformities and intervening facies successions within the lower Kootenai Formation, including within the Great Falls member, indicate different scales of higher frequency subsequences.

METHODS AND TERMINOLOGY

A total of 56 Great Falls member outcrops were examined in detail across the study area (fig. 6; appendix table 1). Most outcrop sites were located by using information in Walker (1974) and from geologic maps (Vuke, 2000; Vuke and others, 2002a,b). The strata were divided into lithofacies and interpreted in terms of facies associations. Lithofacies were designated based on lithology, sediment body geometry, bed features (geometry, contacts, thickness, and physical and biogenic structures), grain size, and thickness trends. Paleocurrent indicators were measured (*n* = 433) from large- and small-scale trough and planar cross-stratification and all other applicable features (e.g., channel axes) using traditional methods (DeCelles and others, 1983). Thickness data, including the approximate location of the depositional zero

edge of the Great Falls member, are compiled from Walker (1974), Vuke (2000), Vuke and others (2002a), and measurements made in this study. Trace fossils were recorded according to lithofacies to serve as supplementary evidence in environmental analysis.

For the convenience of basin-scale mapping, description, and interpretation of depositional environments, individual small-scale lithofacies are integrated into lithofacies assemblages, yet simply referred to as *lithofacies* (after Miall, 2016). Interpreted depositional processes or environments corresponding to the integrated lithofacies scale are referred to as *facies* (Anderson, 1985; Walker, 2006). Facies associations are defined as consisting of one or more lithofacies that represent a distinct environmental setting (Collinson, 1969). This report identifies various estuarine environments. Contrary
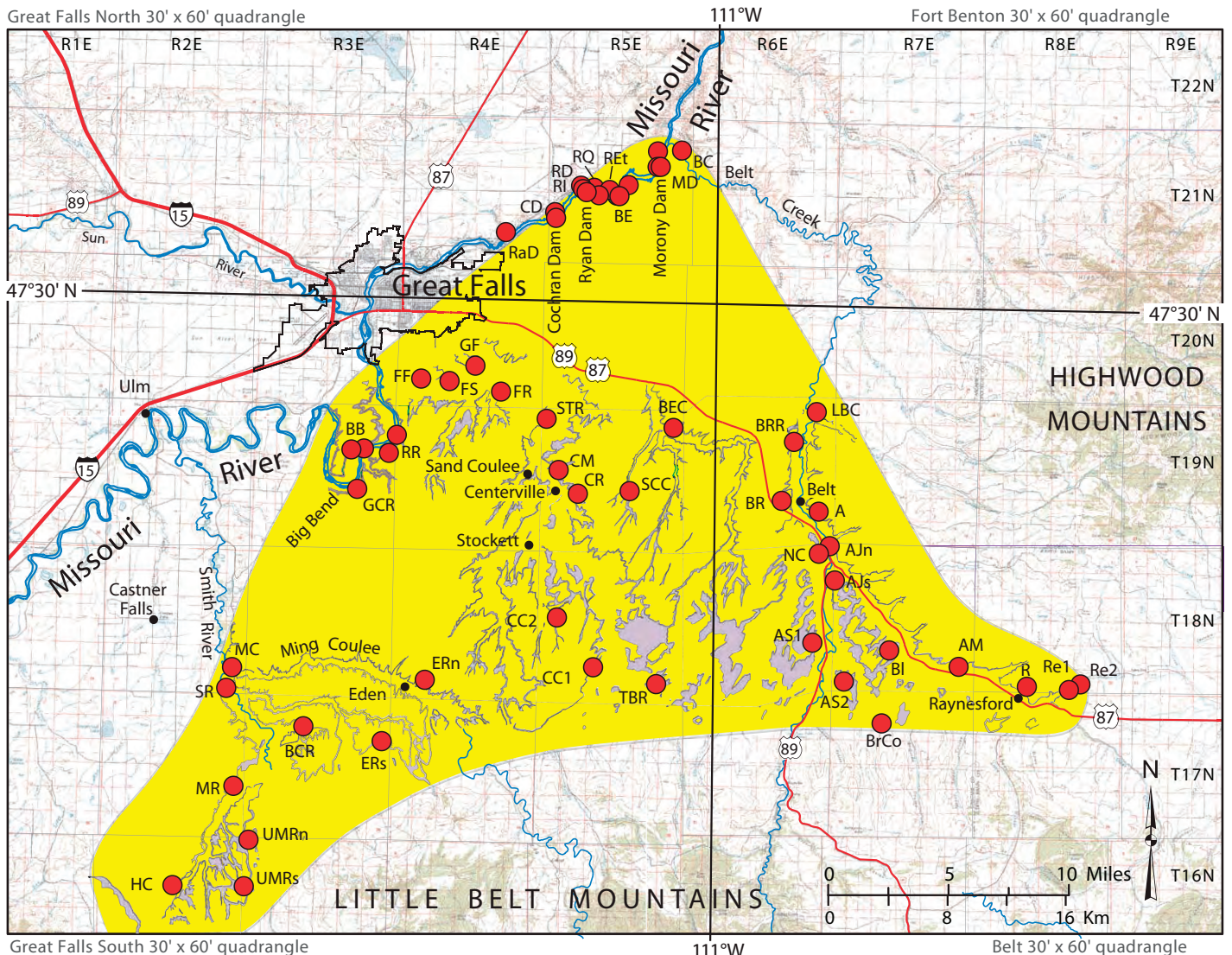
Figure 6. Outcrop sites. Yellow, outcrop extent of Great Falls member; gray, Great Falls outcrops; red circles, with site symbols indicated, studied outcrops (see appendix table 1).

to a salinity-based definition, the term *estuary* is used in this paper as discussed by Dalrymple and others (2012), in which an estuary is a transgressive coastal environment at the mouth of a river that (1) receives sediment from both fluvial and marine sources; (2) contains facies influenced by tide, wave, and fluvial processes; and (3) extends from the landward limit of tidal facies at its head to the seaward limit of coastal facies at its mouth. Our system tract assignments for estuarine and associated nonmarine deposits in the Kootenai sequences follow the convention described by Boyd and others (2006), and those practiced in most studies involving modern estuarine (e.g., summarized in Tessier, 2012) and ancient estuarine foreland basin deposits (e.g., Shanley and McCabe, 1993, 1994, 1995; Hettinger and others, 1993; McLaurin and Steel, 2000; Plint and others, 2001), rather than original definitions for system tracts and conventions of the Exxon group (e.g., Van Wagoner and others, 1988; Posamentier and Vail, 1988). We do this on the basis of (1) high resolution (detailed facies) analysis, (2) internal stratal patterns, (3) recognition that the bulk of the estuarine valley deposits were deposited during a rise in base level at a time when the seaway had migrated well into the nonmarine interior of the foreland, and (4) recognition that final estuary filling was associated with still stand and a subsequent decrease in relative sea level.

SANDSTONE COMPOSITION

Great Falls sandstones typically consist of as much as 98% well-sorted, well-rounded, fine- to medium-grained quartz, with minor amounts of light gray, dark gray, and black chert, and locally as much as 25% limonite specks (Walker, 1974). The most quartz-rich and best-sorted sandstones occur in what are interpreted herein as estuary mouth bar and tidal shoreface facies. Thinning of the Great Falls member towards its southern- and eastern-most depositional extents coincides with a gradual increase in the abundance of more poorly sorted sandstones and significantly higher percentages of chert grains, limonite, and in some instances, a light gray muddy matrix, as well as a general increase in the percentage of interbedded mudstone. Poorer sorting and increased chert and sedimentary clasts also mark the basal parts of facies that overlie a marine erosional (ravinement) surface.

LITHOFACIES, FACIES ASSEMBLAGES, AND DEPOSITIONAL ENVIRONMENTS

The data presented here indicate that the Great Falls member was deposited in a variety of estuarine environments within different scale paleogeographic spaces. These include a large-scale highstand area referred to hereafter as the "main estuary basin" or simply "estuary basin" and within small, isolated, incised valleys encompassed within the boundaries of the highstand estuary basin. The main estuary basin and a case example estuarine incised valley are described in terms of their facies assemblages (FAm and FAv, appendix table 2) and lithofacies (L, appendix tables 2, 3). In some cases, a single lithofacies represents the environmental setting and is thus also ranked on the FA scale.

Main Estuary Basin

Lithofacies within the main estuary basin are grouped into five facies associations (FAm1 to FAm5; appendix table 2).

FAm1: Tidal Flat Complex

FAm1 is represented by tabular-shaped units and subordinate channel-shaped bodies that are exposed in several paleogeographic locations in the estuary basin. The assemblage makes up the southern to northeastern perimeter of the basin where it pinches out to a depositional zero edge (fig. 5). It also occurs in the basin interior within the mudstone-dominated estuary basin facies and as a basin-wide cap to the Great Falls member.

Lithologic Description

Tabular units (L1, 20). Sandstone- and heterolithic mudstone-dominated tabular units (L1) (1–3 m thick) occur singly or as a stacked succession. Rarely, thin tabular micritic limestone beds (L20) containing ostracods and floating sand grains are associated with the tabular sandstone units (fig. 7). The sandstone units are characterized by an erosional base, horizontal to very low-angle beds, and most commonly, by upward fining (fig. 7). However, in some locales, alternating upward fining and upward coarsening tabular units are present (fig. 8), making up fining–coarsening–fining successions. At all locations within the basin, upward fining tabular units cap the Great Falls member, followed by a transition into reddish coastal
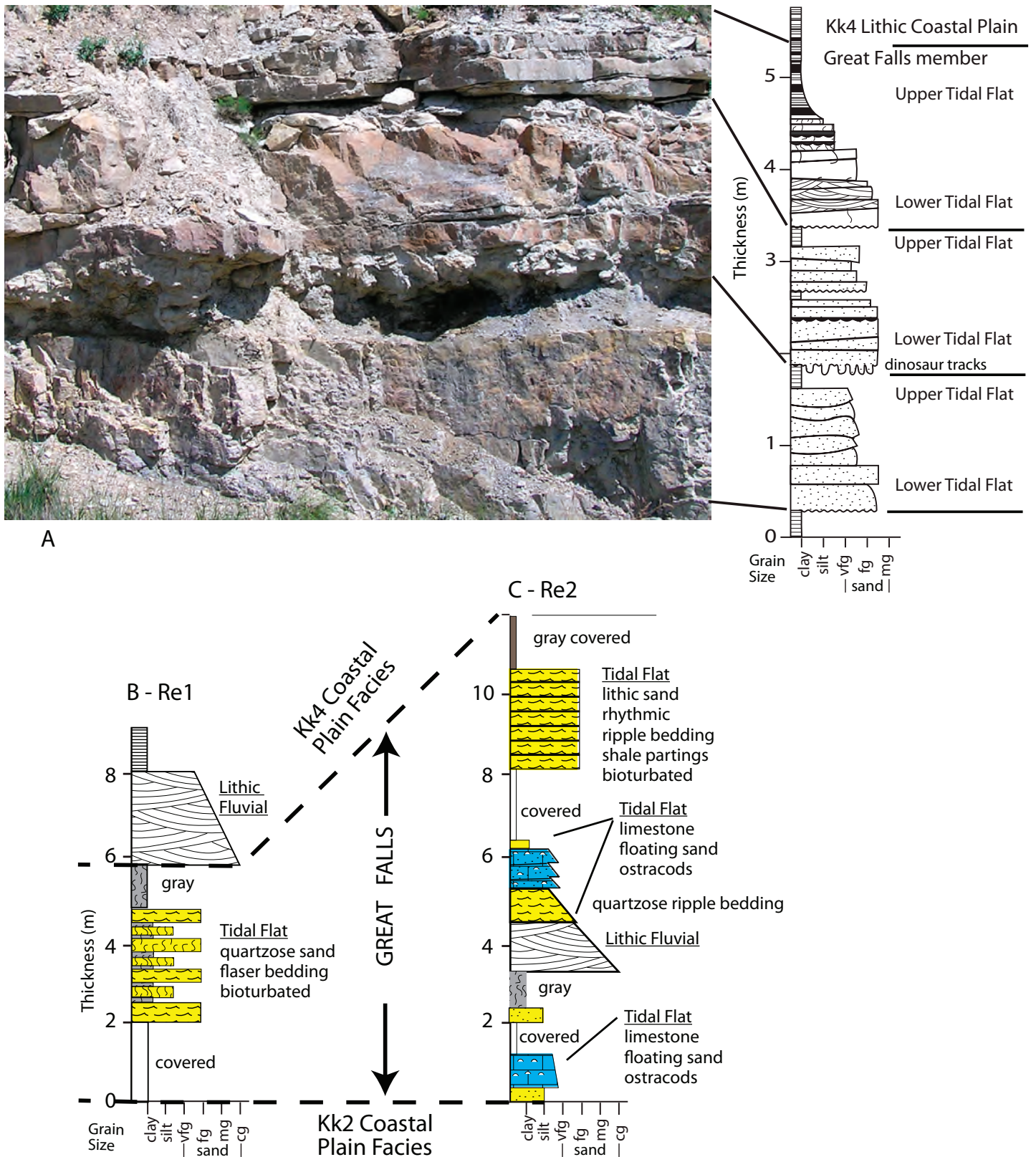
Figure 7. Tidal flat deposits. (A) Upward fining tidal flat facies at Belt road cut (BR). Large bulbous features along the base of the middle unit are deeply penetrative dinosaur tracks (after Englemann and Hasiotis, 1999; Jennings and others, 2006). (B and C) Various types of L1 and L20 tidal flat deposits (colors) in relation to encasing nonmarine deposits (uncolored) near the zero edge of Great Falls deposition in the Raynesford area (Re1 and Re2).
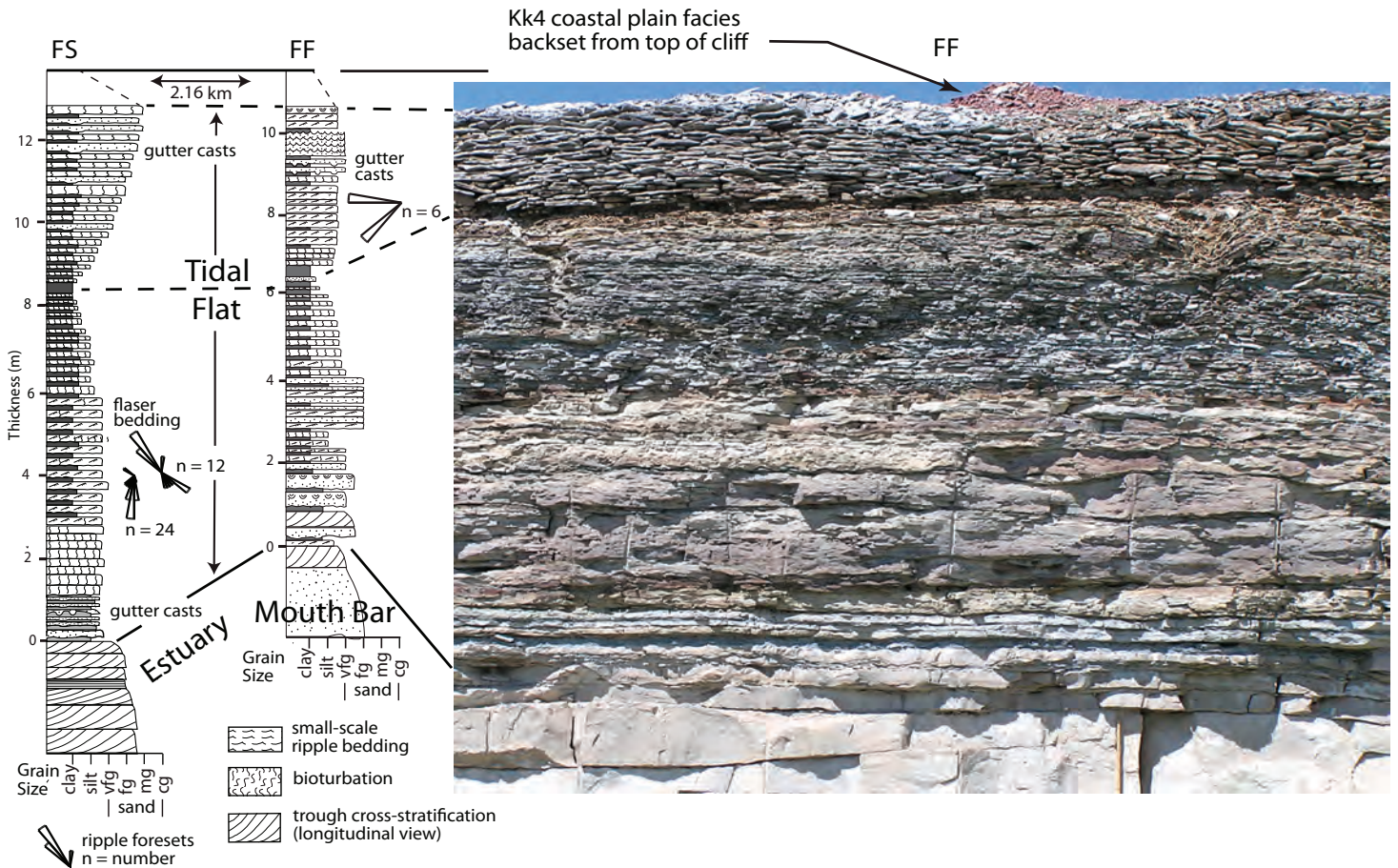
Figure 8. Oblique view of tidal flat facies (L1) overlying estuary mouth bar deposits at the Fisher–Fields road intersection (FF) site and measured sections at FF and the nearby Fields Station (FS) site. Relatively thick upward-fining and upward-coarsening heterolithic successions characterize L2 at these sites.

plain mudstone and lithic fluvial facies of the overlying Kootenai Formation (Kk4; Walker, 1974).

Bedforms include linguoid and sharp- to flat-crested symmetrical ripples. Internally, sandstone beds contain wave ripple cross lamination, flaser to wavy bedding with bimodal (bipolar) foresets (fig. 9) and internal mud drapes, and planar lamination (fig. 10). Small- to medium-scale trough and planar cross-stratification are locally present. Rarely, well-developed, vertically stacked bundles of alternating sandstone and mudstone parallel laminations are also present.

Bioturbation is most common in the mudstone-dominated intervals, but also occurs in sandstone-rich intervals. Identifiable trace fossils include *Cylindrichnus, Psammichnites,* small *Planolites, Spongliomorpha*, possible *Teichichnus, Skolithos,* small *Diplocraterion, Lingulichnus,* horseshoe crab-like crawling and resting traces, arthropod burrows, and penetrative dinosaur tracks (figs. 11–13). In addition, there

are rare occurrences of *Fuersichnus, Naktodemasis, Steinichnus,* earthworm tunnels and pellets, and probable beetle larvae burrows (fig. 12) in reddish upward fining L1 beds that directly underlie the reddish nonmarine Kk4 deposits.

Channel bodies (L8, 9, 13, 14). Channel-shaped bodies accompany the tabular units and are differentiated based upon type of channel fill, whether or not they occur within a single tabular unit or vertically transect multiple units, and by the characteristics of laterally adjacent lithologies. The channel types are designated as quartz sandstone-filled channels within a single tabular sandstone unit (L8; fig. 14A), quartzose heterolithic channels that transect multiple tabular units (L9; figs. 14B,C), mudstone-filled channels that transect multiple tabular units (L13), and muddy lithic-rich sandstone-filled channels, most commonly along the basin margin (L14; fig. 15).
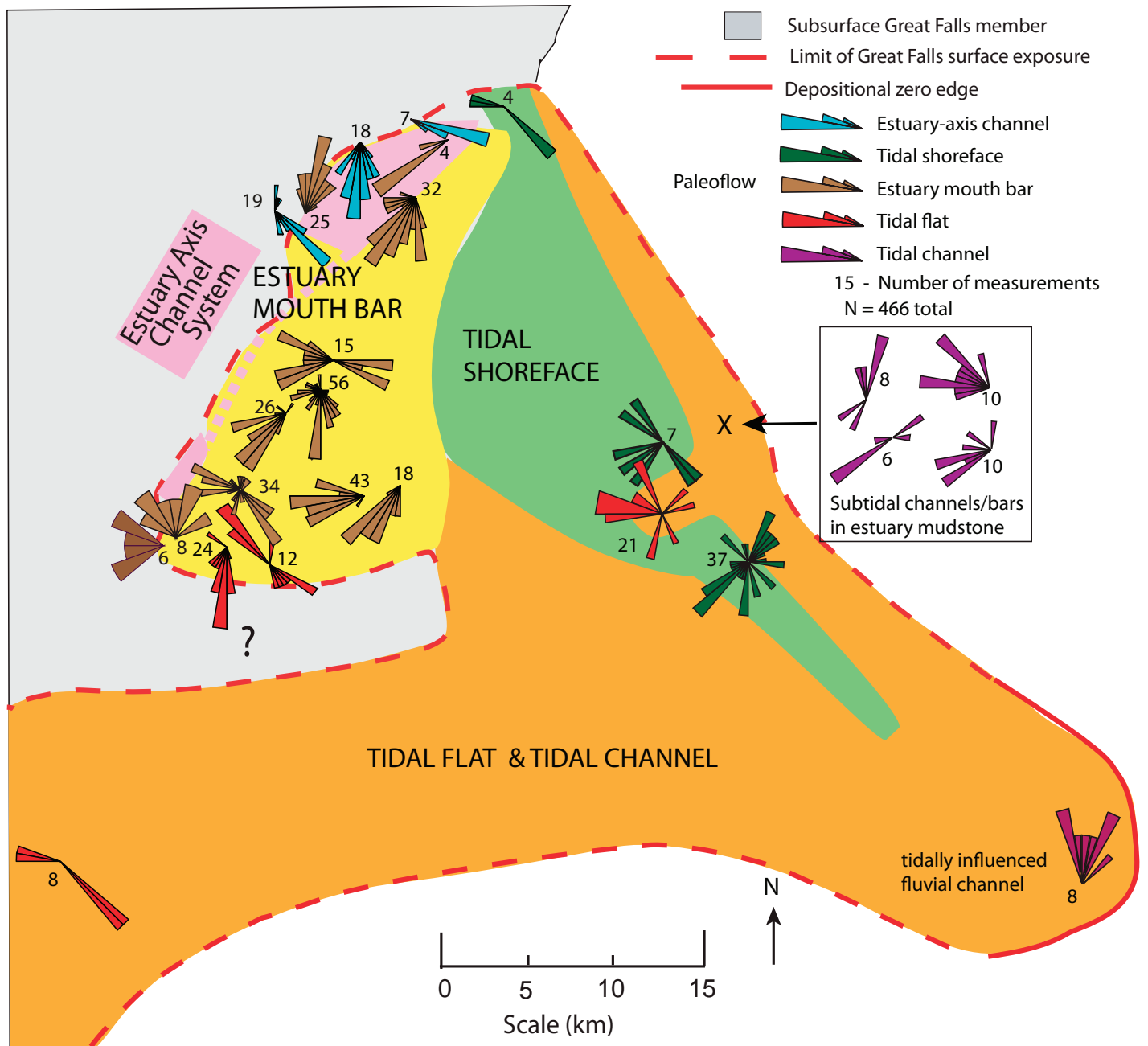
Figure 9. Paleocurrent map for various facies in the Great Falls member. The colored areas indicate the distribution of the prevalent facies type, although facies superposition is typical as reflected by the color of the rose diagrams.

The L8 quartzose channel bodies (within a tabular L1 unit) are relatively small (several to 10 m wide, 1 to several meters thick), have an erosional base, and have very low-angle channel margins (fig. 14A). Internally, they typically contain a thin pebbly layer at their base, undergo slight upward fining and are dominated by horizontal tabular to slightly inclined bedding. Sandstone texture and composition are similar to the tabular unit within which they occur. Cross-stratification with mud drapes is locally abundant.

The L9 quartzose channel bodies, which transect multiple L1 units, are erosional-based, bioturbated heterolithic bodies (tens of meters wide, less than several meters thick) that occur singly to laterally and vertically stacked. Channel fills include upward fining of symmetrically disposed horizontal heterolithic beds that are slightly concave-up along the channel margin, and upward coarsening, inclined heterolithic strata. The inclined heterolithic strata are sometimes highly deformed including small-scale folds, faults, and segmentation in association with abundant penetrative dinosaur tracks (figs. 13D, 14C).
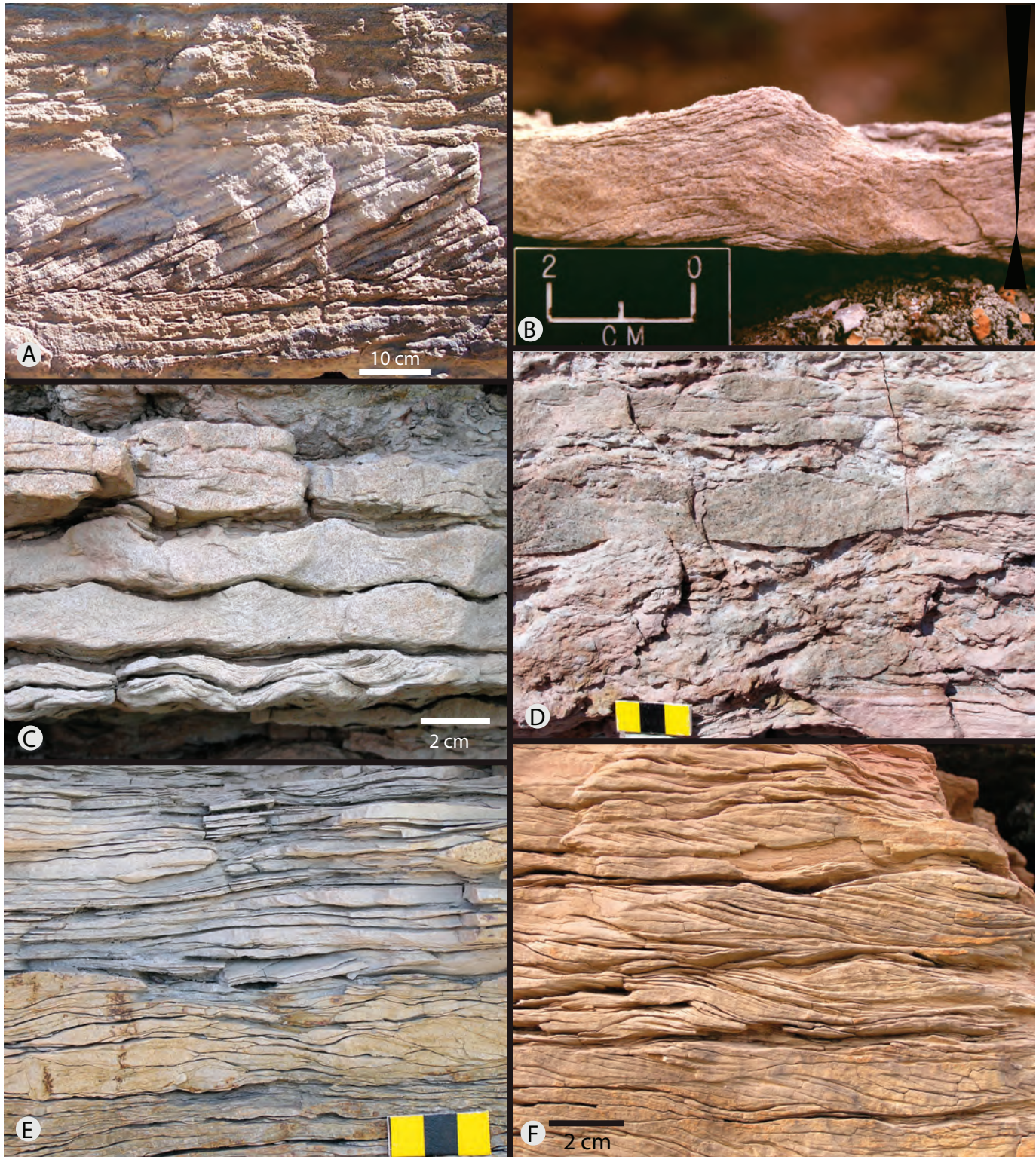
Figure 10. Tidal flat facies: sedimentary structures. (A) Subtidal sandstone exhibiting low-angle ripple bedding and medium-scale cross-stratification with mud drapes. Spring Creek Coulee (SCC). (B) Wave-ripple cross-laminated bed. Ming Coulee (MC). (C) Wavy bedding consisting of rhythmic, bioturbated and non-bioturbated, wave-rippled beds and intervening mudstone laminations. Fisher–Fields road intersection. (D) Heavily bioturbated, wave-rippled tidal bedding. Smith River (SR). (E) Rhythmic wavy bedding, some containing mud-draped current-ripple foresets. (F) Flaser bedded sandstone. Unidirectional ripple foresets with mud drapes reflect strong time-velocity asymmetry. Fisher–Fields road intersection.
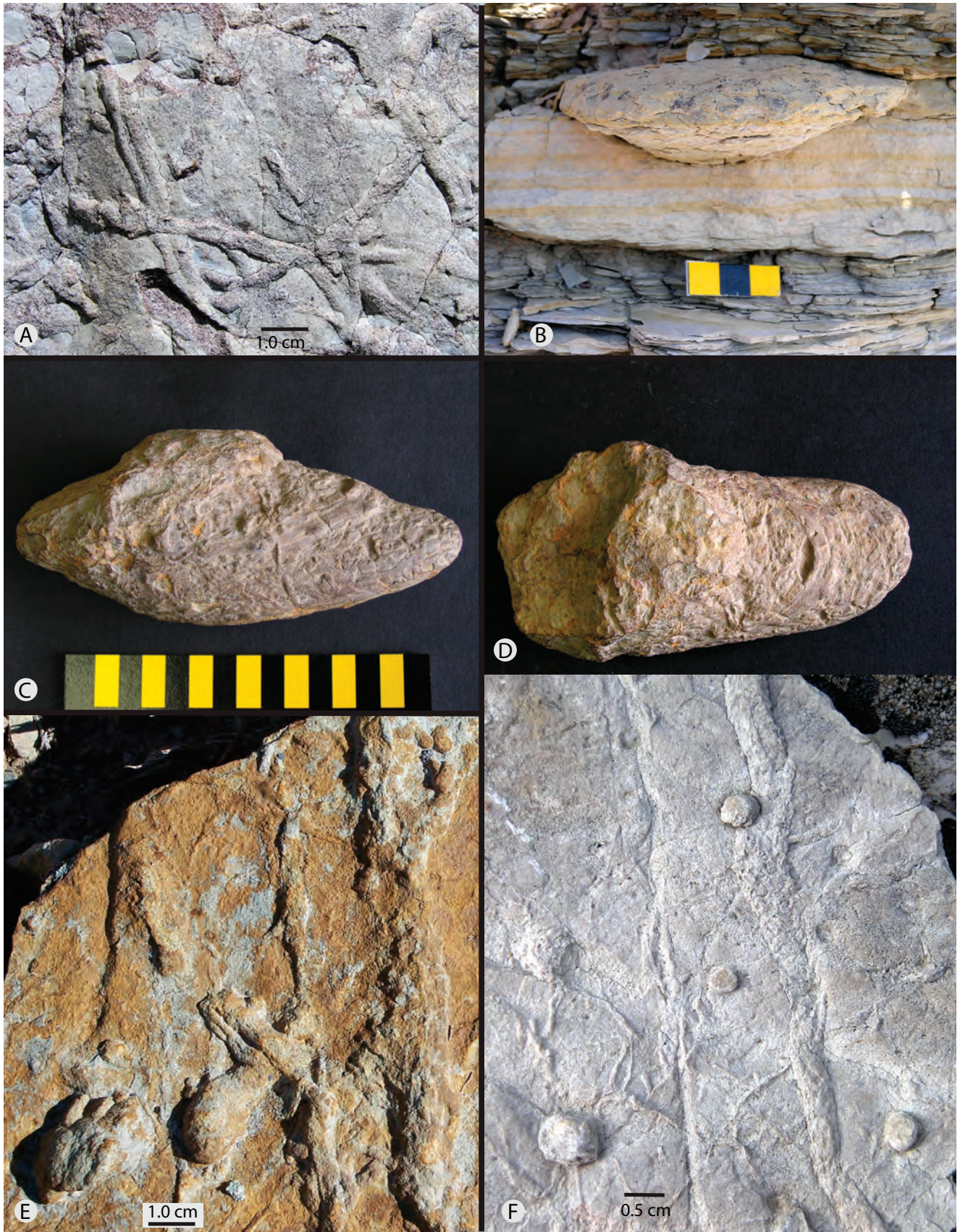
Figure 11. Tidal flat facies: ichnofossils found in association with wave-ripple and flaser bedding. (A) *Psammichnites* on bottom of sandstone bed (transverse ridges poorly preserved). Belt road cut. (B) Arthropod burrow, end view. Scale 3 cm. Fisher–Fields road intersection. (C) Arthropod burrow, side view. Scale 15 cm. Fisher–Fields road intersection. (D) Arthropod burrow, top view of C. (E) *Spongliomorpha*. Spring Creek Coulee. (F) Horizontal and vertical cylindrical burrows with scratch-mark ornamentation; possibly *Spongliomorpha*. Smith River.
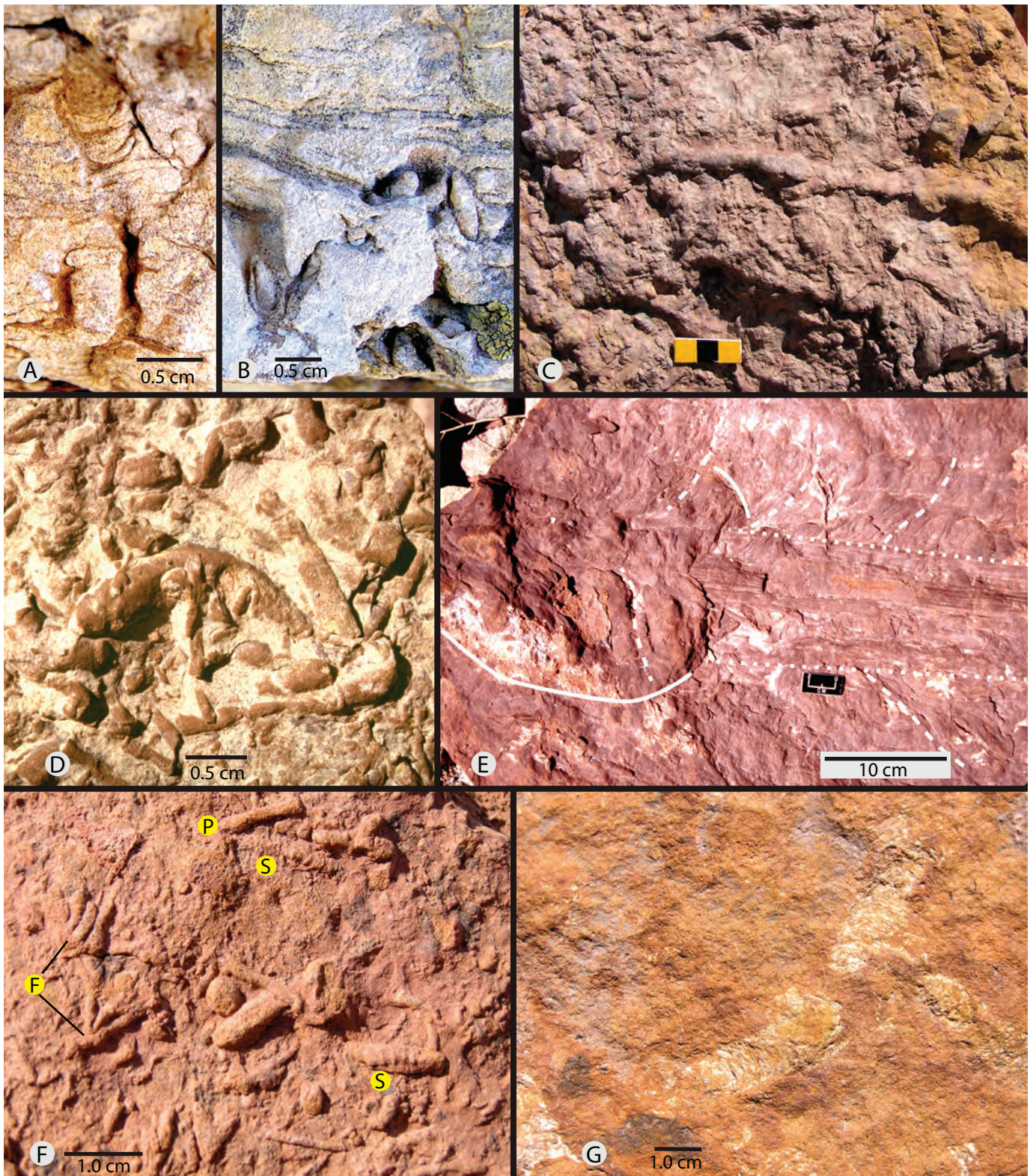
Figure 12. Tidal flat facies. (A and B) Ichnofossils found in association with wave-ripple and flaser bedding; (C through G) ichnofossils in tidal beds at the facies transition between subaqueous tidal beds of the Great Falls member and red continental deposits of Kk4, stained by overlying deposits. (A) *Teichichnus*. Ryan Island (RI). (B) *Cylindrichnus*. (C) Probable earthworm tunnels and pellets. Scale 3 cm. Raynesford (R). (D) *Planolites*. (E) Horseshoe crab-like crawling-to-resting trace. A trailing zone of spine and telson drag marks are present between the subhorizontal dotted lines, leg scratches are parallel to the oblique dashed lines, and carapace margin is indicated by the solid line. Fisher–Fields road intersection. (F) P, *Planolites*, S, *Steinichnus*, and F, *Fuersichnus*. (G) *Naktodemasis*. Belt road cut.
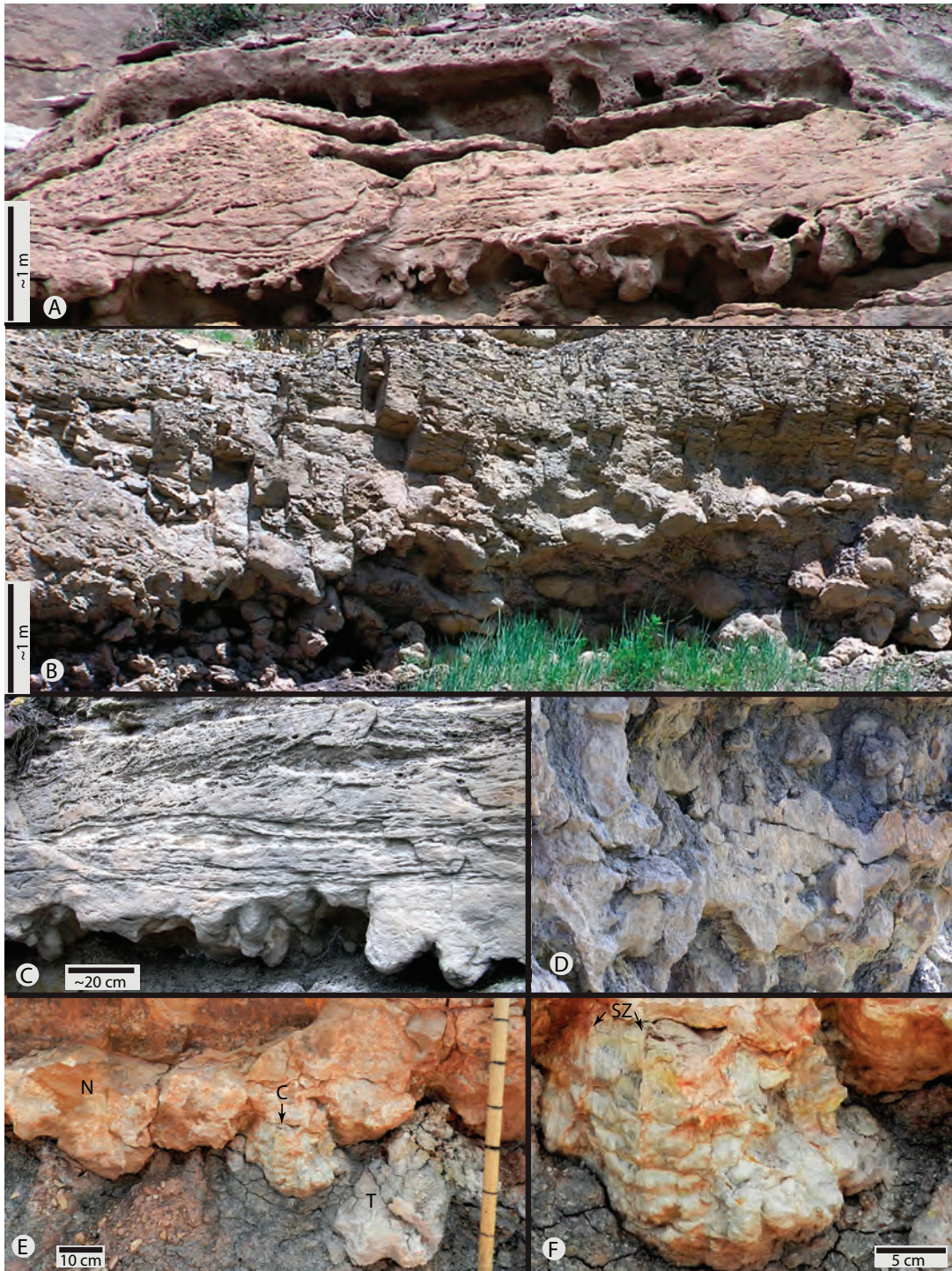
Figure 13. Tidal flat and tidal channel facies: dinosaur tracks. (A) Deeply penetrative under-surface tracks along the base of tidal flat units in the lowermost and uppermost parts of the photo (after Englemann and Hasiotis, 1999; Jennings and others, 2006; Milàn and Bromley, 2006; Platt and Hasiotis, 2006; Jackson and others, 2009). The beds in the middle of the photo contain well-defined tidal structures as well as dinosaur tracks and biodeformation features. The beds with dinosaur tracks are commonly completely bioturbated due to fluidization and mixing from trampling. Ryan Dam power plant cliff (RDP). (B) Pervasive bulbous tracks and biodeformation in the lower part of a tidal creek sandstone unit (~2.8 m thick). Belt road cut. (C) Close-up of lower tidal flat unit shown in A. The unit consists of a completely bioturbated (homogeneous) basal bed containing fully penetrative dinosaur tracks and an amalgamated overlying bed containing trough and bimodal-bipolar cross-stratification. (D) Oblique view of dinosaur tracks and biodeformed bedding along base of tidal channel fill shown in figure 14C. (E) Dinosaur tracks extending below a tidal flat unit including three-lobed track (T) with rounded tips as in ornithopods, multilobed track with internal columns (C), and nondescript bulges (N). Armington Junction south (AJs). (F) Closeup of track in E showing vertical columns bound by smooth, fine-grained, shear-zone walls (SZ) most likely caused by toe or claw penetration.
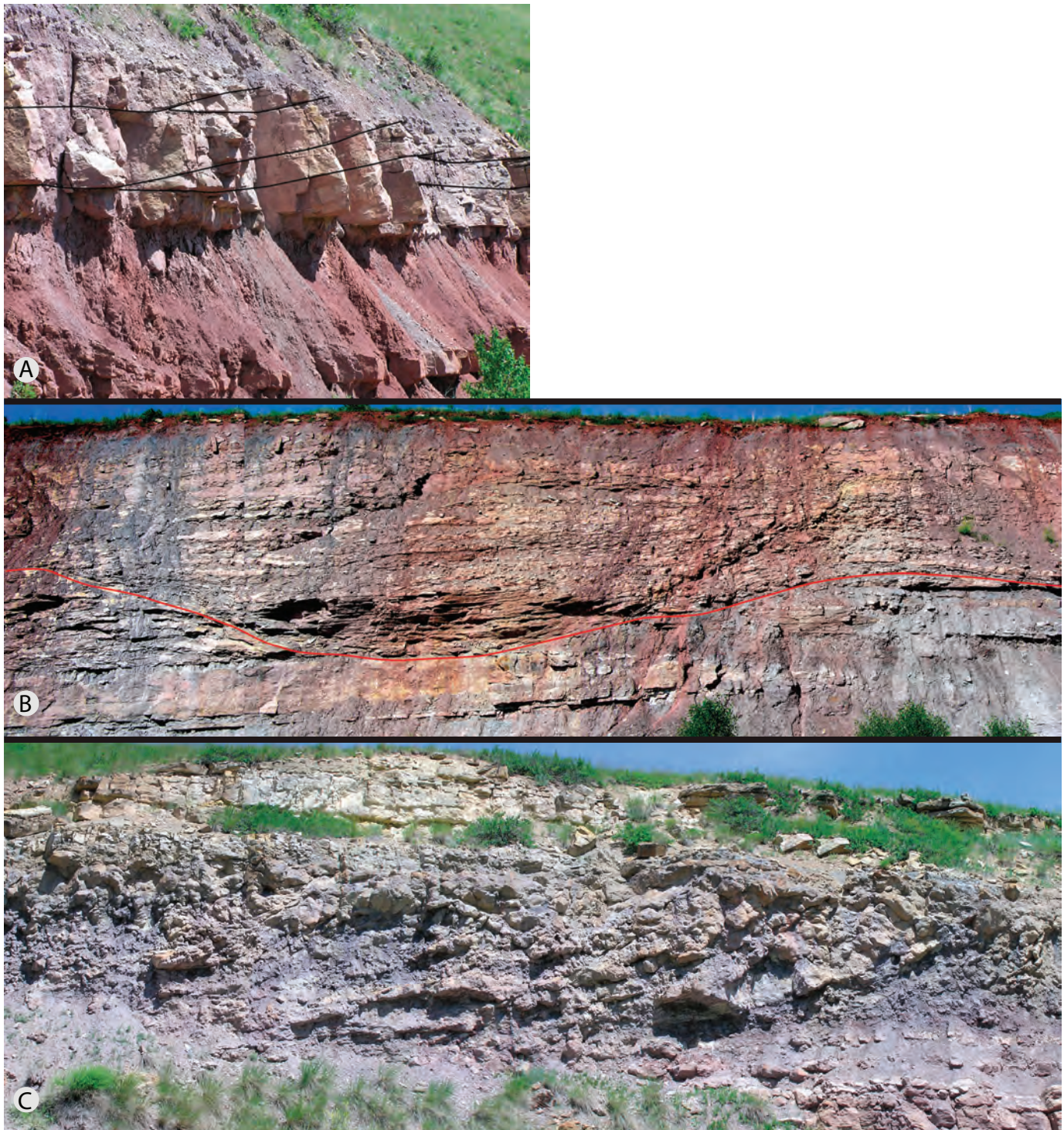
Figure 14. Tidal flat associated channel facies. (A) Quartzose channel body (L8) within a tabular, subhorizontally bedded, tidal flat unit. Unit thickness 2.7 m. Belt road cut. (B) Channel-shaped erosional surface (red line) marks tidal creek incision into underlying heterolithic tidal flat facies (L9). Similar facies above the erosional surface document resumed tidal flat sedimentation. Smith River. (C) Inclined heterolithic channel fill (3.4 m thick; L9) with disrupted bedding primarily due to dinosaur foot compression and penetration (see fig. 13D). Belt road cut.
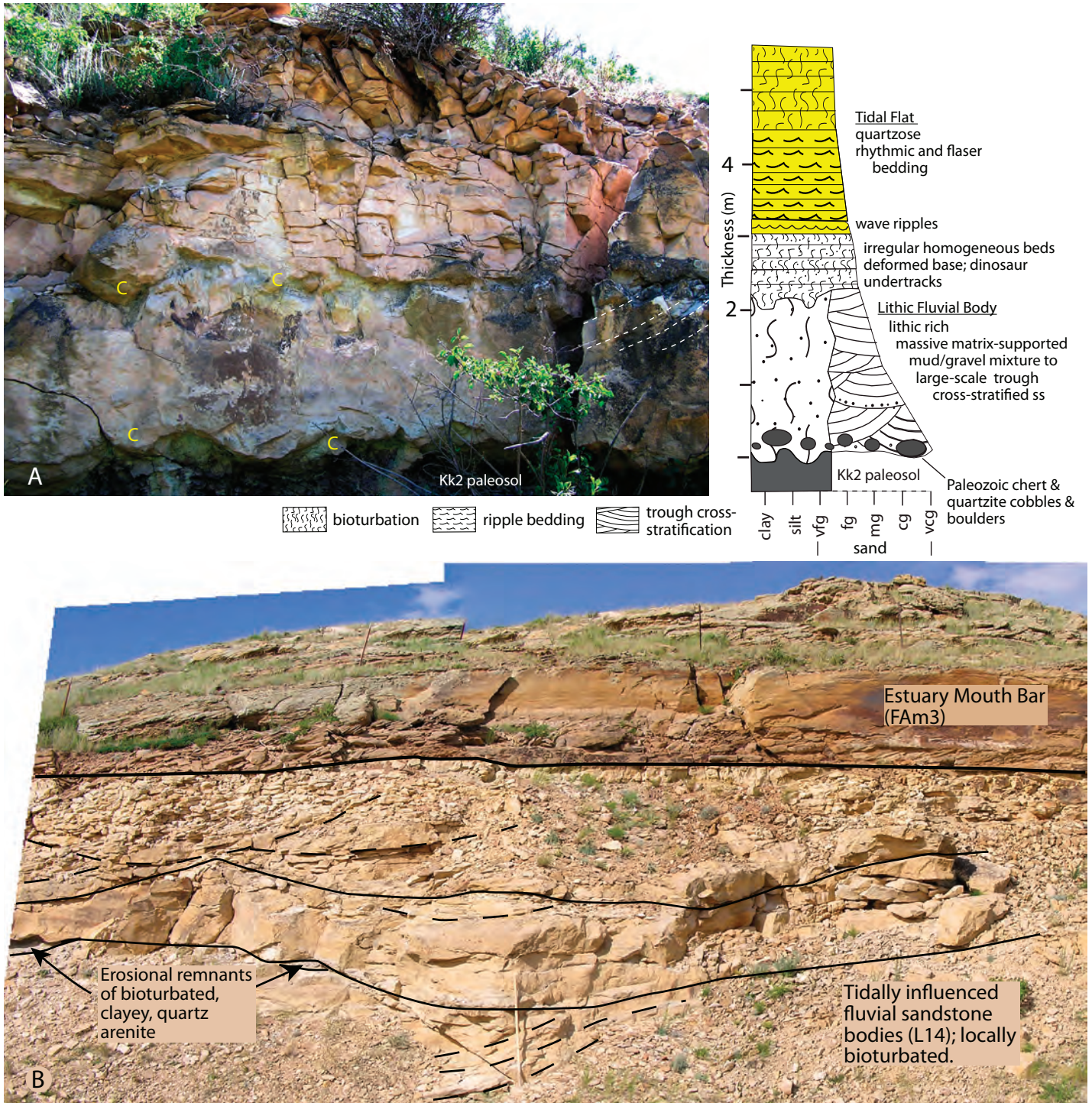
Figure 15. Tidally influenced fluvial deposits. (A) Heavily bioturbated lithic-rich channel body (L14) capped by quartzose tidal flat deposits (L1) near the zero edge of Great Falls deposition in the Raynesford area. Structural overprinting and fabric disruption is most likely due to dinosaur trampling as indicated by undertrack load casts (c) along the soles of the pictured units. Relict large-scale trough cross-stratification indicated by dashed lines. Raynesford. (B) Locally bioturbated, lithic-rich, channel bodies (L14) capped by isolated erosional remnants of clayey, bioturbated, quartz arenite; disconformably overlain by the estuary mouth bar facies. Abundant clay matrix within the lithic and quartzose sandstone is similar to light gray kaolinitic mudstone in L17. Relict large-scale trough cross-stratification indicated by dashed lines. Staff scale 1.5 m. Centerville road cut (CR).

The L13 channel bodies (tens of meters wide, less than several meters thick) are largely to entirely composed of mudstone, and are laterally associated with abundant mudstone-dominated L1 units.

Lithic-rich channel bodies (L14) are typically located along the depositional zero-edge of the basin where maroon nonmarine coastal plain mudstone (Walker, 1974) of the Kk2 and Kk4 underlie and overlie the channel bodies and associated L1 deposits, respectively (fig. 15A). In another case, L14 bodies are erosionally overlain by estuary mouth bar (FAm3) deposits (fig. 15B). The L14 bodies are distinctly different in texture, composition, and organization than the other channel bodies. They are characterized by an upward fining succession (<3 m thick) of conglomeratic coarse- to medium-grained, angular, lithic-rich sandstone that undergoes an upward transition into thin, quartzose L1 deposits (figs. 7C, 15). Depending upon location, the sandstone contains exceptionally abundant gray mud matrix that is similar in appearance to later-described estuary-basin mudstone (L17). Large-scale trough cross-stratification is locally present. In one case, the sandstone is massive, showing a mixed mud–gravel fabric with bulbous dinosaur undertracks, similar to those in L16 and L21, along the base of the body (fig. 15A).

Depositional Processes and Environment

Tidal flat facies (tabular units). The tabular geometry, bedding, and internal sedimentary structures of L1 are consistent with deposition over flat or gently sloping surfaces under mixed tractive current and suspension fall-out conditions coupled with a minor degree of wave influence (e.g., Reineck and Wunderlich, 1968; Weimer and others, 1982; Nio and Yang, 1991; Dalrymple, 2010). The sandstone-dominated units represent relatively high-energy, subtidal to intertidal sand flat to intertidal mixed-flat settings. Basal scour reflects the presence of strong tidal currents along the outer edge of sand flat settings such as those associated with modern estuaries (Dalrymple, 2010). The upward fining L1 units that cap the Great Falls member make up the most convincing case for progradation of laterally adjacent subtidal (sand), intertidal (mixed sand/mud), and supratidal (mud) settings, consistent with models based upon modern tide-dominated estuaries and open coasts (e.g., Dalrymple, 2010; Dalrymple and others, 2012; Daidu and others, 2013). Support for this includes superposition by the nonmarine Kk4 deposits and the presence of terrestrial trace fossils (see below) in the reddish L1 units. In other upward fining cases, the physical and biogenic evidence for an intertidal/supratidal interpretation is not as clear. In those cases, as well as the upward coarsening cases, the textural trends fundamentally represent the stacking of cross-shore textural fining and coarsening trends. Daidu and others (2013) report that in modern, smooth, open-coast tidal flats, textural fining and similar bedding can occur both landward and seaward (deeper) from the sandy upper-subtidal/lower-intertidal zone. Although somewhat moot to our overall interpretation of a tidal flat setting, both upward fining and upward coarsening trends could result from both progradation (Daidu and others, 2013; their fig. 9) or, assuming preservation, from transgression.

Many of the invertebrate ichnofauna indicate a range of marine to brackish environments. However, the absence of a typical marine assemblage, presence of facies-crossing forms, and similarity to Cretaceous brackish water associations (MacEachern and Gingras, 2007; Gingras and MacEachern, 2012), as well as ostracods in associated limestone, suggest physiologically stressed environmental conditions. Moreover, horseshoe crab traces are typically found in facies that represent shallow to very shallow marine to brackish conditions in tidal flat, lagoonal, and estuarine settings (Miller, 1982; Babcock and others, 1995; Rudkin and Young, 2009). The *Fuersichnus, Naktodemasis, Steinichnus, Taenidium*, earthworm, and beetle-larvae burrows make up an assemblage that most likely reflects faunal activity in emergent tidal flats subject to freshwater influx from a nonmarine coastal plain (Buatois and others, 1997; Smith and others, 2008), supported in this case by the superposition of reddish Kk4 nonmarine siltstone and mudstone (Walker, 1974). Correspondingly, the morphology and penetrative nature of the dinosaur tracks record activity on relatively vegetation-free, moist, uncompacted sediments as would occur in a tidal flat-coastal plain margin setting (Platt and Hasiotis, 2006; Laporte and Behrensmeyer, 1980). Overall, the combined ichnofauna, coupled with the sedimentologic data for L1, are most consistent with variable salinity conditions in a tidal flat setting.

Tidal channel and tidally influenced channel facies. Properties of the channel bodies are consistent with those described for modern and ancient tidal flat regions of tide-dominated estuaries and embayments (e.g., Clifton, 1982; Santos and Rossetti, 2006; Hughes, 2012). With the exception of the muddy, lithic-rich channel bodies (L14), the similarities between lithology of the quartzose channel bodies and their tidal flat host rocks clearly reflects tidal flat linkage. Clifton (1982) notes that two scales of tidal channels exist in modern tidal flat settings: (1) small-scale erosional gullies and run-off channels that are perched atop tidal flats and aggrade to approximately the lowest low tide level, and (2) channels that extend well below lowest low tide level. Both types occur in either sandy or muddy settings.

Based upon their occurrence within a single tabular sandstone unit, the L8 channel bodies most reasonably represent runoff channels across a sandy tidal flat. The L9 and L13 channel bodies (truncating multiple units) represent deeper channels in mud flat or mixed mud and sand tidal flat areas (Clifton, 1982; Boyd and others, 2006). The heterolithic bedding and quartzose composition within type L9 channel bodies reflect alternating tractive and non-tractive tidal flow (suspension fallout) with a supply of flood-current transported sand from seaward locations (Clifton, 1982; Dalrymple and others, 1990, 2012; Boyd and others, 2006) or tidal creek reworking of remnant marine sand from higher stand deposits (Frey and Howard, 1986). The upward fining, symmetric-heterolithic units are most reasonably related to the filling of symmetric, straight channel segments, such as can occur in the headward zone of a tide-dominated estuary (Dalrymple and others, 2012), whereas the upward coarsening, inclined heterolithic succession represents sandy point bar accretion (e.g., Hughes, 2012) into a sinuous mud-dominated channel tract.

The lithic-rich channel bodies are a product of base-level rise, fluvial aggradation, and tidal flat development within small paleovalleys along the transient estuary margin, similar to modern systems described by Boyd and others (2006). The exceptionally high abundance of mud matrix most likely reflects high concentrations of suspended mud as occur in upper estuary channels associated with turbidity maxima at the juncture of salinity intrusion

and net seaward flow (Harleman and Ippen, 1969; Allen, 1991). Dinosaur trampling and foot penetration through the fluvial deposits resulted in pervasive bioturbation and structural overprinting.

FAm2: Tide-Dominated Shoreface

FAm2 consists of widespread, typically upward coarsening, sandstone-dominated tabular units (L2; fig. 16, supplementary fig. 1[1]) and scattered hetero-lithic channel bodies (L10; fig. 17) that truncate the tabular units. Excellent exposures up to 12 m thick are present along the Missouri River in the northeastern part of the study area below Morony Dam (MD sites) and to the south at the Belt railroad cut (BRR). Else-where, scattered exposures indicate southward narrowing and thinning parallel to the basin margin.

Lithologic Description

Tabular units (L2). The tabular units occur as several types of bed successions. Most commonly, they are an upward coarsening succession (~2 m thick) of basal mudstone and/or thin heterolithic beds of very fine-grained sandstone and mudstone that grade into thicker-bedded (~0.3–1.0 m), amalgamated, fine-grained or, rarely, medium-grained sandstone with an erosional cap (figs. 16, 18). They may also occur as amalgamated, erosionally bound, sandstone beds of uniform grain size. In some cases, an upward fining succession overlies an upward coarsening succession. As many as five upward coarsening units disconformably overlie nonmarine Kk2 deposits near Morony Dam (fig. 16, supplementary fig. 1).

Sandstone composition is generally >90% quartz; however, the basal disconformity is commonly marked by lithic-rich sandstone or rip-up clast conglomerate, locally containing limestone pebbles derived from the underlying nonmarine Kk2 member. Elsewhere, the basal unit may be mudstone-dominated and rhythmic mud–sandstone couplets (figs. 16, 18). Bedding is sub-horizontal to very low angle and rhythmic, although localized bar-scale (dm wavelength) convex-up bedding may be present (supplementary fig. 1). Lenticular, flaser, and wavy bedding, including bimodal-bipolar ripple forests, are abundant (fig. 19). Bedsets include amalgamated ripple bedding with intervening

[1]Supplementary figures 1–4. These are four photographs showing panoramas of Great Falls member facies and the lower Kootenai Formation, available for download from the M69 page of our website.
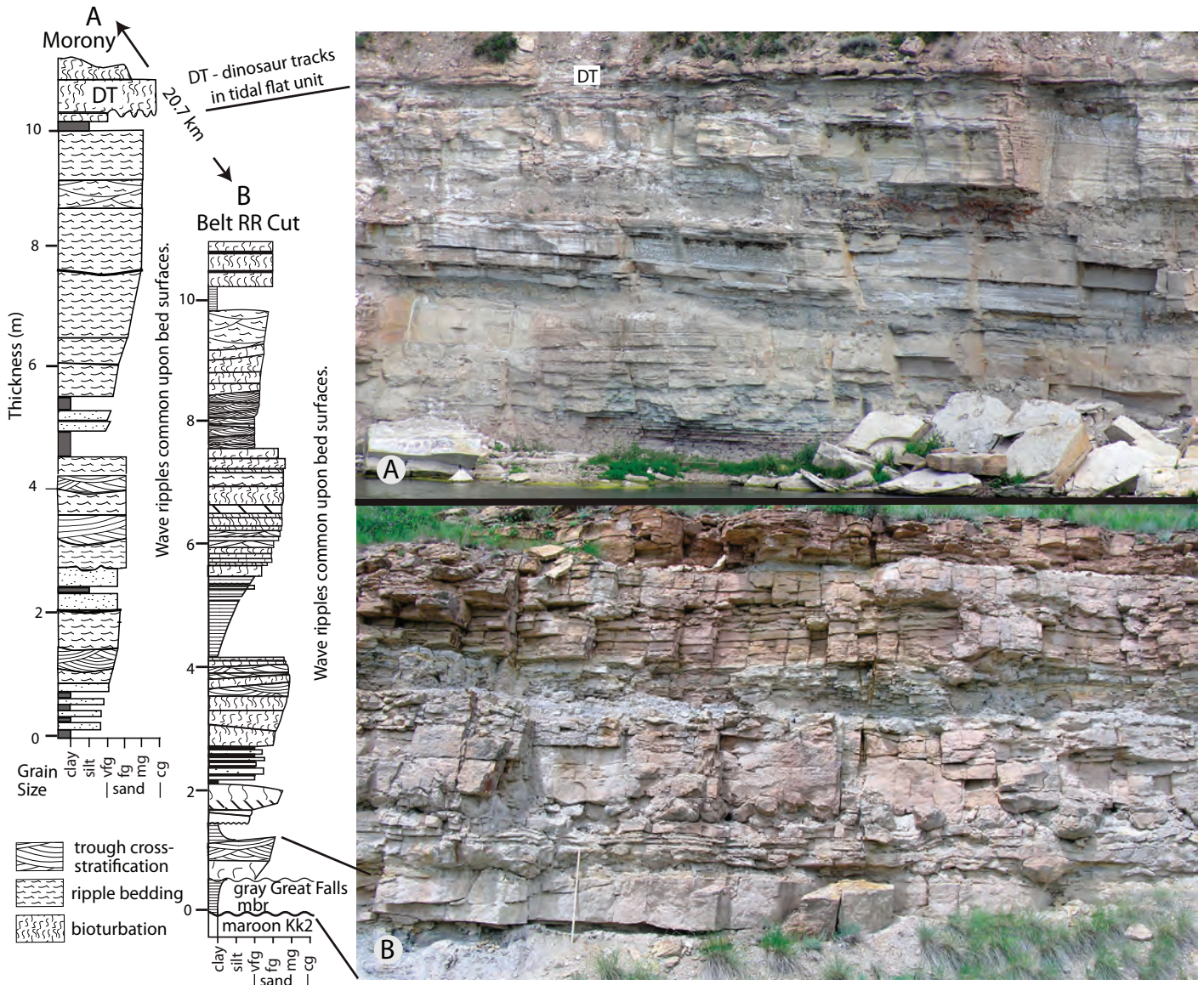
Figure 16. Tide-dominated shoreface facies (L2): measured sections and overview photos. (A) Stacked, tabular, upward-coarsening shoreface units near Morony Dam along the south bank of the Missouri River (MDs1). Dinosaur trampled tidal flat unit (DT) overlying the uppermost shoreface unit. (B) Stacked, tabular, upward-coarsening tabular shoreface units at Belt railroad cut (BRR). Staff 1.5 m.

reactivation surfaces and rhythmically alternating ripple beds and parallel laminations. Millimeter-scale clay drapes are common between parallel laminations, within current and wave ripple cross-lamination sets, and within lateral sequences of small-scale ripple bundles. Lateral successions of larger scale ripple bundles also occur, but are less common (fig. 20). Wave-rippled bed surfaces are common. Scattered, small (1–15 m wide), erosionally based, concave lenses of trough cross-stratified sandstone are locally present within the sandstone-dominated units (fig. 19A). Hummocky and swaley cross-stratification is very rare (fig. 20). Current-ripple foresets range from unimodal to bimodal-bipolar (fig. 9).

Trace fossil abundance in FAm2 is much greater than in FAm1 (tidal flat deposits). In general, there is a mixture of horizontal and vertical assemblages with numerous unidentified feeding traces especially common along bedding planes. In addition to a general bioturbation fabric, ichnofossils include *Arenicolites, Ophiomorpha* (very rare), *Macaronichnus, Planolites, Piscichnus,* possible *Treptichnus*, horseshoe crab-like resting traces, bivalve crawling traces (*Protovirgularia?*), possible shore-crab burrows (figs. 21–23), and rare occurrences of possible *Taenidium* or *Naktodemasis* (fig. 23). At Morony Dam, penetrative dinosaur tracks within FAm1 cap the FAm2 succession (figs. 16A, 20C, supplementary fig. 1).
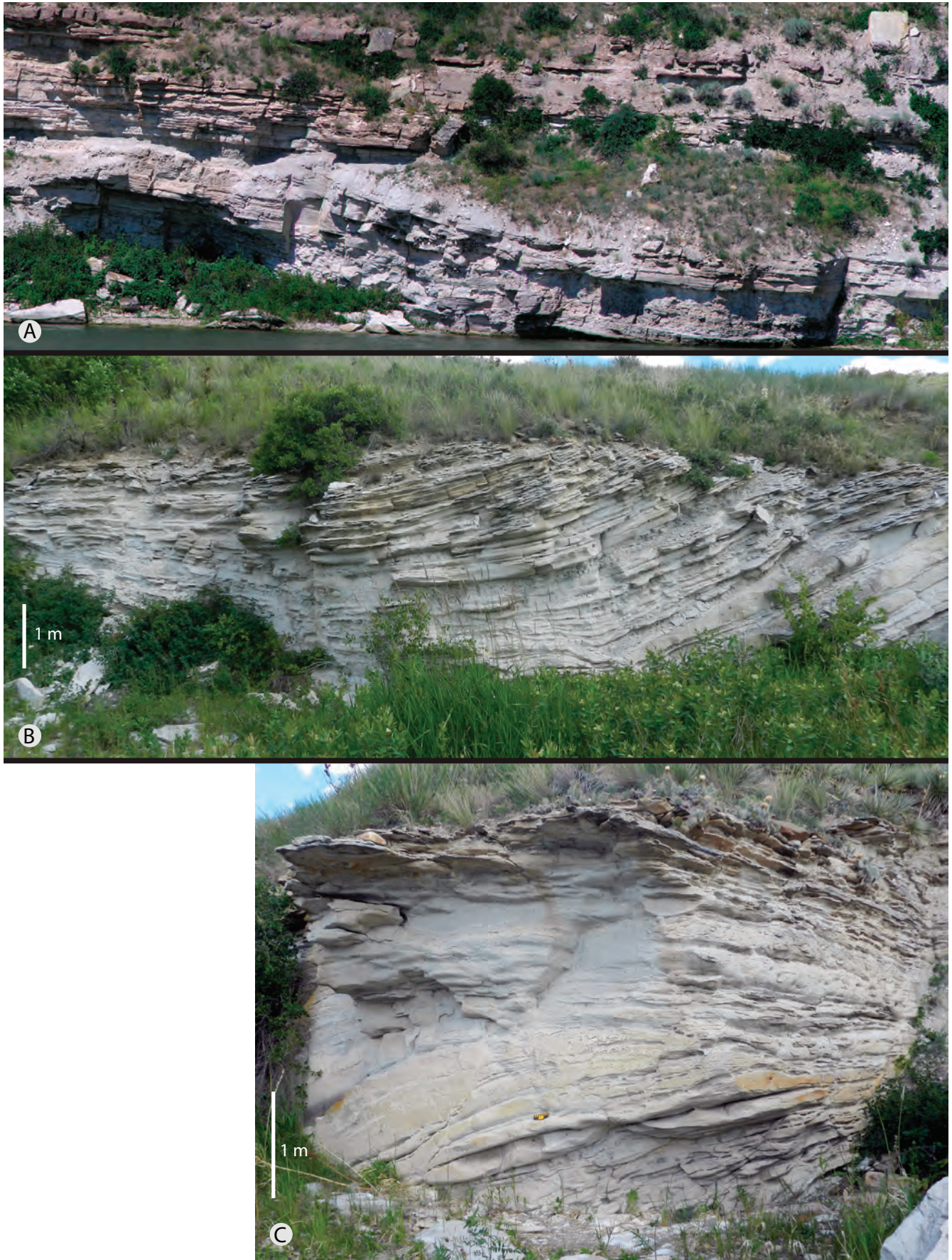
Figure 17. Channel bodies (L10) transecting tabular tidal shoreface units. (A) Large shore-zone channel body encased by tabular shoreface units along the north bank of the Missouri River near Morony Dam (MDn). (B and C) Close-up views of the sandstone body in A, but located along the south bank of the river (MDs2).
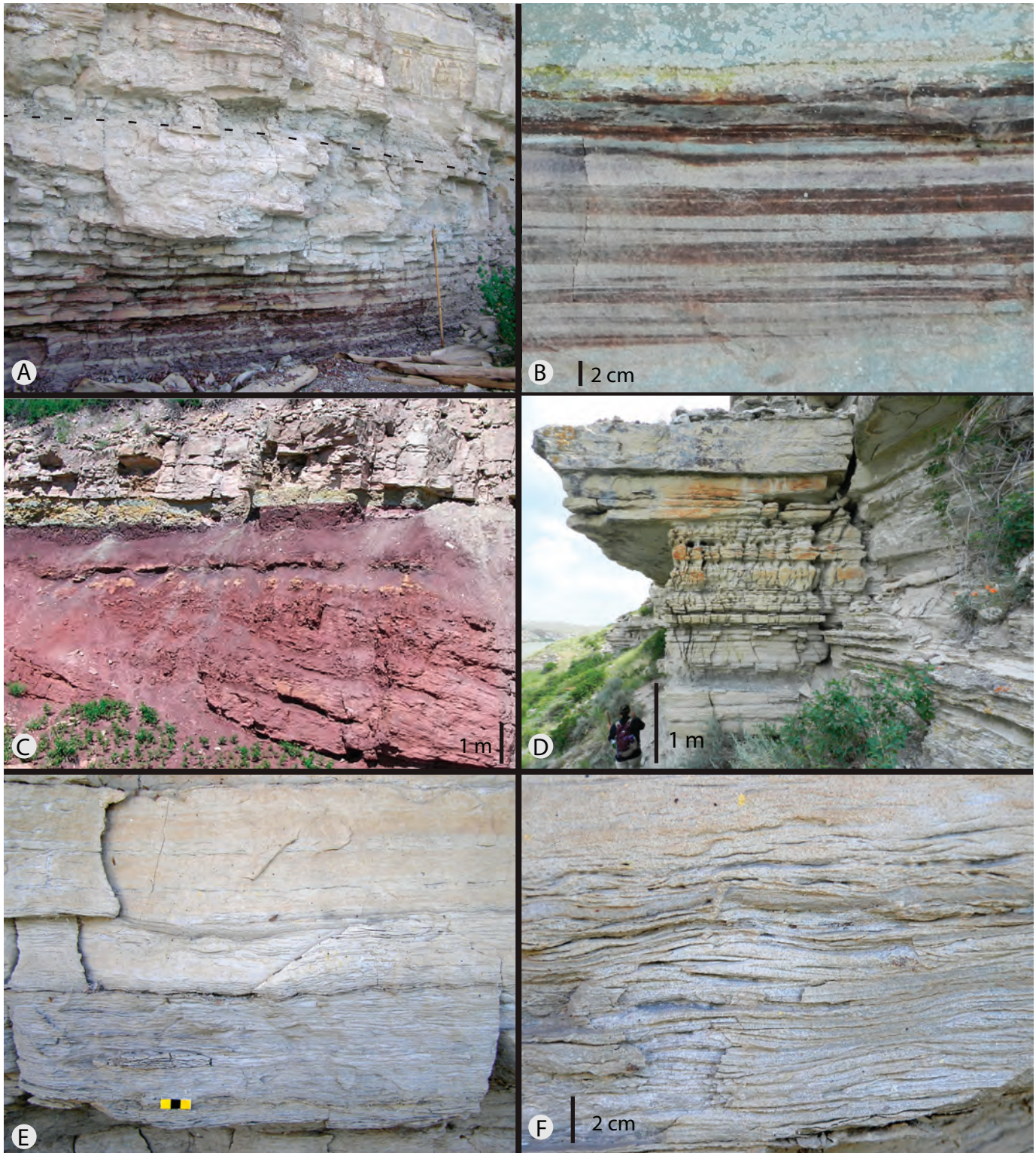
Figure 18. Tide-dominated tabular shoreface facies (L2): bedding and sedimentary structures. (A) Close-up of two stacked upward-coarsening units, separated by an erosional surface (dashed line), at the base of the entire tidal shoreface succession. The basal unit contains red mudstone reworked from non-marine facies of the underlying Kootenai Formation (Kk2). Staff 1.5 m. Morony Dam south. (B) Close up of rhythmic mud–sand couplets in base of photo A, indicative of alternating suspension fallout and tractive flow. (C) Base of the shoreface succession at Belt railroad cut overlying a disconformable ravinement surface above gray estuarine mudstone and a lowstand erosional-surface disconformity that overlies nonmarine, maroon paleosol and fluvial body in the Kk2. (D) Well-developed upward-coarsening ripple-bedded unit. Morony Dam south. (E) Lower part of an upward-coarsening, ripple-bedded unit showing a transition from wavy to flaser bedding. Morony Dam south. Scale 3 cm. (F) Close-up of wavy to flaser bedding in base of D.

Figure 19. Tide-dominated shoreface facies (L2): sedimentary structures. Morony Dam south 1. (A) Tabular and wedge-shaped beds made up of ripple-bedded laminations. Relatively rare trough cross-stratification can also be ripple laminated (lower right). (B, C, D, and E) Various styles of tidally influenced ripple bedding: (B) Wavy bedding consisting of mixed current- and wave-ripple laminations. Wave-ripple bedforms commonly cap current-dominated ripple-bedded units. (C) Flaser bedding consisting of small-scale trough cross-stratification with mm-scale mud drapes. (D) Slightly to heavily bioturbated (top) current-ripple bedding showing bipolar foresets. Current-ripple units are commonly capped by thin undulatory laminations that most likely represent wave reworking during slack water as commonly observed in modern settings. (E) Upward- and downward-inclined sets of small-scale, current-ripple foresets documenting bipolar flow and ripple migration both up and down the slopes of large-scale bedforms.
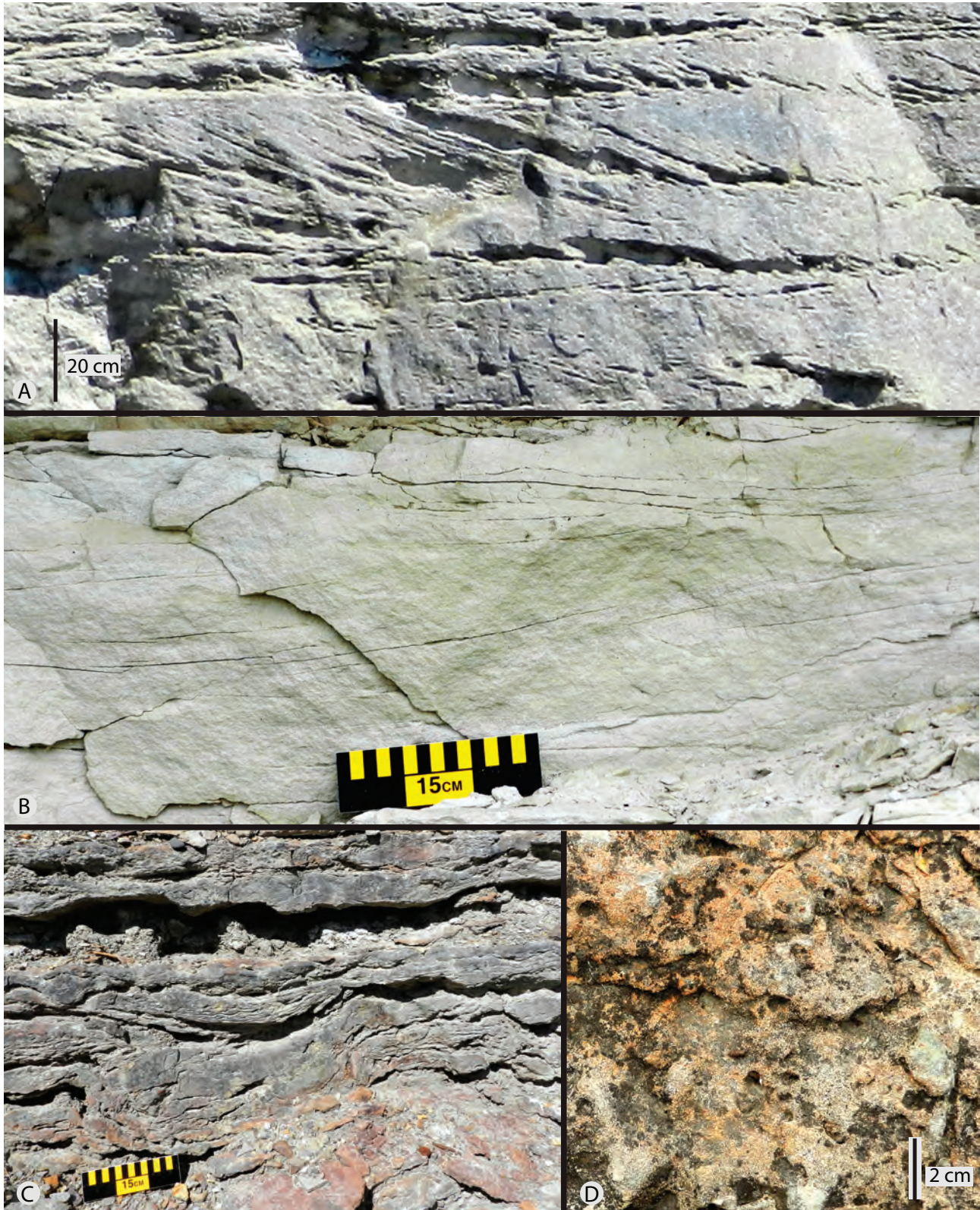
Figure 20. Tide-dominated shoreface facies (L2): sedimentary structures. Morony Dam south 1. (A) Stacked tabular beds containing lateral successions of tidal ripple bundles. (B) Trough or possible swaley cross-stratification. (C) Oxidized, bioturbated, and possibly dinosaur-deformed ripple-bedded sandstone and mudstone firm-ground unit overlying the uppermost shoreface unit, and underlying Kk4 coastal plain facies (not shown). (D) Close up of heavily bioturbated zone (*Glossifungites* ichnofacies?) in the same unit as shown in C.
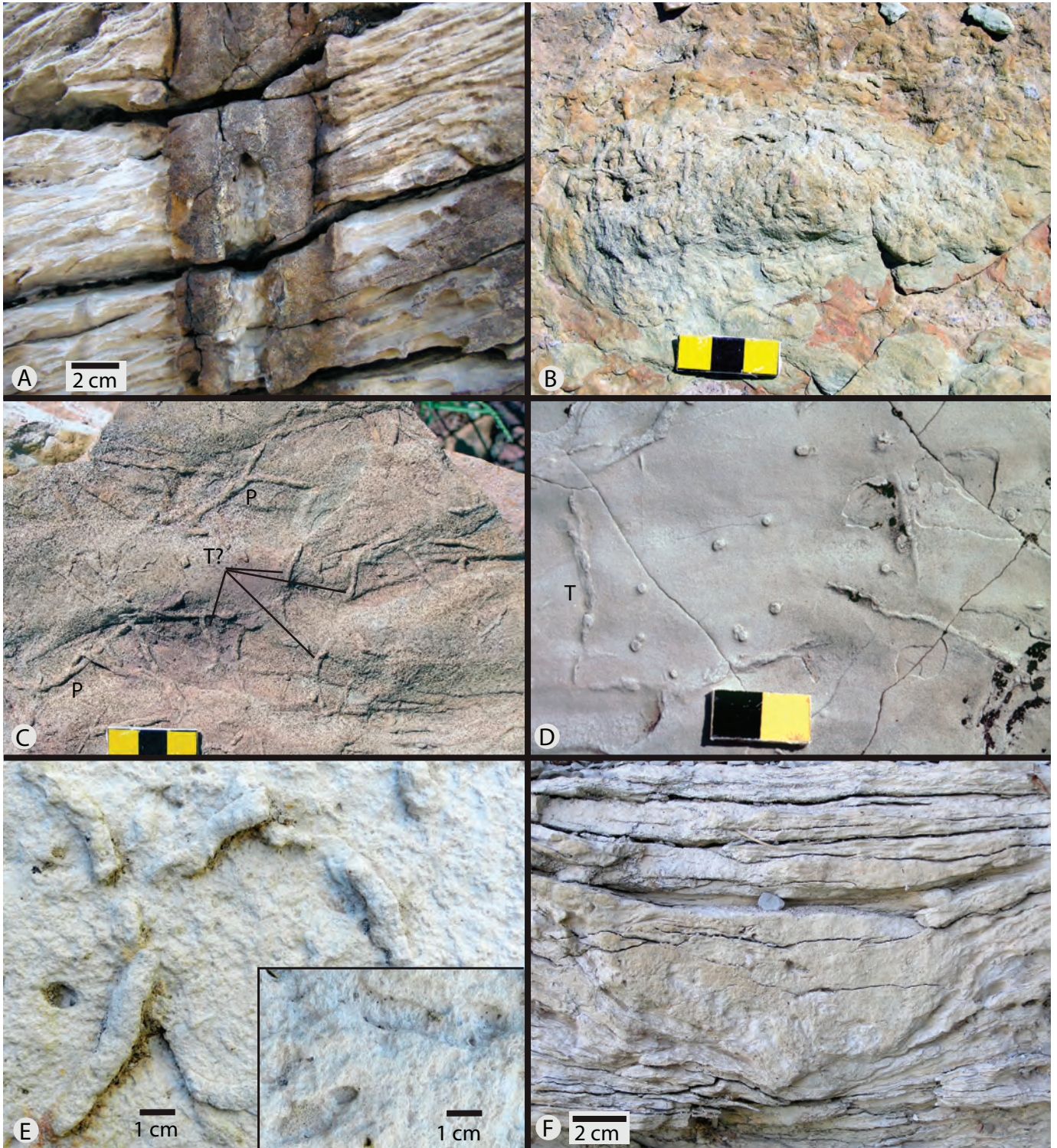
Figure 21. Tide-dominated shoreface facies (L2): ichnofossils. (A) Large diameter vertical shaft, most likely a hematized *Ophiomorpha* burrow. Clayey pelletal lining is present in adjacent, poorly preserved, non-oxidized 1-m-long shafts. Ace Missile (AM). (B) Positive hyporelief of shallow burrow—most likely horseshoe crab based upon wide crescentic impression (carapace margin) along left edge, taper in abdominal width toward right, and possible leg scratch marks along bottom edge of trace. Re-burrowed with *Macaronichnus*. Similar to trace shown in figure 11B. Scale 3 cm. Belt railroad cut (BRR). (C) *Planolites* (P) and possible *Treptichnus* (T) on wave ripples. Scale 3 cm. Morony Dam south 1. (D) Paired *Arenicolites* tubes and possible *Treptichnus* (T) on wave-rippled surface. Scale 2 cm. Morony Dam south 1. (E) *Planolites* and associated burrows with meniscate backfill (inset). Morony Dam south 1. (F) *Piscichnus* (ray feeding structure) similar to that of Howard and others (1977). Morony Dam south 1.
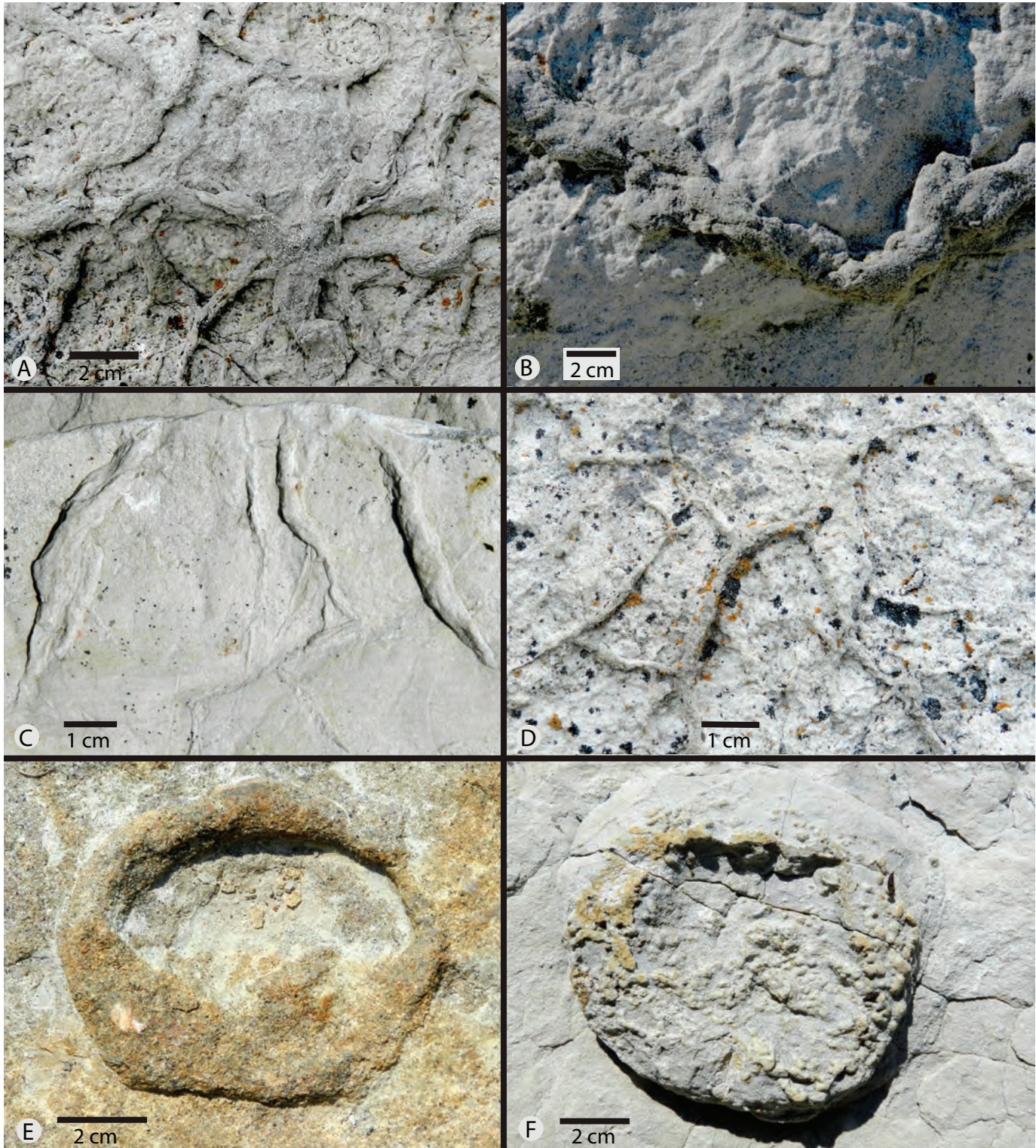
Figure 22. Tide-dominated shoreface facies (L2): ichnofossils. Morony Dam south 1. (A) Large unidentified burrow network following diastasis cracks, and small intervening *Planolites*. (B) Close up of "twisted rope" pattern characterizing the large burrow in A. (C) Discontinuous, emergent and declining, convex hyporelief traces of similar width and "twisted" pattern to those in A and B. (D) Small *Thalassinoides*. (E) Bowl-shaped epirelief of possible fish nest. The coarse, brown, depression floor, raised lip, and host sandstone underlie remnant siltstone, suggesting fish winnowing and stacking of coarser sand as in modern nests. (F) Similar to E and located adjacent to E, but with gray siltstone mantle; fill reburrowed with *Macaronichnus*. Extension of the coarser grained trace rim above the siltstone indicates a contemporaneous silty floor, fish winnowing down to the coarse layer, and subsequent polychaete burrowing of the post-nest fill.
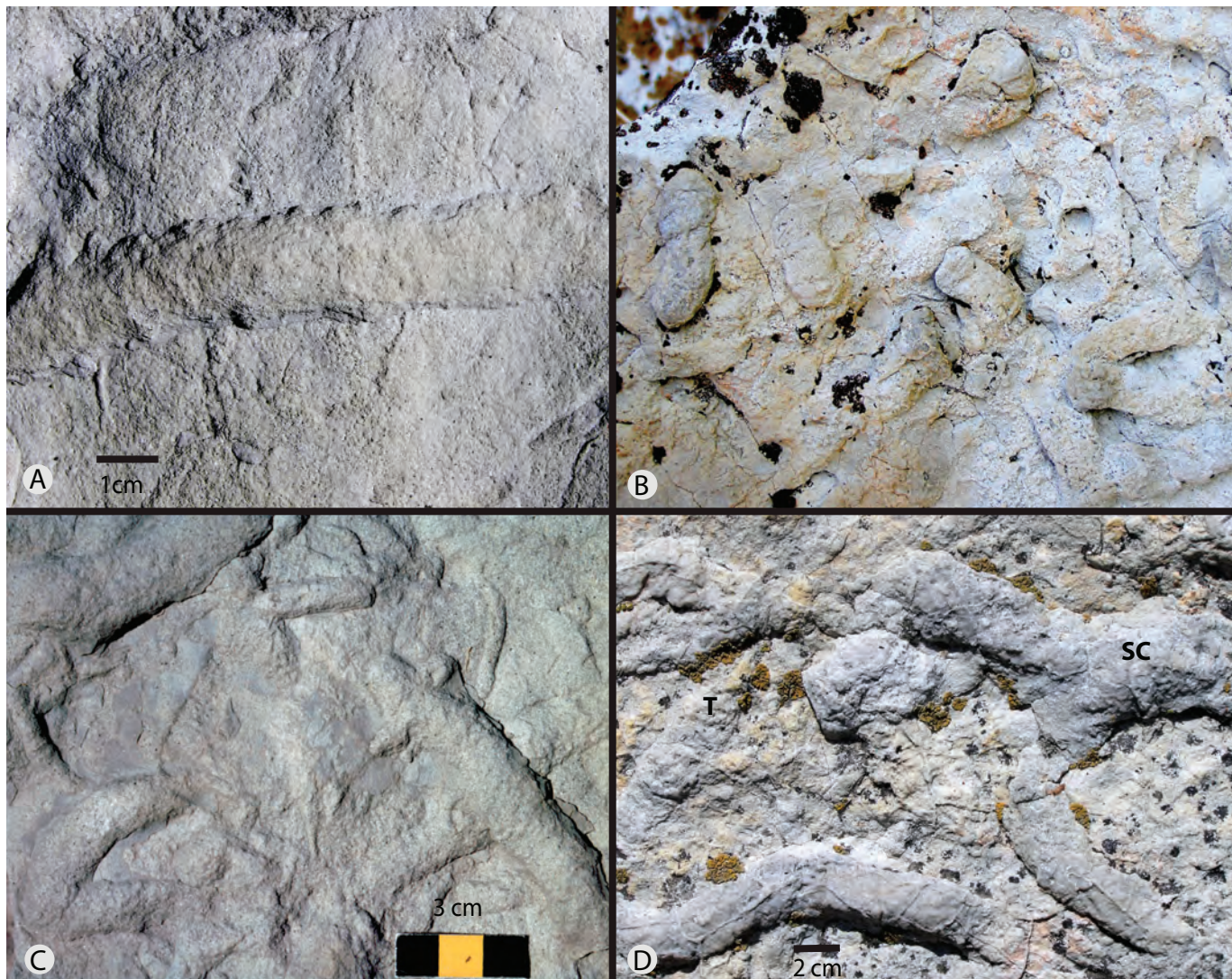
Figure 23. Tide-dominated shoreface facies (L2): ichnofossils. Morony Dam south 1. (A) Bivalve crawling trace, possibly *Protovirgularia* (Carmona and others, 2010). (B) *Taenidium* or possibly *Naktodemasis* with poorly exposed adhesive meniscate backfill (Smith and others, 2008). (C) Unidentified burrows with wall ornamentation. (D) Possible shore crab burrows (SC) and possible *Taenidium* (T).

Channel bodies (L10). At Morony Dam, relatively large (50 to >100 m wide, 5–10 m thick), heterolithic channel bodies are widely scattered within the facies assemblage and exhibit erosional boundaries that transect one or more of the tabular units (fig. 17). In one case (site MDn), multiple channel bodies are stacked vertically upon each other. The composition and texture of the sand fill matches that of adjacent tabular units.

Depositional Processes and Environment

Shoreface facies (tabular units). A tide-dominated, low wave-energy setting is indicated by the abundant rhythmic beds with tidal structures, abundant ripple bedding, lateral ripple-bundle successions, minor occurrence of wave ripple bedforms, wave ripple cross lamination, and paucity of hummocky/swaley cross-stratification (Dashtgard and others, 2009, 2012). The scattered small-scale lenses are consistent with tidal current scour-and-fill. Although tabular bed geometry reflects deposition upon a generally planar surface, the convex-up beds indicate accretion on low-relief bar forms. Rip-up clasts and increased lithic sand along the basal disconformity mark the reworking of underlying nonmarine Kootenai lithologies due to ravinement. The trace fossil suite consists of trophic generalists and facies-crossing forms and is indicative of a marginal marine setting, most likely brackish-dominated (Gingras and others, 2012). As in FAm1, *Taenidium* or *Naktodemasis* may indicate freshwater influence from an adjacent nonmarine setting (Buatois and others, 1997; Smith and others, 2008), again con-

sistent with the presence of nearby nonmarine coastal plain deposits as evidenced by the directly overlying Kk4 (Walker, 1974).

Upward coarsening successions containing wave-formed and tidal structures are typical of progradational shoreface deposits (Clifton, 2006; Dashtgard and others, 2009, 2012; Vakarelov and others, 2012) and progradational open-coast subtidal flats (Daidu and others, 2013, their fig. 9). However, they are also reported for modern transgressive back-barrier tidal flat settings (Flemming, 2012), ancient transgressive estuarine or back-barrier settings that overlie regressive shoreface deposits (Land, 1972; Devine, 1991; Steel and others, 2012), ancient tidally influenced delta fronts, distributary mouth bars, and bayhead delta deposits (Steel and others, 2012; Aschoff and others, 2016). In addition to sedimentologic properties of the Kootenai tabular units, constraints for interpreting the depositional setting include: (1) vertical confinement between a basal transgressive ravinement surface and capping Great Falls tidal flat-to-nonmarine Kk4 coastal plain deposits, (2) association with contemporaneous cross-cutting channels, and (3) lateral association with other tide-dominated estuarine facies (vs. deltaic deposits).

A low wave energy, tide-dominated shoreface setting is proposed for the tabular Great Falls units in L2. However, tide-dominated shoreface deposits are seldom reported for the rock record. This is partially due to only recently established sedimentological criteria for facies identification (Dashtgard and others, 2009, 2012; Frey and Dashtgard, 2012). These criteria, although based upon modern closed-coast settings containing appreciable medium sand to gravel, provide partial support for interpreting the tabular units as representing a tide-dominated shoreface (i.e., a "tide-influenced shoreface" of Dashtgard and others, 2012). Two low-wave energy, open-coast, tide-dominated sites that serve as more satisfactory analogues for the finer grained FAm2 assemblage include the Sapelo Island beach-nearshore zone along the Georgia coast of the United States and the intertidal to subtidal zone along the Nordergründe region of the North Sea. The two areas, although originally presented from shoreface (Sapelo) vs. tidal (Nordergründe) viewpoints, are recognized as having similar profile gradients, grain sizes, and subtidal depths (Reineck and Singh, 1980).

In addition, both areas contain shoreface tracts located between estuaries, wherein a low-gradient, primarily fine sand profile extends seaward and merges with a flatter inner shelf platform.

For comparison with the Great Falls deposits, the diagnostic properties of the Sapelo and Nordergründe shoreface regions are synthesized in appendix table 4 based upon work by Howard and Dorjes (1972), Howard and Reineck (1972), Wunderlich (1972), Reineck and Singh (1980), and Howard and Scott (1983). Hypothetical progradational successions (Reineck and Singh, 1980; parts of their figs. 473 and 496) for both the Nordergründe and Sapelo tidal shoreface regions show strong similarities to vertical trends of slight upward coarsening, such as in the Great Falls member, as well as abundant tidal structures, dominant ripple bedding and parallel laminations, relatively minor scattered trough cross-stratification, and variable amounts of bioturbation. Also important in the modern analogues is the seeming paucity of hummocky and swaley cross-stratification in contrast to the well-established wave-dominated shoreface models.

Overall, the Great Falls stacking patterns are interpreted to represent net shallowing through multiple progradational events. The capping iron-stained and dinosaur-trampled sandstone beds at the top of Morony Dam outcrops are consistent with tidal flat and firm-ground development due to emergence prior to coastal plain deposition of the overlying Kk4. The rare upward fining and erosionally truncated successions that overlie some of the Great Falls tabular units may indicate continued progradation of landward fining intertidal–supratidal sand or, alternatively, a transgressive (deepening) shift of seaward fining shoreface deposits.

Cross-shoreface tidal channel facies. Well-developed tidal channels transect the Nordergründe shoreface (Reineck and Singh, 1980), whereas smaller tidal creek-associated channels extend along shoals into the Sapelo shoreface (Howard and others, 1972). Although details are lacking for the Sapelo channels, the Nordergründe channels extend beyond wave base, erosionally truncate adjacent subtidal deposits, contain sediment and bedding types similar to the adjacent subtidal areas, and upon channel migration, are capped by subhorizontal sand sheets (Reineck and Singh,

1980). The physical attributes are similar to those of the Great Falls channel bodies, and the association of channel bodies and tabular units in the modern tide-dominated shoreface provides support for a similar setting for the Great Falls facies. The succession of stacked channel bodies within FAm2 indicates temporal persistence of a shoreface channel location presumably linked to a temporally persistent shoreward tidal channel.

FAm3: Estuary Mouth Bar

FAm3 is a NNE-elongate (10–15 km wide, >33 km long), upward fining, quartzose sandstone body (5–15 m) that is thickest along the axial zone of the estuary basin and thins toward the estuary basin margins (fig. 5). The eastward edge is fully exposed and in contact with tidal shoreface deposits (FAm2) along

the southern side of the Missouri River gorge between Ryan and Morony dams. To the north and northwest, the deposits extend into the subsurface beneath the Missouri River escarpment. Paleocurrent orientations range from unimodal (most commonly northeast or southwest) to bimodal-bipolar (most commonly northwest–southeast; fig. 9). Two lithofacies constitute FAm3, including a lower, relatively thick (7–11 m), channel-bearing sandstone (L7a) and an upper, thinner (<5–8 m), tabular-bedded sandstone (L7b; fig. 24, supplementary fig. 2).

Lithologic Description

Lower channel-bearing sandstone body (L7a). The lower part of the channel-bearing sandstone rests upon a planar to undulating, erosional surface that truncates FAm4 (figs. 24, 25A). The base contains
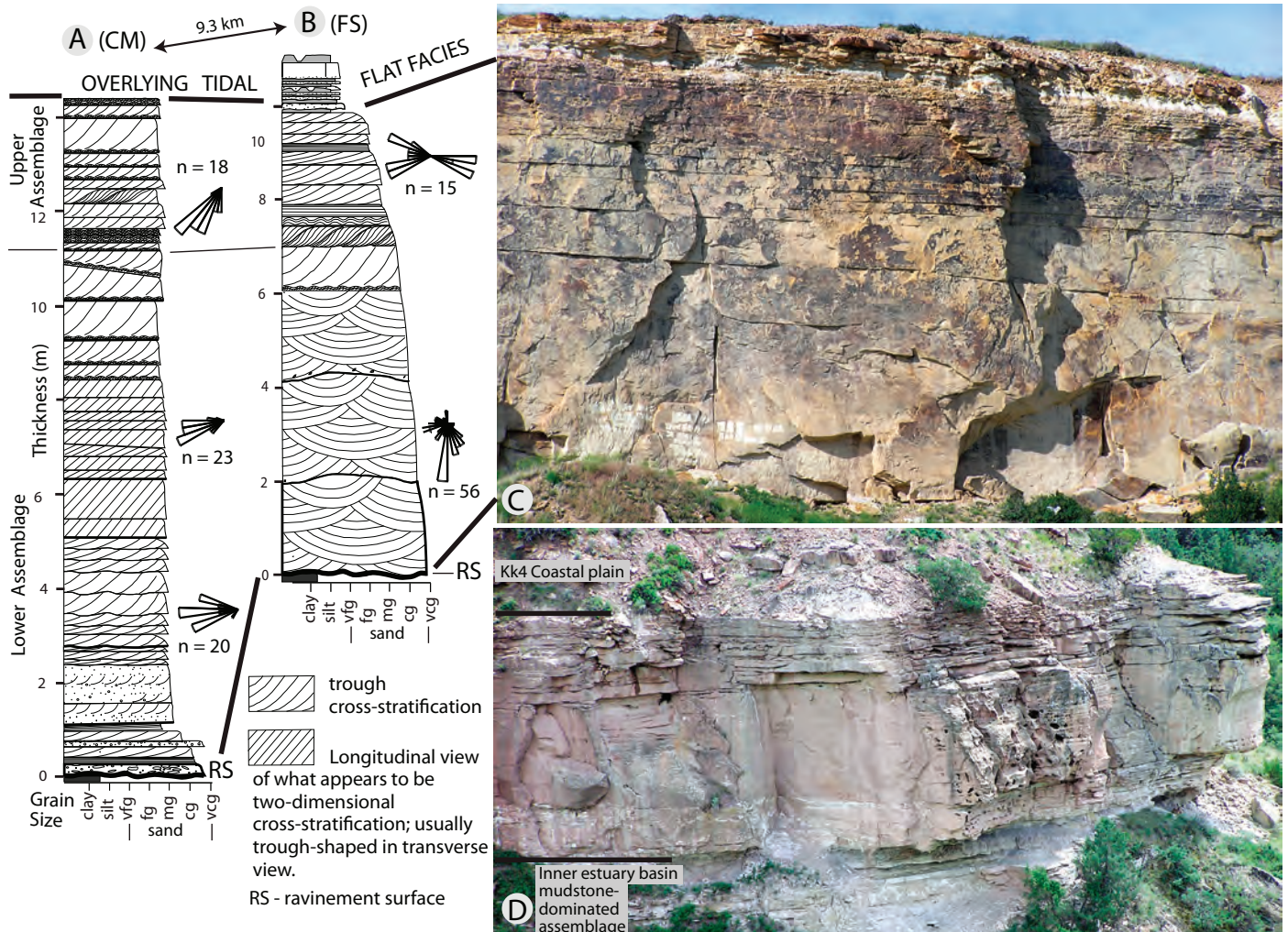
Figure 24. Estuary mouth bar facies association (FAm3). The base of the sandstone body at all locations marks a transgressive surface of erosion developed upon the mudstone-dominated estuary basin facies. (A and B) Measured sections at Centerville mine (CM) and Fields Station (FS). (C) Overview photo at Fields Station. Nearly pure kaolinite of the mudstone-dominated estuary basin facies underlies the sandstone body. (D) Overview photo along the Missouri River gorge at the mouth of Box Elder Creek (BEe). Sandstone body ~12 m thick.
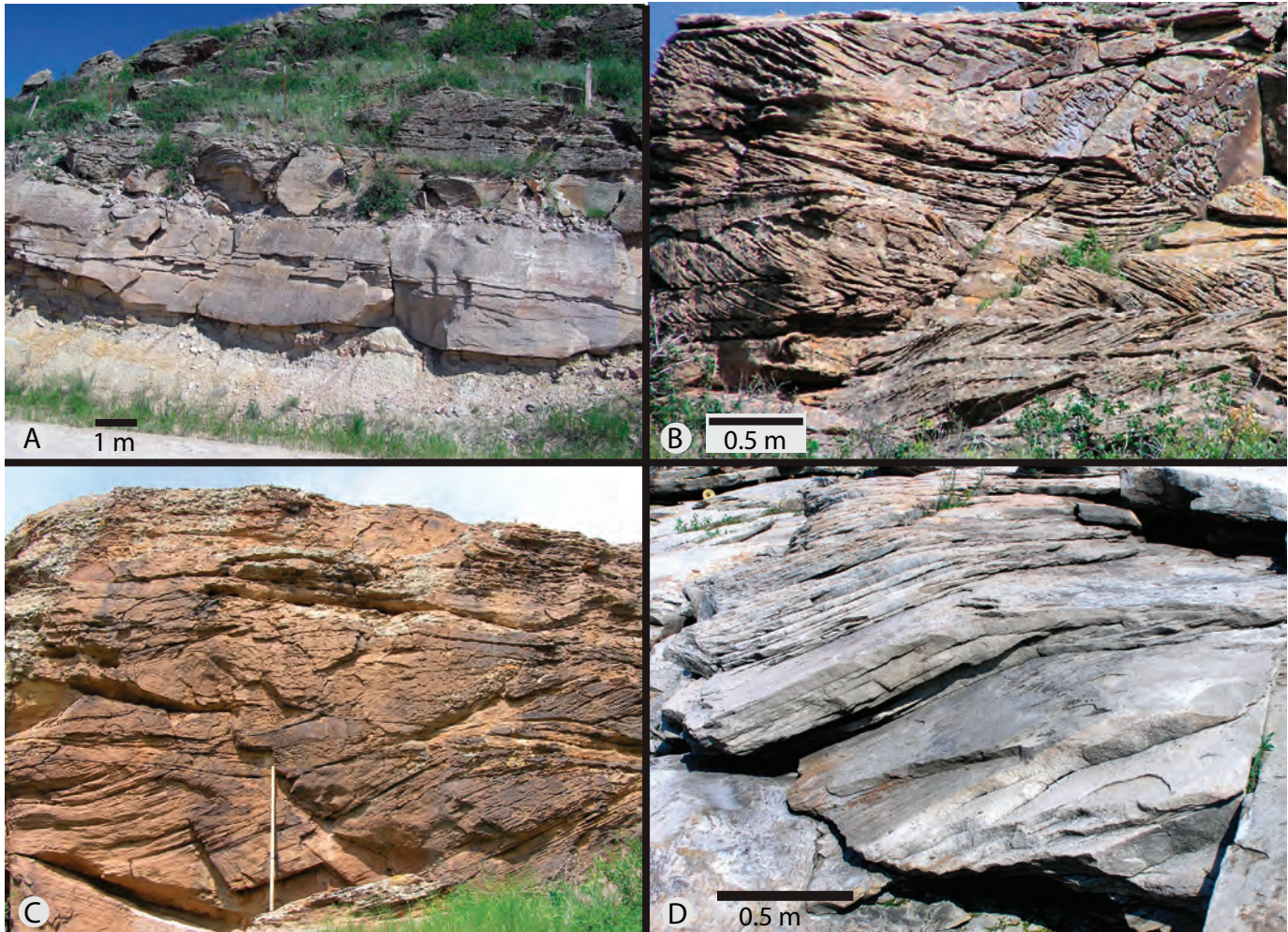
Figure 25. Estuary mouth bar facies (L7a). (A) Concave (channel-form) base of the estuary mouth bar erosionally overlying kaolinitic mudstone and tidal sandstone lenses of the estuary basin facies. Goodwyn Coulee Road (GCR). (B) Stacked tabular sets (left side view) of unimodal trough cross-stratification (front view) recording flood-directed (southward) time-velocity asymmetric flow. River Road 2 (RR2). (C) Very large-scale trough cross-stratification within a channel-shaped body near base of the lower assemblage. The cross-stratification sets overlie concave erosional surfaces and most likely represent infilled channel tracts located between elongate bars. Gibson Flats (GF). Staff 1.5 m. (D) Large-scale planar cross-stratification representing ebb-oriented (northward) dune (sand-wave) migration. South side of Cochran Dam (CDs).

very coarse-grained sandstone and thin conglomerate lenses having a mixture of lithic clasts (mudstone flakes, light gray to black chert sand and pebbles, and quartz pebbles), texturally mature quartz sand, and a light gray muddy matrix similar in composition to that of underlying mudstone (L17) within FAm4. The remainder of the lower sandstone body exhibits slight upward fining, abruptly becoming texturally mature and highly quartzose.

Most of L7a is characterized by large-scale (up to 1–2 m thick) trough cross-stratified units (figs. 25B,C), the erosional bases of which are frequently lined with imbricated pebbles or mudstone rip-up clasts. Upper flow regime, parallel-laminated beds may also be present, predominantly near the base of

the sandstone body. Some exposures demonstrate that these structures are present within several-meter-thick channel-shaped bodies (fig. 25B). Other channel fills are marked by distinct upward fining and thinning successions of large- to medium-scale planar and trough cross-stratified beds. At least six long, narrow, southwest-oriented channel-shaped bodies were noted by Walker (1974), one of which was reported to be approximately 0.4 km wide and >11 km long. In outcrops with orientations oblique or parallel to channel axes, the channel bodies appear as erosional-based, tabular- to prismatic-shaped, upward fining and thinning bed successions. Such outcrops also provide a typical view of amalgamated beds with unimodal, seemingly planar cross-stratification (fig. 26, outcrop
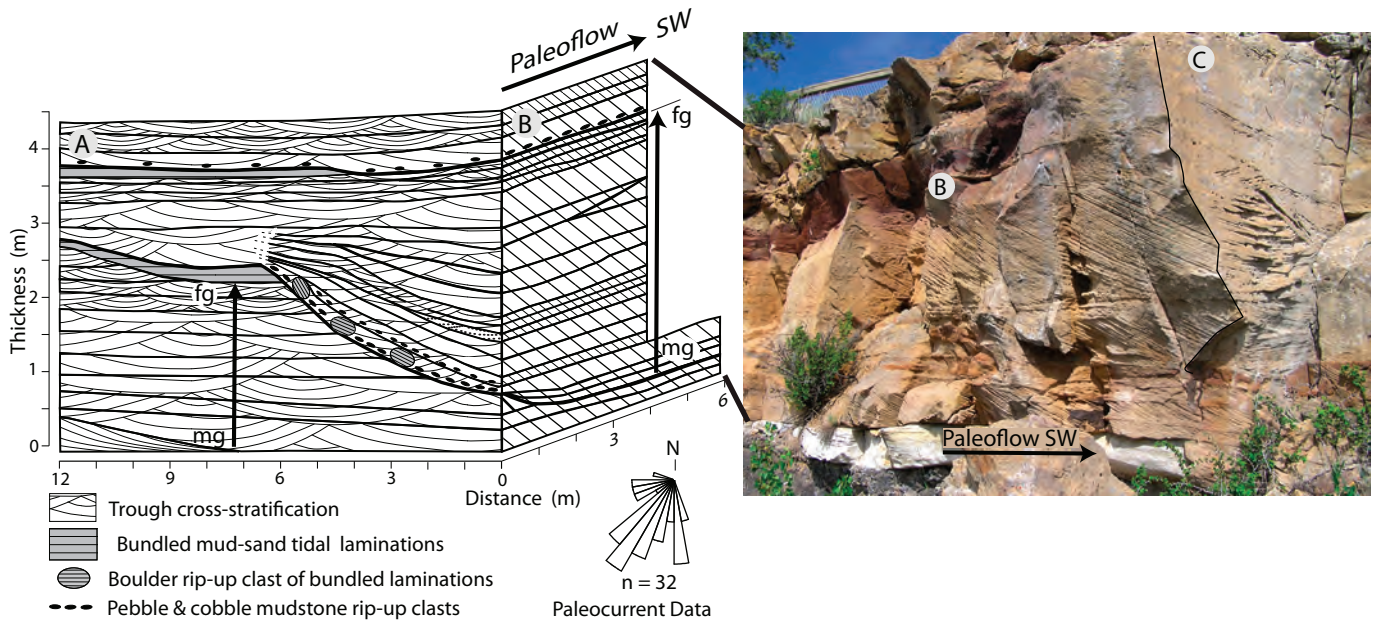
Figure 26. Estuary mouth bar facies (L7a): Inter-bar channel bodies at Ryan Island (RI). Panel B in the sketch corresponds to outcrop face B in the photo. Panel A, not shown in the photo, is located left of B and oriented parallel to C in the photo. The sandstone body erosionally overlies kaolinitic estuary sandstone (white) and mudstone at the bottom of the photo.

face B). However, three-dimensional exposures reveal that trough cross-stratification is by far the most common and that the seemingly planar cross-stratification is due to outcrop orientations parallel or at a low angle to trough and sandstone body axes (figs. 25B, 26). The exposure at Ryan Island (RI) provides excellent flow-transverse and longitudinal views of such a channel body and contains pebble- to boulder-size rip-up clasts of tidal-bundled sandstone–mudstone laminations derived from adjacent beds (fig. 26). Other sedimentary structures within the sandstone body include large-scale, two-dimensional dune forms (fig. 25D), lateral successions of large- and small-scale ripple bundles with rare and partially developed reactivation surfaces (fig. 27A), very rare small-scale bipolar ripple foresets, and very rare mud drapes. Despite composite paleocurrent data for bipolar flow, lowermost parts of the sandstone body, particularly channel fills, demonstrate a unimodal-southwestward dominance. The top of L7a typically consists of similar, but thinner-bedded strata separated by planar to slightly undulatory erosional and seemingly non-erosional surfaces mantled by linguoid, interference, or nearly symmetrical straight-crested wave ripples.

Upper tabular-bedded sandstone body (L7b). The upper sandstone body is a thinner-bedded and typically upward fining succession (<5–8 m thick) of tabular to slightly wedge-shaped beds containing unimodal, large- to medium-scale planar to very wide trough foresets overlain by a thin zone of small-scale, unimodal and bimodal-bipolar, current-ripple bedding and scattered wave ripple cross-laminations. In some cases, stacked two-part bedsets make up smaller scale (½–1½ m thick), upward thinning and fining successions within the upper sandstone body (fig. 27B). Each bedset includes a basal ripple-bedded toeset layer and a conformable overlying thicker and coarser foreset layer commonly containing scattered shale rip-up clasts. The base of the upper sandstone body, as well as the base of internal bedsets, is marked by subhorizontal planar to gently sloping (<10 degrees), curviplanar erosional surfaces. Sloping erosional surfaces are inclined in the direction of foreset dip (fig. 27B), indicating upslope bedform migration. In rarer instances, erosional surfaces are downward sloping relative to foreset orientation, indicating downslope bedform migration. Lateral successions of ripple bundles are sometimes distinct within a bed and demonstrate repeated trends of increasing and decreasing ripple-bundle size (figs. 27B,C). However, in other parts of the same bed, bundles are commonly unrecognizable due to a lack of structural or textural discordance between the bundles. Internally, the ripple bundles are made up of rhythmic two-part (thin–thick) foreset laminations separated by clay parting (fig. 27C). Although rare, simple and
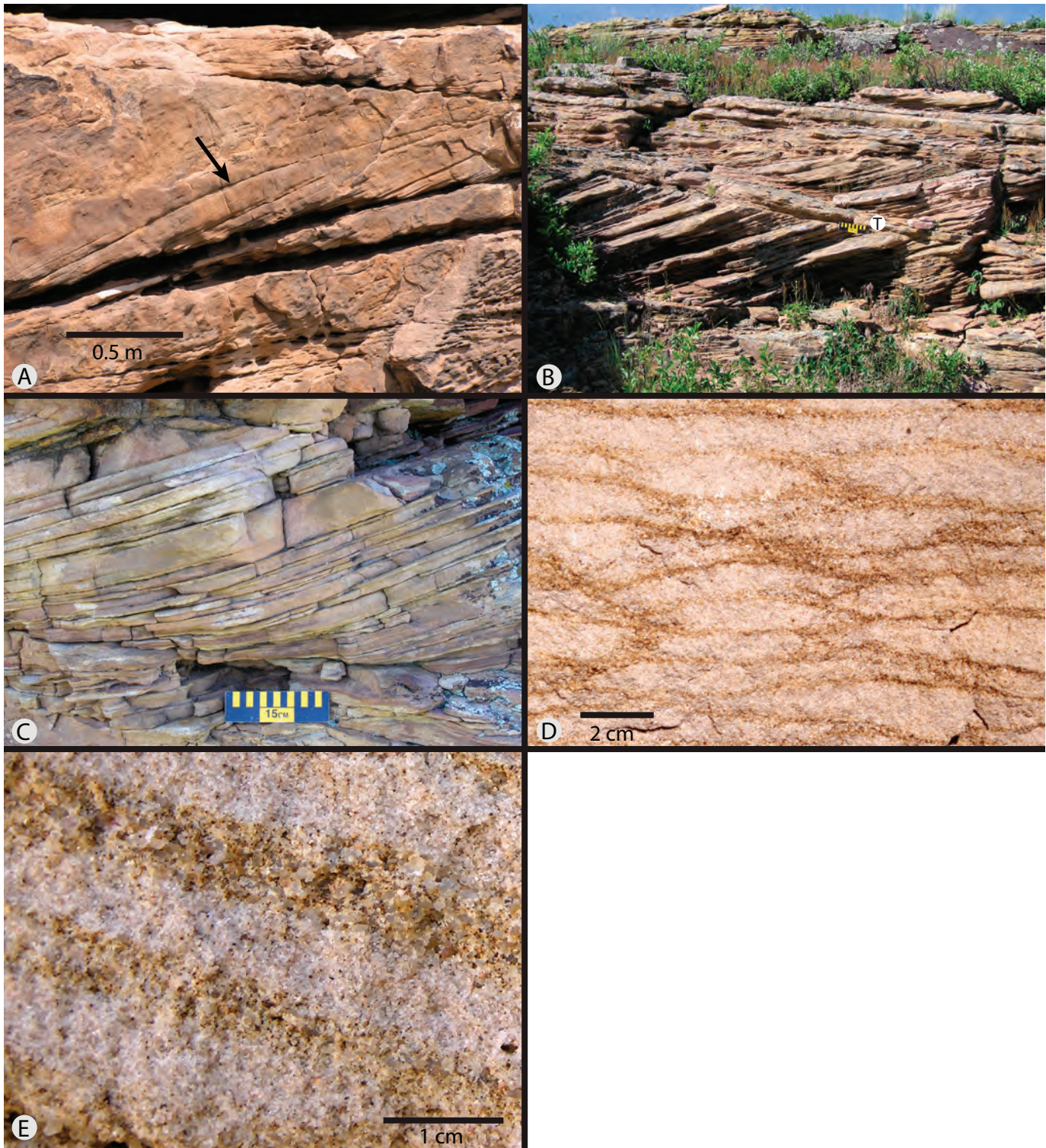
Figure 27. (A) Estuary mouth bar: sedimentary structures. Reactivation surface (arrow). Fisher–Fields road intersection. (B) Upward thinning and fining succession of bedsets. Each bedset overlies an inclined erosional surface, contains a basal ripple-bedded toeset layer (T) and a conformable overlying foreset layer. Foreset thinning-thickening sequences represent neap-spring ripple-bundle migration up the stoss slope of a large bar form. Centerville Mine (CM). Scale 15 cm. (C) Unidirectional two-part thickness sets separated by clay parting laminations document semidiurnal time-velocity asymmetry. Lateral foreset-thickness trends reflect neap-spring cyclicity. Centerville Mine. (D) Flow-transverse view of inversely graded sandstone tongues formed on the lee slope of a two-dimensional sand wave. Fisher-Fields road intersection. (E) Flow-parallel view of dipping, inversely graded sandstone tongues in D.

compound avalanche sand-tongue structures exist in some planar foreset beds (figs. 27D,E).

Trace fossil diversity and abundance in L7a and 7b are exceptionally low. The distribution is heterogeneous and sporadic as defined by Gingras and MacEachern (2012). Trace fossils include *Skolithos* (some clay lined), *Planolites*, and relatively large, but rare, *Diplocraterion* and *Ophiomorpha* (fig. 28).

Depositional Processes and Environment

FAm3 represents a high-energy, tide-dominated shoal system that consisted of elongate (linear) channels and bars. Evidence for an energetic, tide-dominated system includes abundant erosional surfaces, upper flow regime parallel laminations in the lower part of the sandstone body, large-scale dune-related cross-stratification, and tidal current-related structures. The paucity of mud and poorly developed reactivation surfaces separating unimodal cross-strata in both the lower and upper sandstone bodies is consistent with high-energy, but strong time-velocity asymmetry, as in modern settings (Allen, 1980; Dalrymple, 2010).

The basin-parallel orientation of multiple channel bodies within the lower sandstone body indicates elongated tracts of erosion and implies coexistent intervening elongate bars. In modern settings, the outer part of a tide-dominated estuary is marked by a bar complex consisting of elongate (linear) channels and intervening tidal bars (generally 1–15 km length; e.g., Harris, 1988; Dalrymple and Rhodes, 1995; Dalrymple and others, 2012). Net upward fining and thinning through the Great Falls member channel-and-bar units reflect long-term morphologic development and eventual abandonment, whereas smaller scale, textural-structural successions and associated erosional surfaces within the lower and upper sandstone bodies are well explained by fluid dynamics and bedform migration as occurs in modern tidal channel-and-bar systems. For example, in modern settings current speeds are greatest in the tidal channels and decrease toward adjacent bar crests with attendant up-flank fining and a decrease in bedform relief (Dalrymple and others, 2012). With channel migration and bar shifting, basal scour is followed by a net vertical decrease in grain size and bed thickness through the channel fill, as is present in the Great Falls channel bodies. Other smaller scale upward fining and thinning successions,

e.g., within channel fills and adjacent strata, reflect bedset development associated with the migration of smaller bedforms over larger bedforms. Modern flow-transverse simple and compound dunes, mantled with smaller dunes and ripples, are common across tidal sand bars and within channels (Harris, 1988; Dalrymple, 2010; Dalrymple and others, 2012). Planar to undulating erosional surfaces below large-scale trough cross-stratified sets reflect scour-pit migration in front of three-dimensional dunes.

Paleocurrent data for Great Falls indicate that tidal currents were oriented nearly parallel or oblique to the NE–SW-oriented bars and channels. Local unimodal foresets resulted from flood- vs. ebb-current dominance due to lateral separation of flow, a fundamental property of modern estuary mouth bar systems (Harris, 1988; Dalrymple and others, 2012). In particular, modern elongate sand bars are separated by ebb-dominant and flood-dominant channels that result in locally unimodal dune systems of essentially opposite orientation. The dominance of southwestward-unimodal cross-strata in the lowermost sandstone body indicates net sand transport in the headward-estuary, or flood-current, direction. Flood dominance and headward transport of marine, in this case quartzose, sediment has been documented as a fundamental property of modern wide-mouth estuaries wherein tidal currents transport bed material through the lower estuary bar field and into more headward regions (Harris, 1988; Dalrymple and others, 2012). Headward migration of the shifting Great Falls tidal channels, and associated tidal current scour, resulted in ravinement and coarse-grained deposition including the mixing of reworked, underlying nonmarine, lithic-rich material and seaward-derived mature quartz sand. The upward transition into clean quartz sand reflects flood-current dominance and net headward transport of seaway-derived sand. Overall, the tidal ravinement process accounted for disconformity development at the base of the main sandstone body.

The upper sandstone body represents a transitional change from the high-energy and deeper channel-and-bar system to a shallower, lower energy setting in which currents and waves reworked a finer grained mantle of sand. The continued upward decrease in bed thickness as well as increased abundance of planar cross-stratification and bimodal-bipolar foreset ori-
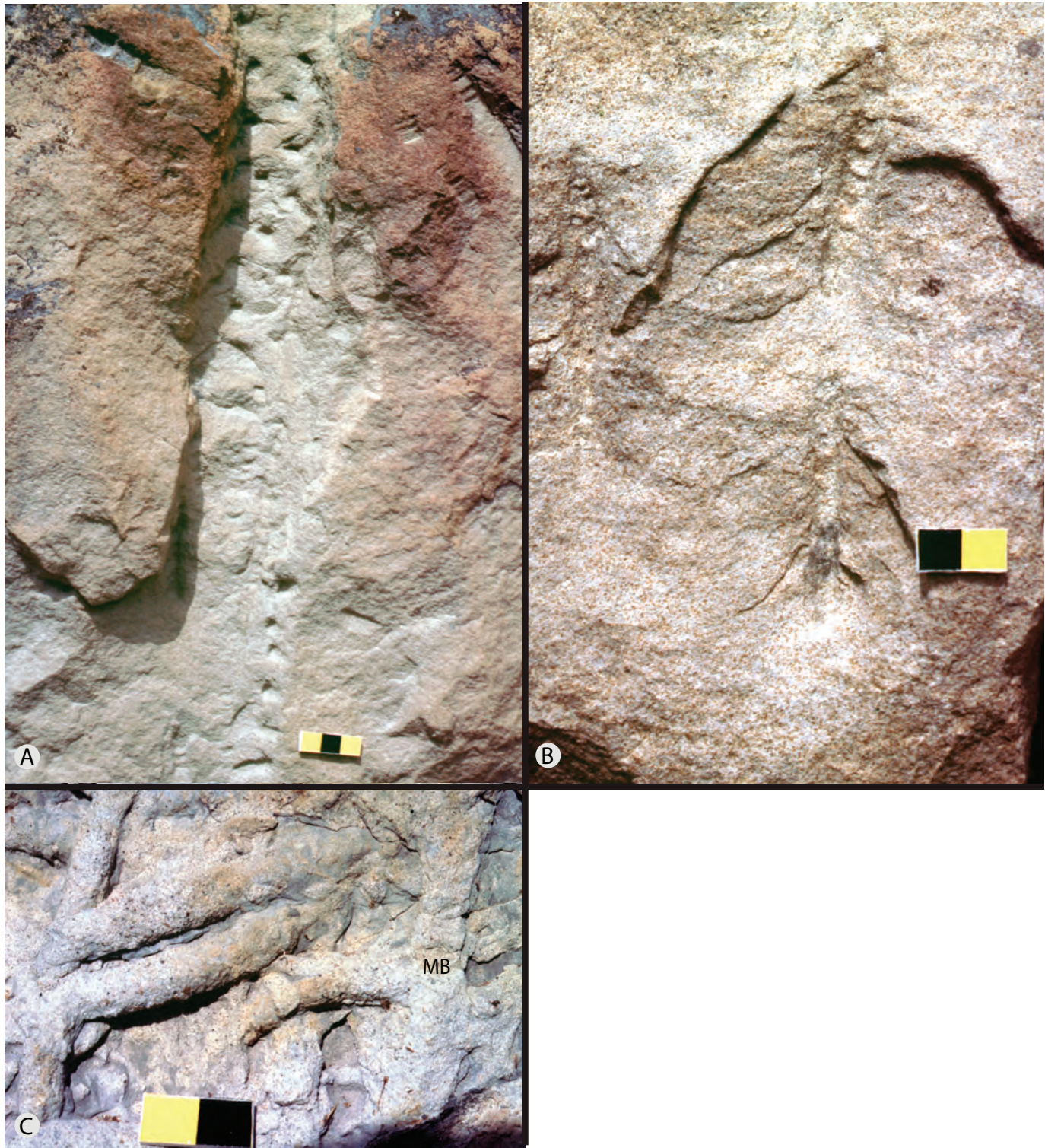
Figure 28. Estuary mouth bar: ichnofossils. (A) Probable *Ophiomorpha* with clay lining weathered out; lower main sandstone body. Scale 3 cm. Ryan quarry (RQ). (B) *Diplocraterion*; lower main sandstone body. Scale 2 cm. Ryan quarry. (C) *Planolites* and cylindrical burrow with vaguely meniscate backfill (MB in photo); upper transitional subfacies. Scale 2 cm. River Edge Trail (REt).

entations collectively indicate predominant smaller scale, two-dimensional ripples associated with a net decrease in flow regime and decreased time-velocity asymmetry. Ripple bundle thickening and thinning are a product of neap-spring cyclicity, whereas the internal thin–thick foreset laminations document semidiurnal cyclicity. The subhorizontal and sloping low-angle erosional surfaces resulted from episodic beveling as occurs along the faces of modern sand bars (Dalrymple, 2010). Similarly, stacked bed sets resulted from

the migration and buildup of smaller dunes and ripples along the beveled surfaces (Allen, 1980). During quiescent conditions, avalanche sand tongues resulted from gravity collapse of high-angle frontal slopes of two-dimensional dunes and large ripples (Buck, 1985; Hunter, 1985).

Overall, the estuary mouth bar sandstone body reflects initial landward encroachment and buildup of a high-energy system followed by eventual regression-associated abandonment. The ichnogenera make up an impoverished marine assemblage that is consistent with a high-energy and brackish water to possibly marine estuarine setting in which episodic erosion and/or sediment deposition are typical (Desjardins and others, 2012; Gingras and MacEachern, 2012; Gingras and others, 2012). Such settings include tidal bars and subaqueous dunes that develop in brackish estuaries and funnel-shaped bays (Dalrymple and others, 2012; Desjardins and others, 2012). Studies of modern and recent tide-dominated estuary systems indicate that as the rate of sediment supply to the estuary exceeds the rate of relative sea level rise, the estuary fills, sand bar morphology changes, and sand bars prograde seaward (Johnson, 1977; Allen, 1982; Harris, 1988; Dalrymple and others, 1992). Bars become broader and shallower, and intervening channels become diminished and stranded as the estuary fills (Stride and others, 1982; Harris, 1988). Overall, estuary filling and seaward progradation account for the late-stage facies change in the Great Falls sand bar system as does superposition by tidal flat and estuary channel facies.

FAm4: Inner Estuary Basin

A mudstone-dominated facies assemblage (<0.1–11 m thick; fig. 29, supplementary fig. 3) extends southward (1) along the basin axis and (2) in a relatively narrow zone along the eastern basin margin (fig. 5). Although gray mudstone (L17) is dominant, several other lithofacies representing short-term environmental changes as well as an axial channel within the inner basin are present.

Lithologic Description

Gray mudstone (L17). In the basin axis depozone, gray kaolinite-rich to exceptionally pure kaolinite mudstone is present (or has been mined out) directly underneath the estuary mouth bar facies (figs. 24D, 25A). In some locales, darker gray carbonaceous mudstone (fig. 29C) and thin coal (Walker, 1974) are present. Composition of the clay is unknown for the eastern depozone. Where exposed adjacent to the tidal shoreface facies (site BC), the assemblage contains an upward coarsening shoreface-like sandstone unit near its base, similar to upward coarsening units in the adjacent shoreface exposure (CM sites). A general bioturbation fabric is common.

Maroon mudstone (L19). Thin (<15 cm), mottled maroon and gray mudstone layers with blocky ped and plant bioturbation fabric, gray rhizohaloes, drab haloes, and localized small-scale slickensides are relatively rare, but scattered through the assemblage.

Tabular sandstone (L3, 4) and tabular heterolithic (L5) units. Up to six widespread tabular units of fine-grained sublitharenite (~1–6 m thick) may be present (figs. 29A,D,E). In some cases, underlying heterolithic units (~1–3 m thick) of very fine-grained sandstone and mudstone beds (5–50 cm thick) show a transition up to thicker bedded (~0.3–1 m) amalgamated, fine-grained sandstone of the tabular units. Heterolithic units above the tabular sandstones, if present, make up a subsequent upward fining trend. Trace fossils include *Planolites, Skolithos, Taenidium*, and scattered unidentified ichnogenera. General bioturbation is locally common.

Erosional surfaces typically underlie and are present within the sandstone units. Grain size is commonly uniform throughout a unit with slight upward fining at the top. Erosional surfaces are also common within the heterolithic intervals.

Figure 29 (opposite page). Inner estuary basin facies assemblage (FAm4). (A) Mudstone-dominated succession along Belt Creek (BC) near the Morony tidal shoreface facies. Tabular sandstone bodies within the mudstone succession represent sheet sands of uncertain lower intertidal or subtidal origin. (B) Flaser bedded sandstone within estuary mudstone truncated by the overlying estuary mouth bar sandstone body at Ryan Island. Scale 15 cm. (C) Dark carbonaceous mudstone underlying estuary mouth bar sandstone body at Ryan Island. Scale 15 cm. (D). Close up of parallel lamination-dominated tabular tidal sand-flat body (L3) within the inner estuary basin assemblage at Belt Creek. (E) Internal architecture of three cross-stratification-dominated tabular tidal sand-flat bodies (L4) within the inner estuary basin assemblage at Little Belt Creek (LBC).

The sandstone-dominated units are either dominated by parallel lamination (fig. 29D) or cross-stratification (fig. 29E). In the parallel lamination-dominated units (L3), trough and very low-angle parallel laminations may be present in the lower part of the unit. Although rare, laminations are locally convex-upward rather than subhorizontal. Ripple bedding and pervasive bioturbation may also be present in the top 10–50 cm.

The cross-stratified units (L4) are marked by amalgamated medium- to large-scale trough cross-stratified beds in the lower part and ripple-bedded medium- to large-scale foresets or low-angle to horizontal ripple-bedded laminations in the upper part. Alternating bundles of parallel and rippled laminations may also be present. Mud rip-up clasts mantle some of the erosional surfaces and wave ripple bedforms mantle bed surfaces. Paleocurrent distributions are unimodal to bimodal-bipolar.

Sandstone beds within the heterolithic intervals (L5) contain flaser bedding, mud-draped trough cross-stratification, and alternating ripple bedding and parallel lamination. Bioturbation fabric is typically abundant.

Lensoidal heterolithic unit (L12). A relatively widespread (hundreds of meters) and thin (~4 m) plano-convex unit of quartzose sandstone (L12) is encased within gray mudstone-dominated lithologies (L17) in the basin axis depozone of FAm4 along the Missouri River gorge (fig. 30; site BEw). The unit contains one to several stacked lensoidal bodies that have a laterally changing subhorizontal to concave scour base that, in some cases, truncates underlying bodies. The bodies generally fine and thin upward into heterolithic beds from amalgamated sandstone or thicker heterolithic beds along the base. Trough cross-stratification is present above the scour base, and bedding is dominantly subhorizontal throughout each
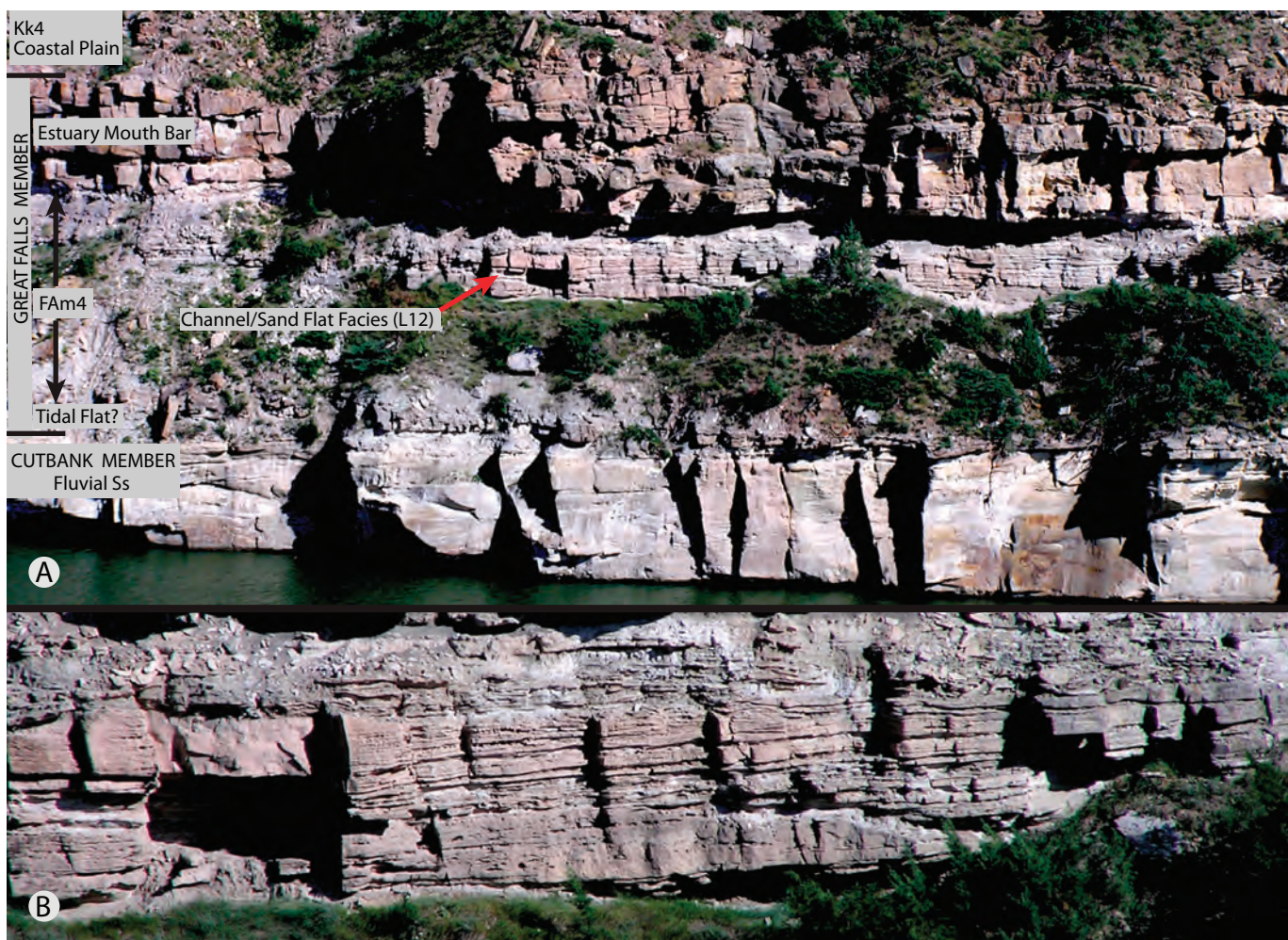
Figure 30. Axial inner-estuary channel (L12) along Missouri River gorge (BEw). (A) Overview of lower Kootenai Formation showing facies succession and L12 within the inner estuary facies assemblage (FAm4). (B) Close up of L2 showing stacked sandstone bodies and concave-shaped scour base. Maximum thickness ~4 m.

body. Estimated heterolithic body, concave-scour, and trough cross-strata orientations indicate roughly basin-axis-parallel paleoflow.

Depositional Processes and Environment

The combination of lithofacies represents a low-energy, estuarine, mud-rich basin that intermittently contained subtidal or intertidal mud flats, sand flats, mires, thin soils and, near the basin axis, an axial channel-related system. The gray mudstone (L17) represents estuary entrapment of fine-grained sediment, similar to that reported for modern systems (Harris, 1988; Dalrymple and others, 1992). Kaolinite, generally considered an end-member weathering product, is also present in Kk2 coastal plain (including paleosol) deposits that lie below and laterally adjacent to the Great Falls member deposits (Walker, 1974). Thus, the nonmarine units most likely served as a nearby source of kaolinite that became reworked and redeposited in the low-energy central zone of the estuary basin, analogous to tidal current-scoured and fluvial-derived mud in modern estuaries, e.g., the Moreton embayment, Australia (Harris, 1988). The carbonaceous mudstone and thin coal deposits indicate settings with restricted circulation, poor drainage, and localized mire development, whereas the maroon mudstone (L19) reflects relatively short periods of emergence and soil development.

The tabular sandstone and heterolithic units (L3, 4, 5) indicate a dominance of tidal processes in intertidal to subtidal sand flat settings as documented in modern environments (Dalrymple, 2010; Daidu and others, 2013). The cross-stratified units reflect stronger current activity in subtidal settings and the convex bedding suggests localized bar development. Facies shifting and stacking due to changing depth is the most likely cause of vertical transitions between the heterolithic units and amalgamated sandstone beds. The trace fossil assemblage, combined with low diversity and abundance, and absence of a typical marine assemblage, is reflective of environmentally stressed conditions such as in brackish water estuarine settings (Keighley and Pickerill, 1994; Savrda and Nanson, 2003; Gingras and MacEachern, 2012; Gingras and others, 2012).

The lensoidal heterolithic unit (L12) most likely represents an axial channel-and-sand flat setting within the mudstone-dominated part of the central basin. Lensoidal geometries with basal scour and confinement by mudstone indicate an initial history of channelized flow. The upward transition into widspread, subhorizontal heterolithic beds further indicates rhythmic tractive-slack deposition over relatively flat areas above the channel base.

FAm5: Estuary Axis Channel System

Facies association 5 (L11) is exposed above estuary mouth bar deposits along the Missouri River between Ryan and Cochran Dams and near Big Bend (BB1; fig. 5). The deposits pinch out a short distance east of Ryan Dam and to the southeast where they are laterally confined by subtidal and intertidal flat deposits. Toward the north and west, the deposits extend into the subsurface where the lateral extent is unknown. At Ryan Dam (RDs), a basal erosional surface exhibits at least several meters of scour into underlying estuary mouth bar deposits (figs. 31A, 32A). Here, the assemblage includes a ~40-m-thick succession of laterally and vertically stacked channel bodies (fig. 31). Individual channel body orientations are approximately NE–SW and transect the Missouri River gorge at a high angle, indicating a >5 km width between pinch-out boundaries for the channel complex. The deposits are described below on two architectural levels: within channel body, and stacked channel body successions.

Lithologic Description

Within Channel Body. The channel bodies have a distinctly concave erosional base, cross-channel widths of several meters to >20 m scale, and thicknesses of a meter to the 10 m scale (fig. 31C). Erosional patterns and remnant parts of channel bodies demonstrate lateral and vertical truncation of preceding channel deposits. Three varieties of upward fining channel fills include amalgamated sandstone-dominated, heterolithic-dominated, and mudstone-dominated. The sandstone is quartz-rich and clayey to clean with a well-sorted framework. Sand size ranges from coarse to very fine. Mudstone rip-up clasts are locally common. Bed geometry ranges from inclined heterolithic to an upward succession of symmetric-concave to subhorizontal bedding. In one case, an inclined heterolithic-bedded paleo-slump block exhibits over-steepened beds and penetrative
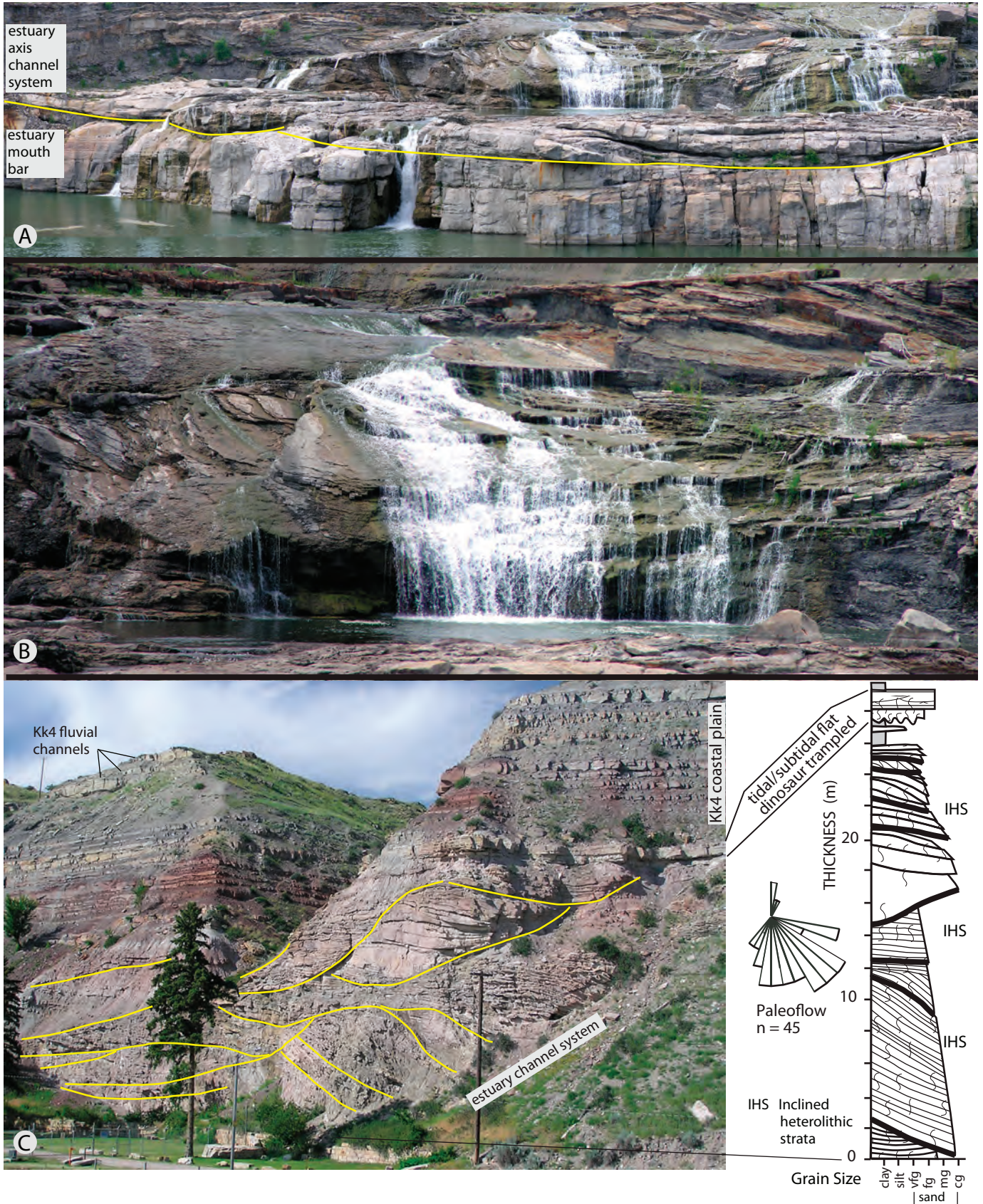
Figure 31. Estuary axis channel system (FAm5). (A) Estuary axis channel sandstone bodies erosionally overlying the estuary mouth bar facies. Yellow line, erosional surface. Ryan Dam spillway (RDs). (B). Very large-scale trough cross-stratification within an estuary channel sandstone body in the lower part of the estuary-channel succession (RDs). (C) Upper part of the estuary axis channel system overlain by Great Falls tidal flat and Kk4 coastal plain deposits. Yellow lines, margins of stacked channel bodies. Ryan Dam power plant cliff (RDp).
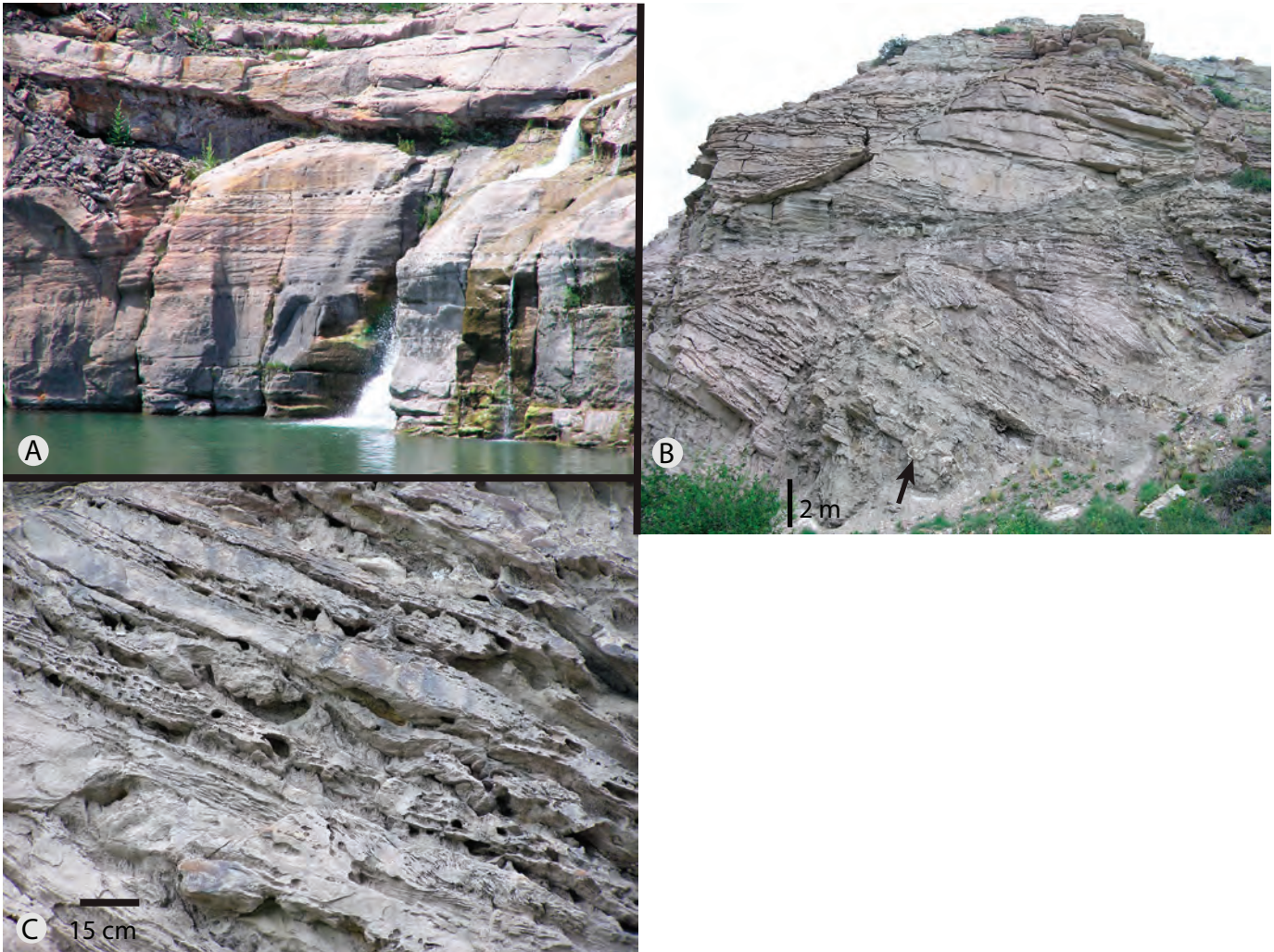
Figure 32. Estuary-axis channel system (FAm5). (A) Close up of the concave base of an estuary channel body erosionally overlying stacked cross-stratified sets of the estuary-mouth bar facies. Photo is located at the left side of figure 31A. Ryan Dam spillway. (B) Stacked estuary channel bodies containing inclined heterolithic strata. The channel bodies are those shown in the stratigraphic section of figure 31C. Arrow indicates location of dinosaur track (shown in fig. 33D) within paleo-slump block. Ryan Dam power plant cliff. (C). Close up of B showing regular heterogeneous bioturbation pattern of inclined heterolithic strata. Ryan Dam power plant cliff.

dinosaur tracks (figs. 32B,C). Slightly convex-up cross-channel bedding is rare. Horizontal heterolithic (L5) and mudstone beds (L17) commonly flank the channel margins. Sedimentary structures include medium- to very large-scale trough cross-stratification (widths up to 8 m, thicknesses up to 4 m; fig. 31B), abundant small-scale current-ripple bedding, mud drapes, rhythmic (tidal) bundles of parallel lamination (fig. 33A), gutter casts, flute casts, and wave ripples. Paleocurrent data are unimodal southward to southeastward, and bimodal-bipolar with a dominant southeastward mode (fig. 9). The modal orientations roughly align with the elongate estuary basin axis.

The channel bodies contain small, mixed horizontal and vertical tubular trace fossils and are sporadically up to 100% bioturbated. Identifiable forms are relatively few and include *Siphonichnus* (Zonneveld and Gingras, 2013), transported worm tubes, and penetrative dinosaur tracks (fig. 33). Regular heterogeneous trace-fossil distributions (Gingras and MacEachern, 2012) are common in inclined heterolithic strata wherein the muddy intercalations are heavily bioturbated and the sandstone beds less bioturbated (fig. 32C).

Channel body successions. Two successions of stacked channel bodies are superposed at the Ryan Dam sites (RDs and RDp; figs. 31A,C). Each succession shows net upward fining and consists of sandstone-channel bodies overlain by heterolithic channels, or basal heterolithic channels overlain by
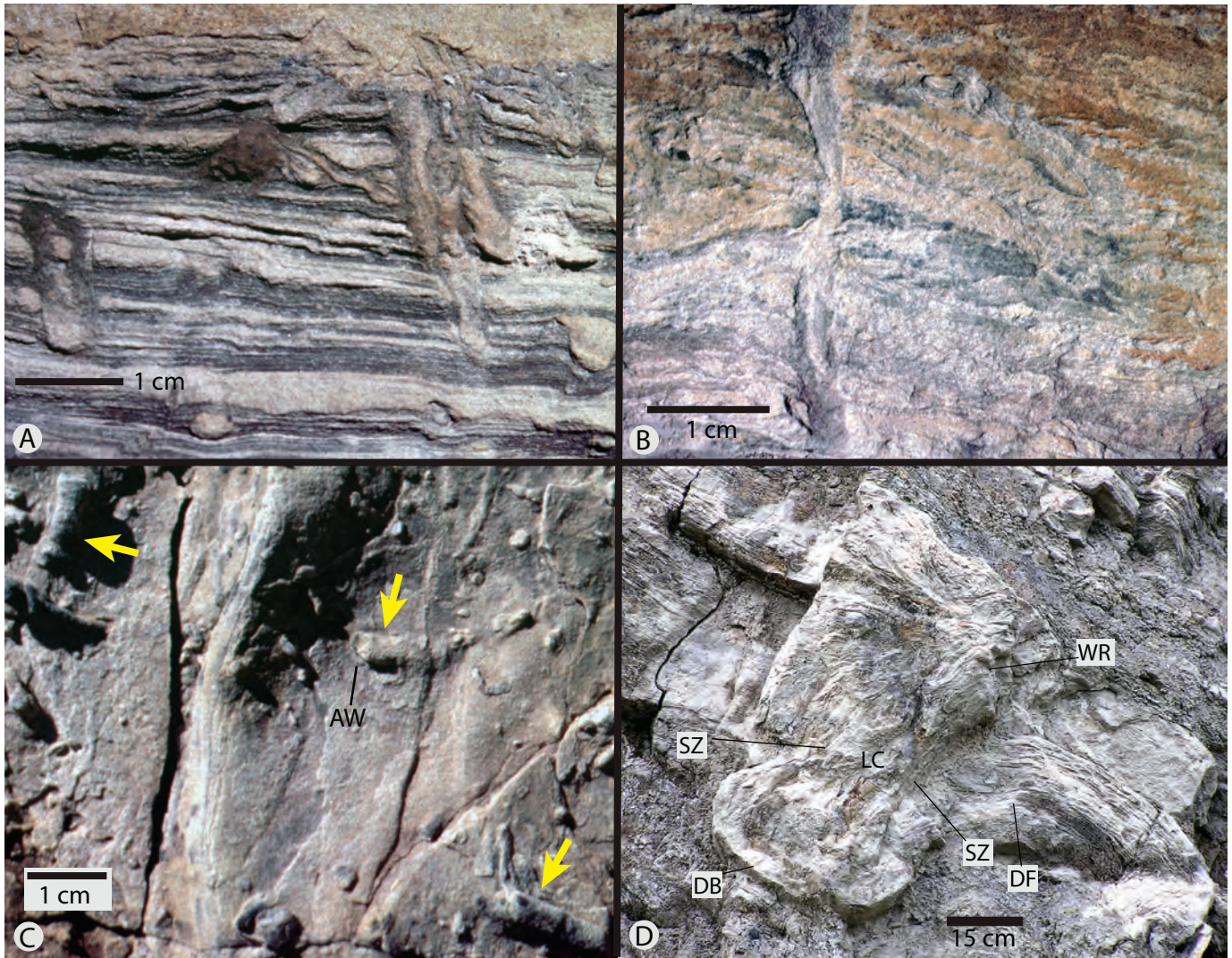
Figure 33. Estuary channel facies: ichnofossils. Ryan Dam power plant cliff. (A) *Siphonichnus* transecting stacked neap-spring tidal bundles of parallel laminations. (B) *Siphonichnus* transecting heavily bioturbated parallel-laminated tidal bundles. (C) Transported worm-tube segments (arrows), with agglutinated wall structure (AW), on wave-rippled surface. (D) Dinosaur track in inclined heterolithic point-bar strata (arrow in fig. 32B). Diagnostic features include: displacement bulb (DB), smooth shear-zone walls (SZ) along the leg cast (LC), and down fold (DF) formed during the penetration phase; withdrawal rim (WR) formed during the extraction phase (after Englemann and Hasiotis, 1999; Jackson and others, 2009; Jennings and others, 2006; Milan and Bromley, 2006; Platt and Hasiotis, 2006).

mudstone-dominated bodies, suggesting an idealized succession of sandstone-to-heterolithic-to-mudstone channels. Channel body thickness decreases upward within each succession from about 4–5 m (maximum) along the base to about 2 m (maximum) near the top. Sand within the channel bodies typically ranges from coarse- and medium-grained in the lower channel bodies and fine- to very fine-grained in the upper bodies. However, strong textural variability may be present between adjacent channel bodies. Coarse-grained basal channels contain locally abundant mudstone rip-up clasts and plant debris, including large tree fragments. The degree of bioturbation increases upward in association with upward fining.

Depositional Processes and Environment

The physical properties of the channel bodies and channel body successions are consistent with those reported for axial estuary channel systems, particularly along the inner part of modern tide-dominated estuaries (Clifton, 1982; Dalrymple, 1992; Dalrymple and others, 2012; Hughes, 2012). As documented in modern environments, lateral migration of axial tidal channels produces cut-and-fill facies that exhibit upward fining over a sharp erosional base (van Straaten, 1954; Hughes, 2012). Also, the inner part of modern tide-dominated estuaries is typically flanked by mudflats (Dalrymple and others, 2012)

similar to the off-channel mudstone in FAm5 as well as accounting for the common occurrence of mudstone rip-up clasts in the channel bodies.

The medium- to very large-scale trough cross-stratification reflects the presence of similar sized three-dimensional dunes, typical of modern sand-filled channels in meso- and macrotidal estuaries (Dalrymple and others, 1978; Visser, 1980; Clifton, 1982; Dalrymple, 1984; Elliott and Gardiner, 2009). Localized unidirectional paleocurrent data indicate southward-dominant, time-velocity asymmetry in some locations compared to flow reversal toward the northeast in other locations, also consistent with the lateral separation of flood-and-ebb current dominance in estuary channel systems (Clifton, 1982; Hughes, 2012). Wave ripples in the channel bodies confirm some wave influence in an otherwise tide-dominated setting. Upward fining within channel bodies of modern infilling channels reflects a reduction in flow strength sometimes related to lateral movement of the channel and altered tidal conditions at a site (Hughes, 2012).

The invertebrate ichnofossils coupled with low diversity, absence of a marine assemblage, diminutive sizes, and locally intense bioturbation are consistent with brackish water salinity (Dalrymple and others, 1990; MacEachern and Gingras, 2007; Hughes, 2012). The regular alternation of bioturbation intensity in inclined heterolithic strata reflects the influence of tidal and possibly seasonal rhythms upon both point bar deposition and bed colonization (Gingras and MacEachern, 2012). Dinosaur tracks document the presence of large vertebrates surrounding the estuary channel system and, similar to modern and ancient fluvial point bars (Laporte and Behrensmeyer, 1980), they most likely caused bank failure and the destruction of primary bedding.

The lateral and vertical pattern of intersecting channel bodies, combined with relatively coarse-grained sand along channel bases (including lag), and inclined heterolithic channel fill, document the existence of a complicated channel network, abundant tidal point bars, and lateral channel migration as occur in inner estuary systems (Clifton, 1982, 1983; Rahmani, 1988). In addition to point bars along sinuous channel tracts, longitudinal bars can be common in sandy estuarine tidal channels (Clifton, 1982), and

may account for the occasional convex sandstone fill in some of the Great Falls member estuary channel bodies.

The erosional juxtaposition of a wide, axial, estuary channel succession upon the estuary mouth bar facies in the northern part of the study area marks a change from a deeper, more open-basin setting to a shallower setting. Thus, a decrease in relative sea level caused sandy, lower estuary channels to extend seaward, migrate laterally, and scour into subjacent high-energy sand bar deposits. Net upward fining and thinning of channel bodies and increase in bioturbation through a succession is consistent with progradational stacking of an estuary system that had a headward decrease in channel depth and energy. For example, studies of modern estuaries show that the lower reaches are dominated by strong tidal currents with greater scour potential, greater channel depths, more wave activity, and a greater supply of oceanic sand than in the headward reaches (e.g., Frey and Howard, 1986; Fenies and Tastet, 1998; Dalrymple, 2010; Dalrymple and others, 2012). The lateral textural trend associated with decreasing headward energy in modern tide-dominated estuaries is headward fining with increased muddy channel fill toward the mixed marine-fluvial zone (Clifton, 1982; Frey and Howard, 1986; Dalrymple and others, 2012), thus accounting for upward fining in a progradational succession. Also consistent with progradation is the thin tidal flat cap to the Great Falls successions as typical of modern estuarine tidal flat and channel systems (Clifton, 1982).

Incised Valley

An incised paleovalley, about 24 m deep and 240 m wide (Hopkins, 1985) with predominantly estuarine fill, is well exposed in the northeast corner of the study area adjacent to Morony Dam (MDs3; fig. 34, supplementary fig. 1). The paleovalley is marked by a broad, U-shaped erosional surface that begins below the top of the Great Falls member, truncates the adjacent Great Falls member tidal shoreface (FAm2) succession, and extends downward to near the top of the Cutbank Member. A very low-angle erosional interfluve surface lies atop the adjacent shoreface succession, descends toward, and connects with the paleovalley margin. Heterolithic levee, splay, and localized channel fill units (Hopkins, 1985) overlie the interfluve
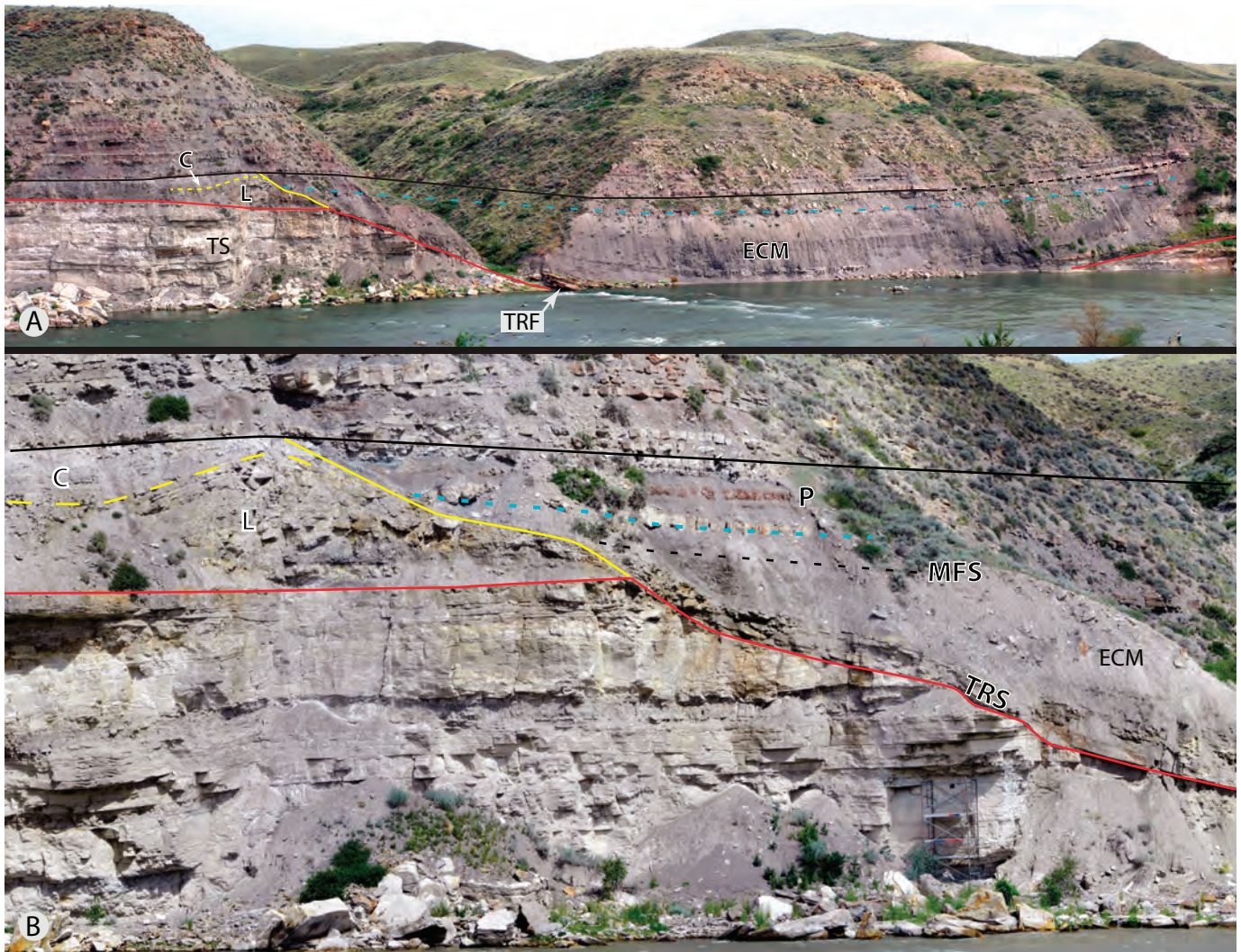
Figure 34. Incised valley below Morony Dam (MDs3). (A) Incised paleovalley with predominantly estuarine mudstone fill truncating laterally adjacent tidal shoreface facies (TS). Colored lines: Red, erosional surface along the paleovalley side and atop the correlative, low-angle, interfluve surface; solid yellow, constructional upper margin of the paleovalley; dashed yellow, delineates the shape of a valley-side levee system; blue, base of lacustrine limestone (FAv4) and fluvial sandstone (FAv5) unit with dinosaur tracks (fig. 36); black, contact between the Great Falls member and Kk4 nonmarine coastal plain facies. C, heterolithic back-levee channel; ECM, estuary center mudstone (FAv3); L, heterolithic levee-splay system; TRF, tidally reworked lithic-fluvial sandstone (FAv1) along thalweg of the paleovalley (fig. 35A). (B) Close-up of the paleovalley side consisting of a lower incisional and upper constructional margin. C, heterolithic back-levee channel; ECM, estuary mudstone (FAv3); L, heterolithic levee-splay system; P, paleosol (FAv6); TRS, transgressive quartzose sandstone (FAv2). Colored lines: dashed black, maximum flooding surface (MFS) marked by upper limit of transgressive sandstone; others, same as above.

unconformity and make up a constructional upper margin to the paleovalley (fig. 34). The main valley fill consists of a succession of six facies associations that are described in ascending order. The entire incised valley succession is overlain by nonmarine coastal plain deposits of Kk4 (Walker, 1974).

FAv1: Tidally reworked fluvial channel

Lithologic description

An upward fining, channel-shaped sandstone body (L15) lies along the thalweg of the incised valley (TRF

in fig. 34A). The sandstone is coarse- to medium-grained and lithic-rich. Sedimentary structures include lateral successions of medium- to large-scale ripple bundles with mudstone drapes and southwest-oriented foresets, vertically stacked bundles of two-part sandstone–mudstone parallel laminations, and wave ripple bedforms (figs. 35A–C). *Cochlichnus*, medium- to very small-sized *Thalassinoides*, very small paired burrows (most likely *Diplocraterion*), and small, unidentified, horizontal tubular traces are present along clayey bedding planes (figs. 35D,E).

Depositional Processes and Environment

The geometry and composition of the sandstone body are similar to those of lithic-fluvial sandstone bodies in the nonmarine Kootenai members. However, the physical structures reflect rhythmic tidal processes. The combination of low trace fossil diversity and abundance, absence of a typical marine assemblage, presence of facies-crossing trophic generalists, and diminutive size is indicative of environmentally stressed conditions such as in brackish water estuarine settings (Gingras and MacEachern, 2012; Gingras and others, 2012). The paleoflow direction of Kootenai fluvial systems is generally northward (Walker, 1974; Berkhouse, 1985). However, the opposing foreset directions of FAv1 most likely reflect southward flood-current reworking up the paleovalley, similar to flood-current directions in the larger scale estuary basin. Overall, composition of the sandstone body and its location along the thalweg of the paleovalley suggest sediment delivery by a presumably northward-flowing fluvial stream to a coastal margin with subsequent estuarine tidal reworking (e.g., Bjerstedt, 1987).

FAv2: Transgressive Shorezone Sandstone

Lithologic Description

A 2-m-thick, medium- to fine-grained quartzose sandstone lens (L6) sharply overlies the basal lithic sandstone body and thins laterally to where it disconformably onlaps the lower wall of the paleovalley (fig. 35F). The unit fines and thins upward from amalgamated, parallel-laminated sandstone beds into ripple-bedded and heavily bioturbated heterolithic beds that show a rapid transition into an overlying mudstone lithofacies (L18). Trace fossils include small *Thalassinoides* (fig. 35E) and unidentified vertical burrows.

Depositional Processes and Environment

The upward trends in texture and physical and biogenic structures indicate progressive energy decrease in a deepening, tidally influenced, marine or brackish shorezone system. Flood-current transport most likely resulted in the encroachment of quartzose sand into the paleovalley estuary, similar to that documented for large, modern tide-dominated estuaries (Boyd and others, 2006; Dalrymple and others, 2012). Similar to FAv1, the trace fossil assemblage is indicative of environmentally stressed conditions such as in brackish water estuarine settings.

FAv3: Estuary Center Mudstone

Lithologic Description

A 16- to 18-m-thick, organic-rich, gray mudstone (L18) transitionally overlies FAv2 and makes up most of the paleovalley fill. Microfossils include palynomorphs, dinoflagellates, and acritarchs (Burden, 1984).

Depositional Processes and Environment

The organic-rich mudstone indicates a low-energy setting with a relatively low degree of oxygen mixing. Burden (1984) interpreted the microfossil assemblage as marine or brackish. Overall, the upward succession from FAv2, interpreted salinity, and confinement of FAv3 between paleovalley walls represents progressive inundation of the paleovalley and landward migration of the estuary, resulting in a setting similar to mud-dominated central-basin zones in some modern estuaries (Dalrymple and others, 1992).

FAv4: Carbonate Lake or Pond

Lithologic Description

A 30- to 50-cm-thick molluscan packstone/wackestone (L21; bottom half of figs. 36 A,B) is present near the top of the valley fill (fig. 34). Disarticulated and fractured mollusk shells are abundant. The bed is deformed, including downward projecting columnar zones and small-scale faults (figs. 36B,D). The columnar deformation zones align with bulbous load casts similar in structure to penetrative dinosaur tracks and under tracks in L1 and L9. Shell orientations range from bed-parallel to randomly mixed and small-scale fault aligned.

Depositional Processes and Environment

Based upon compositional makeup and environmental contraints indicated by bounding lithofacies (L16, L18, L19), the limestone is interpreted to represent a freshwater lacustrine setting. Modern, carbonate mud-producing lake deposits with localized development of molluscan shell hash are described by Schnurrenberger and others (2003). Moreover, an analogous upward transition from estuary central-basin mud to freshwater lake deposits has been documented in Holocene deposits (Buso and others, 2013). Deformation and fabric disruption in FAv4 resulted from post-depositional trampling by dinosaurs. Although vertebrate trampling of Jurassic palustrine–lacustrine carbonate settings has been demonstrated (Jennings and others,
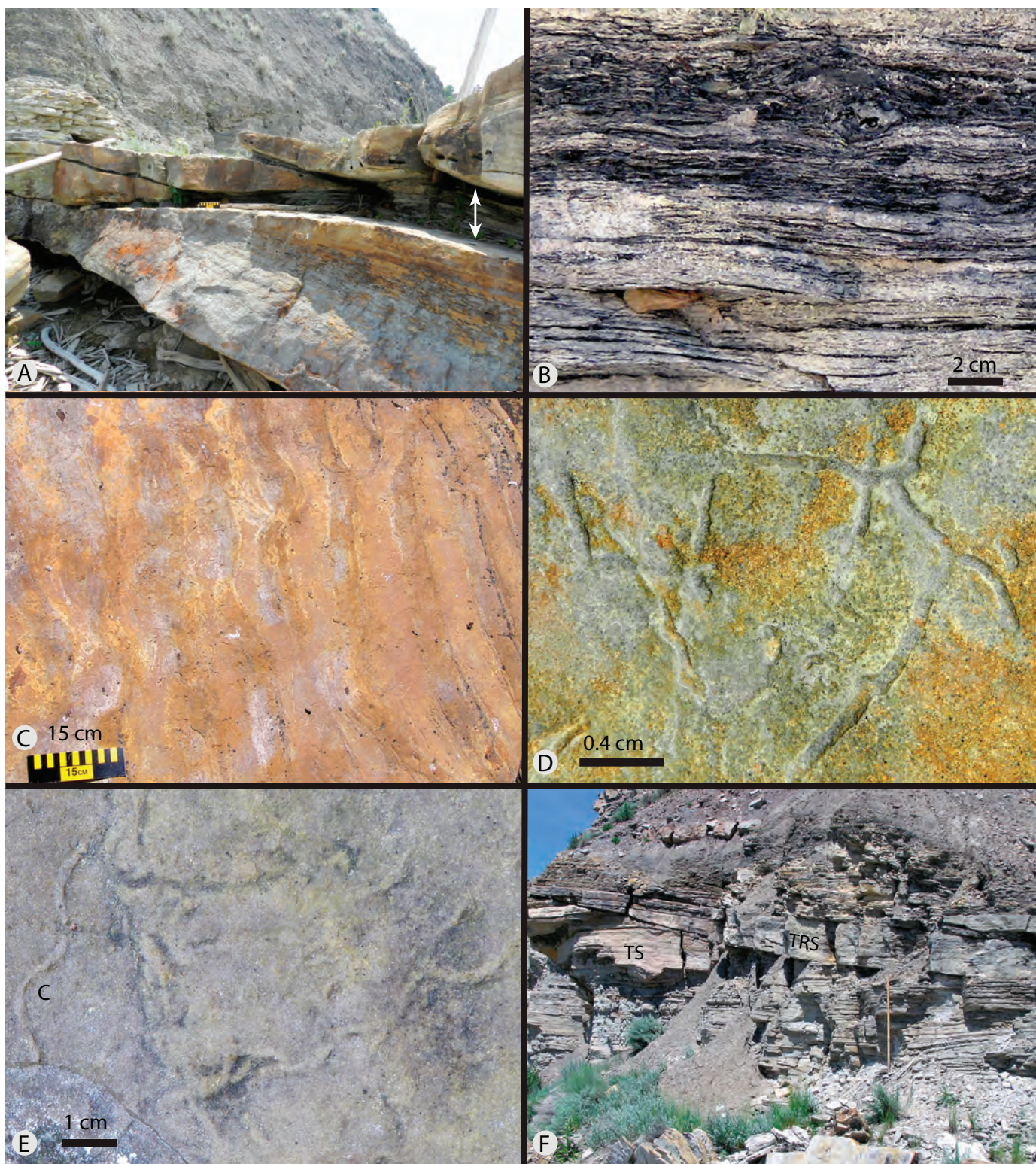
Figure 35. Incised valley fill: basal part. Morony Dam (MDs3). (A) Tidally reworked lithic-fluvial sandstone (FAv1) in foreground overlain by upward fining estuarine sandstone (FAv2) and mudstone (FAv3) in background. Rhythmic ripple bundles, draped with multiple mudstone–sandstone laminations, are oriented southwestward, in the general flood-current direction. Total thickness of sandstone unit about 90 cm. (B) Stacked two-part sandstone–mudstone laminations below the upper ripple-bundle unit in A (white arrow) indicating tractive-suspension fallout cycles. (C) Wave ripples capping ripple-bundled sandstone in A. (D) *Thalassinoides* on wave-rippled surface in C. (E) *Cochlichnus* (C) on wave-rippled surface. (F) Transgressive, upward fining, quartzose sandstone lens (TRS) onlapping truncated tidal shoreface facies (TS) along the lower part of the paleovalley margin. Staff 1.5 m.
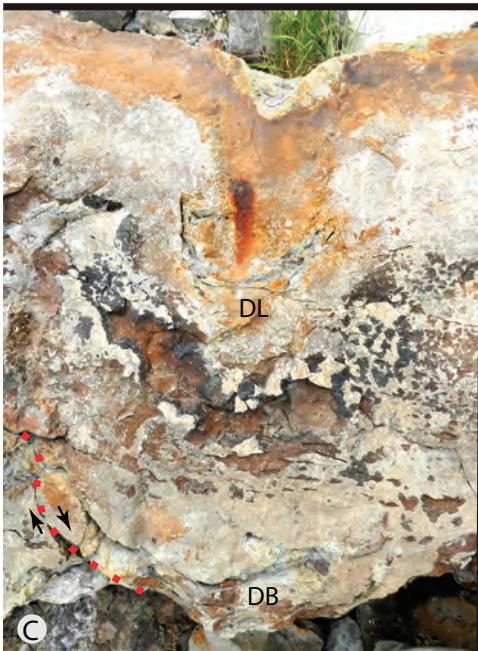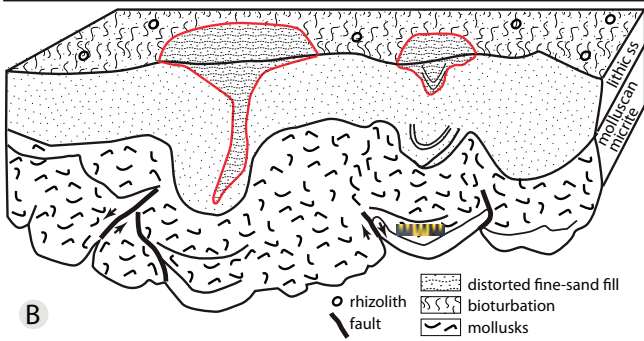
Figure 36. Dinosaur-trampled limestone and sandstone unit in uppermost part of paleovalley. Morony Dam (MDs3). (A and B) Cross-sectional overview and corresponding sketch of trampled lithic sandstone and molluscan micrite. Downward-deformed contacts between beds and laminations within beds are superposed and aligned with bulbous protrusions along the sole where sediment was pressed by feet into underlying mud (after Englemann and Hasiotis, 1999; Jackson and others, 2009; Jennings and others, 2006; Milan and Bromley, 2006; Platt and Hasiotis, 2006). The large conical structures in the top of the unit (red in B) are most likely of combined foot insertion and subsequent collapse/fluidized flow origin (Buck and Goldring, 2003). The scales in A and B are in matching locations. (C) Close up of cross-sectional view of dinosaur trace (at location of scale in A and B) showing downward deformed laminations (DL), displacement bulb (DB) and displacement fault (red dotted line). (D) Limestone in lower part of B and C showing disarticulated and fractured mollusk shells with a partially deformed fabric including a penetration-related shear zone along left side of photo. (E) Sole of trampled bed showing bulbous under-track trace fossils containing concave-upward laminations.

2006), penetrative deformation extending downward from the overlying facies (FAv5) precludes a distinct FAv4 temporal association.

FAv5: Fluvial Channel

Lithologic Description

A thin (10–50 cm) lensoidal, lithic sandstone (L16) made up of coarse- to medium-grained angular siliciclasts lies atop FAv4 (upper half of figs. 36A,B). The bed is texturally homogeneous and biogenically deformed, similar to FAv4. Downward-projecting deformation columns and bulbous sole casts extend from FAv5 into FAv4 and align with the deformation columns and load casts in FAv4 (figs. 36A–C). In addition, the uppermost part of the bed contains 100% small-scale bioturbation, rhizoliths, and surficial conical pits aligned with some of the deformation columns.

Depositional Processes and Environment

Despite a lack of diagnostic physical structures, this facies most likely represents fluvial influx of lithic sand similar to FAv1. The continuity of biogenic-deformation structures with those in FAv4 documents post-depositional dinosaur trampling and foot penetration through moist semicohesive substrates (Laporte and Behrensmeyer, 1980). The complete bioturbation, destruction of primary structures, and development of structureless bedding in fluvial channel deposits by dinosaur trampling is well documented (Engleman and Hasiotis, 1999; Platt and Hasiotis, 2006). The large conical structures in the top of FAv5 most likely represent a combination of foot insertion and consequent fluidized flow (Buck and Goldring, 2003), whereas rhizoliths document rooted-plant development across the surface.

FAv6: Paleosol

Lithologic Description

A meter-scale mottled maroon and gray mudstone (L19) is present above FAv5 (fig. 34B). The mudstone contains a blocky ped and plant bioturbation fabric, gray rhizohaloes, drab haloes, and localized small-scale slickensides.

Depositional Processes and Environment

The mudstone represents full emergence of the paleosetting, floodplain development, and pedogenesis. In general, the paleosol properties are commensurate with wet-and-dry seasonality in a sub-humid to arid climate (Retallack, 1990; Birkland, 1999).

ENVIRONMENTAL ARCHITECTURE— SPATIAL DISTRIBUTION OF FACIES ASSEMBLAGES

The spatial distribution of facies within the main basin and incised valley serve to define the environmental architecture of the different depositional spaces. For the main estuary basin, the facies patterns are presented in terms of those associations that characterize the basin margin vs. the basin interior. In contrast, a relatively simple vertical succession makes up the paleovalley fill.

Main Basin

Basin Margin Facies

FAm1, representing tidal flat and associated channel facies, is the sole assemblage making up the Great Falls member along the eastern and southern margins of the basin (Figs. 5, 37, 38). The western margin is not exposed, but subsurface data (Walker, 1974; Carstarphen and others, 2011) suggest that the western margin of the marine basin is not far to the west of the outcrop extent. Along the basin margin, FAm1 disconformably overlies Kk2 nonmarine coastal plain mudstone and lithic-rich fluvial bodies, and is conformably overlain by Kk4 nonmarine coastal plain and lithic-rich fluvial bodies (fig. 39; Walker, 1974).

Basin Interior Facies

Axial and transverse patterns across the tidal basin fill define the fundamental distribution of environments within the main estuary. The axial trend from the southern terminus of the basin, through the central part of the fill, is from basin-margin facies (FAm1) to estuary mouth bar (FAm3) and tide-dominated shoreface (FAm2) facies in the wider northern part of the basin (fig. 5). The cross-basin trend in the northern locale is from basin-margin facies to muddy estuary basin (FAm4), to tide-dominated shoreface, and to estuary mouth bar facies in the central part of the basin.

In all cases, the vertical successions disconformably overlie nonmarine Kk2 or Cutbank Member deposits and are capped by tidal flat facies that transition into overlying Kk4 nonmarine coastal plain deposits (Walker, 1974). Several types of vertical successions are present beneath the estuary mouth bar
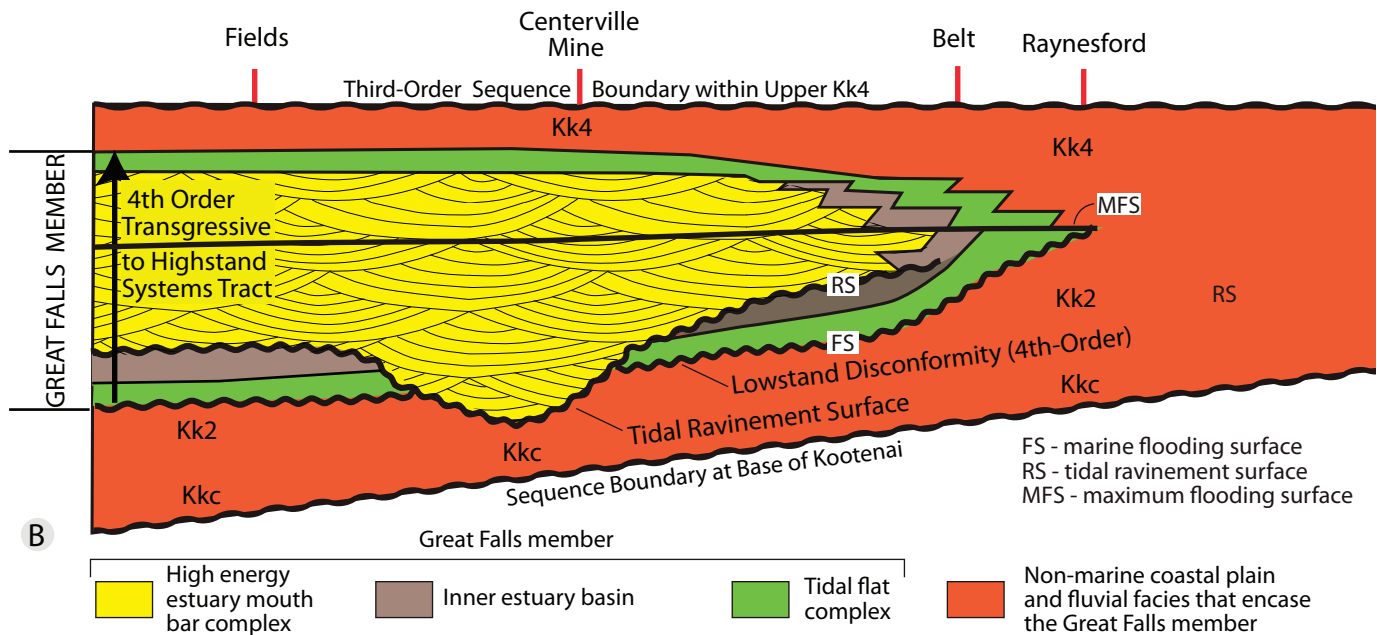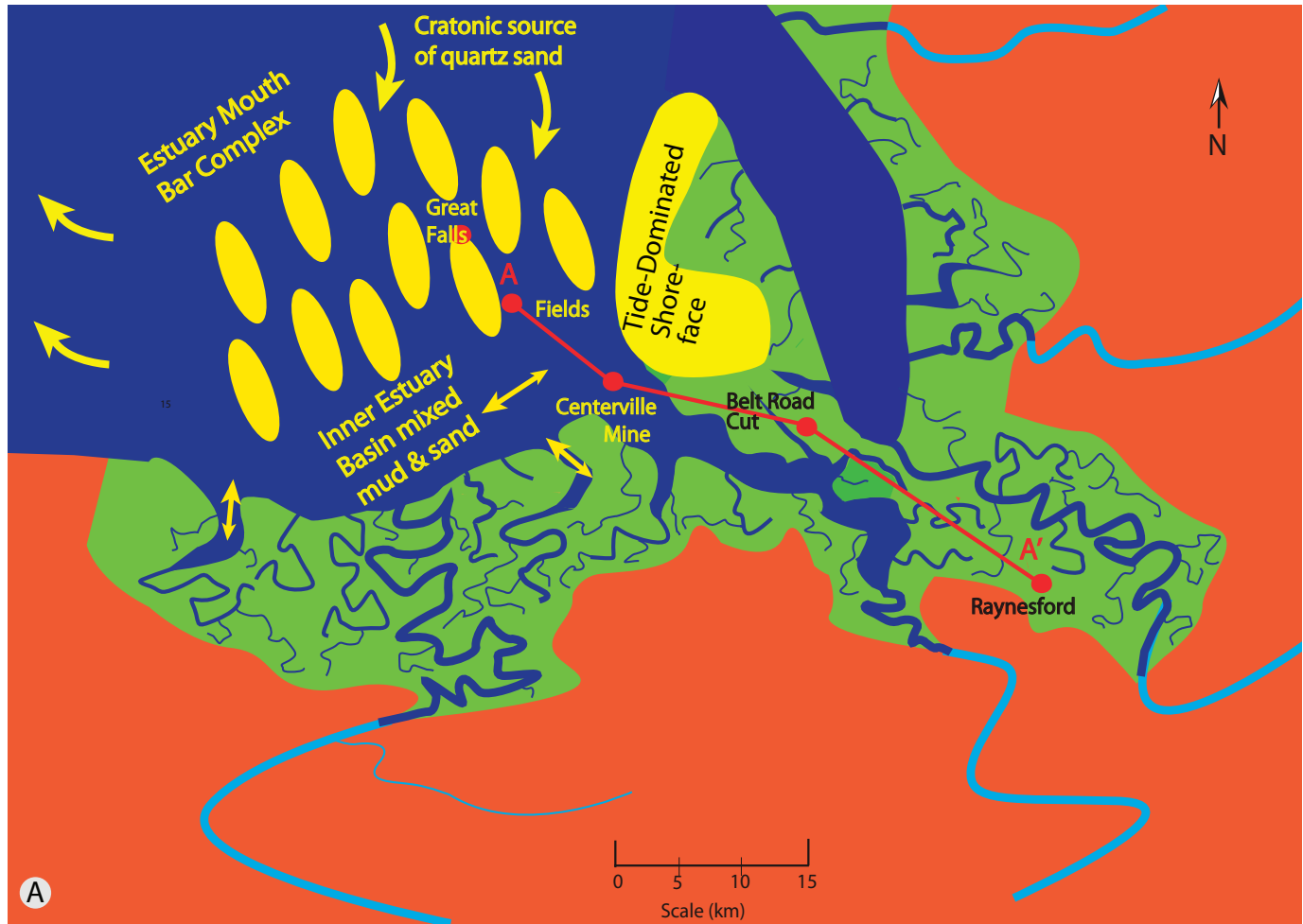
Figure 37. (A) Schematic reconstruction of the tide-dominated estuary-like terminus of the pre-Albian sea in northern Montana. Arrows depict the general circulation pattern. (B) Schematic longitudinal section along A–A' showing distribution of facies within the Great Falls member resulting from transgressive onlap of tidal flat, estuary basin, and estuary mouth bar facies followed by progradation of basin-margin tidal and coastal plain facies (Kk4). The erosion beneath the estuary mouth bar is due to high-energy tidal scour along inter-bar channels. Incision into the basal Cutbank Member (Kkc) most likely took place along a preexisting lowstand incised valley.
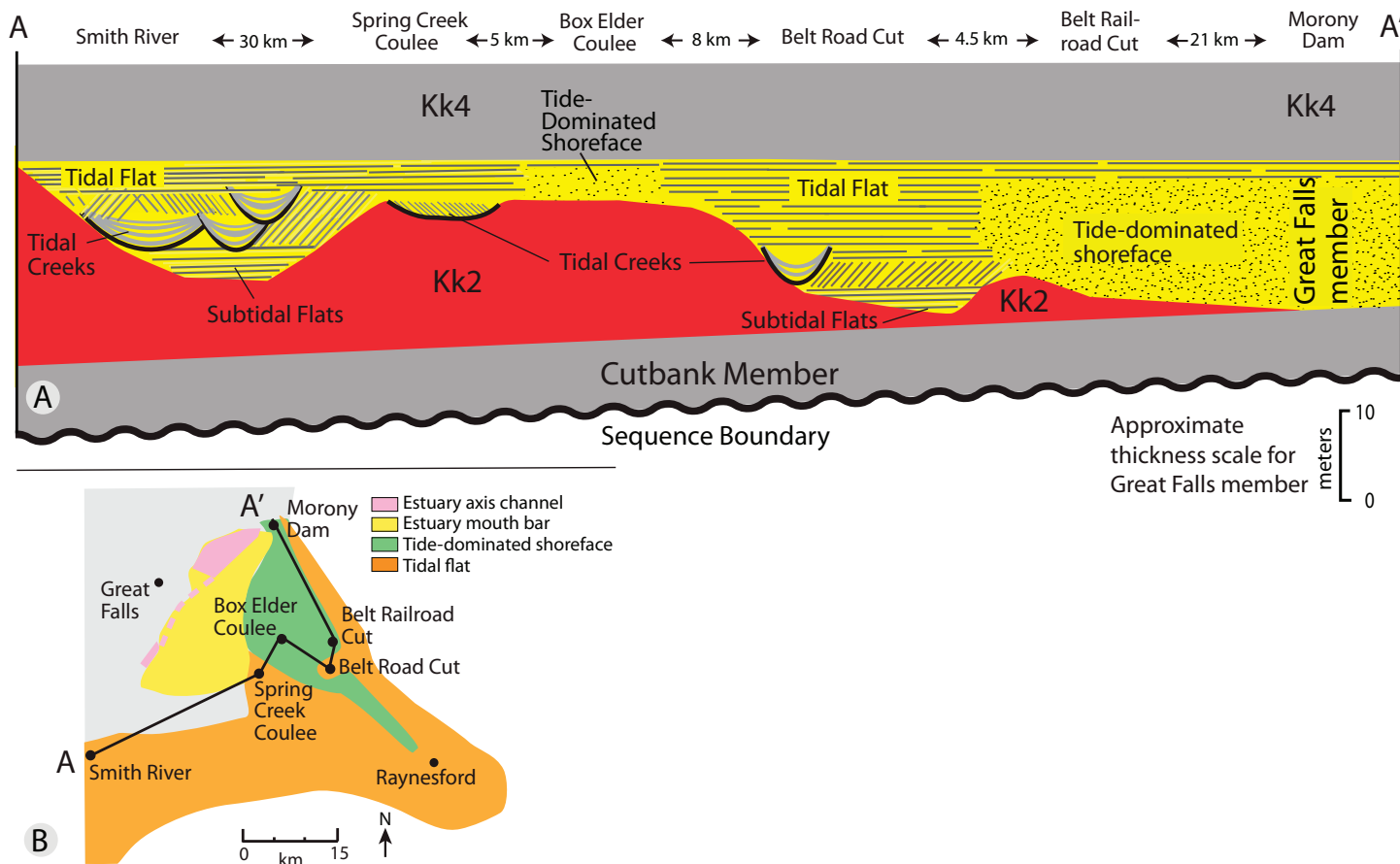
Figure 38. (A) Panel diagram of facies within the Great Falls member along section line A–A' in map B illustrating relationships with incised valleys. The topographic relief along the top of Kk2 is based upon measured sections at each site using the top of the Great Falls as a datum. Because of limited outcrop control, the paleotopography along the Great Falls–Kk2 contact is not intended to represent the actual number and width of incised valleys.

depending upon location. The most common vertical trend is from basal tidal flat (FAm1) to muddy estuary basin (FAm4) facies to FAm3. Near its eastern margin of occurrence (sites CM and CR), the estuary mouth bar typically rests upon very thin estuary mudstone (< 50 cm thick) or tidal creek facies (L14; fig. 15B). In other locales, it directly lies upon nonmarine Kk2 and Cutbank Member lithologies (figs. 37–39). Two types of vertical successions continue upward from the estuary mouth bar deposits. In many locales, a relatively thick (up to 15 m) tidal flat succession (FAm1) caps the estuary mouth bar facies, marking the top of the succession (fig. 8 and Big Bend to Fields Station area in fig. 39). In other locales, the estuary mouth bar facies is erosionally overlain by the estuary axis channel facies (FAm5), which is then followed by thin capping tidal flat deposits (fig. 39).

Along the northeastern side of the basin interior, vertical successions include Cutbank fluvial deposits or remnants of nonmarine Kk2 strata disconformably overlain by tidal shoreface or muddy estuary basin facies. Both of these successions are conformably overlain by Kk4 nonmarine coastal plain deposits. At Morony Dam (MDs3), the shoreface succession is locally truncated by the incised valley (fig. 34, supplementary fig. 1).

Incised Valley

A relatively simple vertical succession makes up the incised valley fill. The succession begins along the paleovalley thalweg with tidally reworked, fluvial channel deposits (FAv1) that disconformably overlie fluvial Cutbank Member sandstone and possibly thin remnant Kk2 lithologies. FAv1 is sequentially overlain by transgressive quartzose sandstone (FAv2) and relatively basin-center mudstone deposits (FAv3). The mudstone is then overlain by thin carbonate lake/pond (FAv4) and fluvial (FAv5) deposits followed by two thin basin-center-type mudstone intervals and paleosol (FAv6). The top of the succession is conformably overlain by nonmarine Kk4 coastal plain deposits (Walker, 1974).
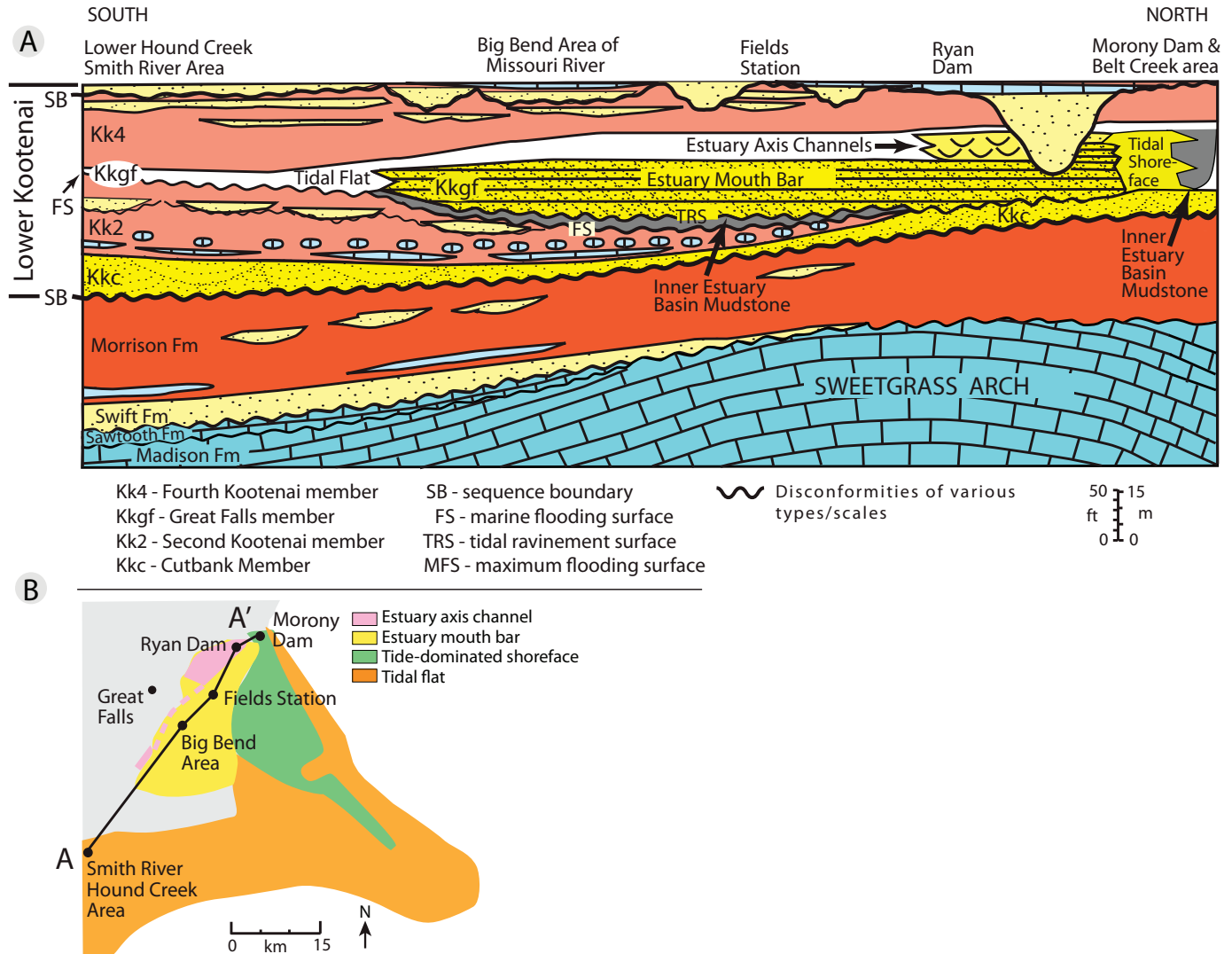
Figure 39. (A) Schematic cross-section of the lower Kootenai Formation and underlying stratigraphic units across the Sweetgrass Arch (A–A' in map B) including facies distribution within the Great Falls member. Also schematized are sequence-stratigraphic surfaces. Modified from Walker (1974) and Schwartz and others (2006).

DEPOSITIONAL MODELS

The main tidal basin and the incised valley exposure represent different scales of accommodation associated with marine flooding of an incised landscape. Our primary focus is upon the depositional model for the main tidal basin, which is treated in greater detail than the incised valley example.

Main Estuary Basin

We interpret the overall Great Falls member to have been deposited in an elongate, low-accommodation, tide-dominated estuary tract. Although depositional models for estuaries are well established, case examples of tide-dominated estuaries in the ancient record are relatively rare (e.g., summary by Tessier, 2012). The following sections provide an assessment of paleogeography (basin geometry and physical boundaries) and depositional architecture of the main estuary basin.

Paleogeography and Pre-Estuary Incision

Although the current definition of an estuary (Dalrymple, 2006) does not require the drowning of an incised valley as originally specified by Dalrymple (1992), the presence of wave and tidal deposits restricted to an incised valley constitutes compelling evidence for estuarine deposition. The following stratigraphic properties of the Great Falls member are consistent with criteria for recognizing incised valleys (Boyd and others, 2006).

The southwestern, southern, and eastern limit of Great Falls exposure coupled with thin tidal flat (FAm1) occurrence along the main basin margins

define a lobate, northward-opening shape for the tidal basin as well as mark the southward limit of marine encroachment (fig. 5). Isopach data define northward thickening (~25 m maximum) and prismatic cross-basin (~50 km maximum width) cross sections that indicate a valley-like paleotopography, consistent with the dimensions of large paleovalley-associated estuaries (Boyd and others, 2006). In addition, the disconformity beneath the Great Falls member indicates a generally concave, pre-depositional landscape developed upon nonmarine Kootenai strata. Kk2 deposits beneath the disconformity were largely to entirely eroded in the central basin compared to basin-margin sites where thin Great Falls tidal flat facies overlie greater thicknesses of fine-grained, nonmarine Kk2 strata (figs. 37, 39; Walker, 1974; Schwartz and others, 2006).

A northward paleotopographic gradient for the region is indicated by northward-directed paleocurrent data from lithic-rich, fluvial sandstone bodies directly below and above the Great Falls member (Walker, 1974), as well as by northward-directed paleocurrent data from lithic-rich, tidally influenced, fluvial facies (e.g., L14; fig. 15A) at the margins of the tidal basin. Overall, a northward-opening depression containing Great Falls member deposits is consistent with lowstand erosion and development of a large-scale, longitudinal, paleovalley tract within the foreland.

Facies Distribution and Tidal Dominance

Estuaries contain a characteristic, although often complicated, mix of marine, estuarine, and terrestrial facies (e.g., Tessier, 2012). Fundamental environmental components and facies of the Holocene-based, tide-dominated estuary model include: (1) a broad, outer estuary axial zone with elongate tidal sand bars and/or sand flats commonly flanked by wave-influenced shorefaces and beaches and (2) a narrower inner estuary axial zone containing a transitional tidal-fluvial channel-sand belt and in some cases, sand flats dominated by upper-flow-regime parallel laminations, and (3) mixed and muddy tidal flat and marsh deposits that can fringe both the inner and outer axial zones (Dalrymple, 1992; Dalrymple and others, 1992, 2012). The inner estuary transitional-channel belt is predicted to have a straight–sinuous–straight channel pattern and mark the area of bedload convergence from both fluvial and marine sources (Dalrymple and others, 1992, 2012).

Many aspects of the Great Falls facies distribution indicate a tide-dominated estuary system. The northward axial trend from the southern basin-margin tidal flat complex (FAm1) to the estuary mouth bar (FAm3) corresponds with the facies distribution in a funnel-shaped open-mouth estuary as opposed to that of a barrier-fronted, wave-dominated estuary (Dalrymple and others, 1992). Although outcrops for testing contemporaneous connectivity of axial tidal channels through the mid-estuary position, that is, between the estuary mouth bar and basin-margin deposits, are missing, quartzose and lithic-rich channel bodies (L9, L14) do transect the tidal flat facies (L1), documenting the presence of inner estuary tidal channels and tidally influenced fluvial channels. The tidal flat facies (L1) in the headward zone was not observed to be upper-flow-regime; however, the quartzose composition does indicate tidal current dominance that resulted in net headward transport of marine sand.

Other facies relationships provide supporting stratigraphic evidence for the presence of axial tidal channels through the inner estuary. Estuary axis channel (FAm5) and flanking muddy inner estuary (FAm4) deposits progradationally cap the estuary mouth bar assemblage, documenting seaward migration of a sinuous channel system and fringing mud-rich zone that were previously headward of the estuary mouth bar. Analogously, the seaward migration of inner estuary zones, including the sinuous tidal channel reach, with progradation upon estuary mouth bar deposits is well documented for Holocene deposits (Woodroffe and others, 1989; Dalrymple and others, 1992). Other evidence for an inner estuary axial channel system in the Great Falls member includes L12 (appendix table 2) within inner estuary basin deposits (FAm4) that underlie the estuary mouth bar (fig. 30). This stratigraphic relationship demonstrates the erosional abutment of axial channel deposits against fringing inner estuary, mudstone-dominated facies, as predicted by Dalrymple and others (1992), and occurrence of a mudstone-dominated estuary zone prior to transgressive superposition by the estuary mouth bar.

The basin-transverse facies trend from estuary mouth bar to tide-dominated shoreface, estuary mudstone, and basin-margin tidal flat environments is also consistent with modern tide-dominated estuary mouth settings. As summarized by Dalrymple and

others (2012), shoreface deposits are not unique to wave-dominated estuaries, but can occur marginal to estuary shoal systems where tidal current influence weakens relative to wave influence. Moreover, they report that at some point along the outer margin, the beach shoreface ends and is abruptly replaced by tidal flats and salt marshes somewhat similar to the Great Falls member pattern (figs. 5, 39). Although a beach shoreface typically develops near the headward end of the elongate sand bar complex, they report that the system can migrate farther into the estuary as the estuary transgresses, most likely explaining the landward extent as illustrated in figure 5.

An aspect of sandy tidal flat (FAm1) occurrence at the basin margin is problematic with regard to the tide-dominated end-member model. We recognized sandy tidal-flat-associated deposits as marking the basin margin rather than mudflat or marsh deposits as predicted in the model. Although FAm1 was present at or near the depositional margin, this may reflect the relative ease of identifying tidal–subtidal sandstone and heterolithic beds rather than thin mudstones representing mudflat or marsh settings.

Sequence Stratigraphic Evidence for Tidal Dominance

Many studies of tide-dominated estuary infill refer to sequence stratigraphy concepts for the recognition of tidal dominance (e.g., Dalrymple, 1992; Zaitlin and others, 1994; Plink-Björklund, 2005; Tessier, 2012). Although outcrop data in this study are insufficient to precisely reconstruct the full distribution of Great Falls member paleoenvironments and are primarily limited to the transgressive and highstand system tracts, the data are sufficient to identify bounding surfaces (transgressive flooding, tidal ravinement, and maximum flooding) and the makeup of the transgressive and much of the highstand system tracts of a higher-order sequence (figs. 37, 39, 40) within the lower Kootenai.

The transgressive flooding surface for the sequence is marked by the basal contact between estuarine deposits (FAm5 and/or FAm1) and underlying nonmarine deposits of Kk2 or the Cutbank Member (figs. 37, 39). Recognition of the maximum flooding surface, and thus the distinction between transgressive and highstand systems tracts, is more problematic.

In landward reaches of the Great Falls estuary, the highstand turnaround point between landward- and seaward-stepping successions was not recognized. However, in outer estuary locations where estuary mouth bar deposits are present, the vertical transition to progradational deposits is well exposed. Here we place the maximum flooding surface within the estuary mouth bar at the contact between the lower channel-bearing sandstone body (L7a) and upper tabular-bedded sandstone body (L7b; fig. 37). As discussed earlier, changes at this position signify a change in sand bar morphology due to progradational estuary filling (Johnson, 1977; Allen, 1982; Harris, 1988; Dalrymple and others, 1992). The vertical facies succession above L7b (either to FAm1 or FAm5-to-FAm1) is consistent with continuing seaward progradaton and thus our placement of the maximum flooding surface.

A distinct tidal ravinement surface underlies the estuary mouth bar, which extends at least 15 km up the estuary axis. The ravinement surface is highly erosional in what seems to be a rising and falling manner and ranges from cutting into underlying inner estuary deposits (FAm4) to partially or completely cutting through nonmarine Kk2 deposits where it overprints the transgressive flooding surface (fig. 37). Moreover, based upon isopach data for the estuary mouth bar deposits (fig. 5), the tidal ravinement surface has a roughly hemi-conical shape that tapers and rises in the headward direction.

The highstand system tract contains facies fundamentally similar to those in the transgressive tract. Major differences from the transgressive system tract include: (1) a reversed vertical facies succession and thus a seaward shift of inner estuarine facies, (2) volumetrically less estuary mouth bar deposits, (3) volumetrically greater sinuous, axial channel deposits, and (4) gradational capping by delta plain Kk4 deposits (Walker, 1974).

Key features of transgressive system tracts in tide-dominated estuaries include: (1) the tract normally contains all sedimentary bodies and facies successions that typify different components of a tide-dominated estuary system and (2) the facies successions demonstrate sea level rise as indicated by a transgressive stacking (landward-shift) pattern (Dalrymple and others, 1992; Zaitlin and others, 1994; Plink-Björklund, 2005; Tessier, 2012). Such is the case with the Great

STUDY AREA

NE Basin Interior (site MDs) ← 21 km → N Basin Interior (site FS) ← 24 km → SE Basin Margin (site BR) ← 38 km → S Basin Margin (site SR) ← 220 km → SW Montana

Sequence boundary of Porter and others (1993)

Coastal floodplain, splay and distributary deposits in deltaic setting.[8]

Incised valley fill

Tidal flat

Estuary Mouth Bar

Tidal flat

Tidal flat

Tidal shoreface

5th Order TST to HST

TRS

Inner Estuary Basin

FS

Debris flow

conglomerate

Paleosols[6]

Lithic fluvial[5]

Paleosols[4]

Lacustrine limestone and dolomite[3]

Paleosol dominant[2]

Lithic braided fluvial[1]

K-J MORRISON FM.

FS

Kk4 / HST

Great Falls mbr / TST

Kk2 / TST / HST

Cutbank Mbr / TST / LST ?

Sequence 3 / Sequence 2 / Sequence 1

Third-Order Sequence

Study area scale 20 m

Upper fine-grained mbr

Paleosols; lacustrine, swamp and fluvial deposits[7]

Lacustrine limestone[6]

Lower calcareous mbr

Paleosols; localized pond, lake, swamp and fluvial deposits[5]

Middle fine-grained mbr

Lithic fluvial[4]

Second sandstone mbr

Paleosols; localized pond, lake, swamp and fluvial deposits[3]

Lower fine-grained mbr

Lithic braided fluvial[2]

First sandstone mbr

Braided-fluvial incised valley fill[1]

Basal cgl. mbr

SW MT scale 100 m

K-J MORRISON FM.

J MORRISON or Tr DINWOODY FM

Cutbank, Kk2 and Kk4 Unit Descriptions

Sequence 3

8. Transition above Great Falls member with upward coarsening from carbonaceous shale to massive red mudstone and interbedded widespread tabular, cross-stratified, red sandstone.

7. Great Falls member - see text.

Sequence 2

6. Dominantly purple and red mudstone paleosols (internal features similar to below); minor gray mudstone.

5. Broadly lenticular lithic-fluvial bodies flanked and interbedded with purple and red mudstone paleosols (similar to 2 below); sandstone horizon rests upon bleached gray erosional surface. Regionally widespread, inversely graded, matrix-supported limestone-mudstone pebble/cobble debris-flow conglomerate.

Sequence 1

4. Dominantly purple and red mudstone paleosols (internal features similar to 2 below), includes kaolinized and silicified beds; minor gray mudstone.

3. Micritic limestone and dolomite dominant. Interbedded with red to purple mudstone paleosol, gray calcareous mudstone, and thin fine-grained fluvial sandstone

2. Red to maroon calcareous mudstone paleosols with horizonation, calcrete nodules, calcified root structures, blocky ped structures, clay cutans, small-scale slickensides and rhizocretions. Also gray mudstone-filled channels and thin oxidized sandstone splays with drab halo structures and root casts.

1. Widespread, coarse, chert-rich, dominantly trough cross-stratified sandstone making up channel bodies of variable thickness upon the sub-Kootenai unconformity. Chert pebbles/cobbles along base.

EXPLANATION

FS - flooding surface
TRS - tidal ravinement surface
LST - lowstand or degradational* system tract
TST - transgressive or transitional* system tract
HST - highstand or aggradational* system tract

〰️1〰️ Disconformities (various types/scales) in chronological order

1,2,3 - lower boundaries of sequences 1, 2, 3

* Nonmarine sequence terminology of Currie (1997)

Lower Kootenai Unit Descriptions

Sequence 3

7. Mudstone paleosols and lacustrine siliciclastics similar to lithofacies association #3 small, isolated sandstone and conglomerate fluvial bodies.

6. Lacustrine micritic limestone interbedded with mudstone and rare thin siltstone and very fine-grained sandstone.

Sequence 2

5. Similar to lithofacies association #3.

4. Widespread lithic-fluvial unit primarily made up of lenticular sandstone and intraformational limestone/mudstone-pebble conglomerate bodies; flanked and interbedded with red/green mudstone paleosols, sandstone splay, and calcareous siliciclastic and silty limestone lacustrine deposits.

Sequence 1

3. Red and green mudstone paleosols with mottling, calcrete nodules, massive bedding and local bioturbation; mixed lacustrine and scattered muddy fluvial siliciclastics.

2. Widespread, coarse, chert-rich, dominantly trough cross-stratified sandstone making up channel bodies of variable thickness upon the sub-Kootenai unconformity. Chert pebbles/cobbles along base.

1. Chert-clast conglomerate locally with capping trough-cross-stratified sandstone, or isolated conglomerate lens encased in mudstone.

Figure 40. Representative stratigraphic sections illustrating the relationship between depositional architecture and system tract designation in the lower Kootenai Formation. The panel extends southward, left to right, from estuary mouth settings to headward, tidal-flat-dominated settings along the southern margins of the study area. At the far right is a tentative correlation with lower Kootenai strata in southwestern Montana. Descriptions and interpretations of lower Kootenai strata in the Great Falls area adapted from Walker (1974), Schwartz and others (2006), Pankowski (2007), this study, and in southwest Montana from Holm and others (1977), DeCelles (1986), and Gresh and others (2017).

Falls member. Although highstand system tracts in modern tide-dominated estuaries differ greatly in terms of facies successions (Tessier, 2012), the facies components of the Great Falls highstand systems tract are fully consistent with tide-dominated estuarine settings and a seaward shift in those environments. The tidal ravinement surface is judged to be one of the most significant stratigraphic features for discriminating between tide-dominated and wave-dominated estuaries (Tessier, 2012). Compared to wave-dominated estuaries, where the tidal ravinement process is restricted to the estuary mouth barrier inlet, tidal currents in tide-dominated estuaries are stronger, scour sediment beneath the relatively widespread estuary mouth bar-and-channel complex, and extend headward where they are produced by erosion along the base of channels associated with sand bars and flats (Zaitlin and others, 1994; Tessier, 2012). The result is a generally concave, headward-narrowing, erosional surface that manifests: (1) partial to complete erosion of transgressed inner estuary deposits, (2) possible amalgamation with the transgressive flooding surface and possibly the sequence boundary, especially in the seaward zone, (3) possible erosion of underlying stratigraphic units, and (4) shallower levels of erosion in the upper reach. Also, in contrast to the wave-dominated highstand systems tract, there is a greater likelihood of preserving tide-dominated sand bodies, in particular, mouthward-extending and capping axial tidal channel deposits showing evidence of tight meandering (e.g., FAm5; Dalrymple and others, 1992; Tessier, 2012). Great Falls member stratigraphy displays these properties.

Axial Trends in Composition and Texture as Evidence for Tidal Dominance in a River-Associated Estuary

The composition and texture of Great Falls and marginal sandstones make up definitive trends along the estuary axis. Tidally influenced, generally northward-directed, fluvial bodies along upper (southern) reaches of the estuary (e.g. L14; fig. 15) supplied coarse-grained, texturally immature, lithic-rich sand to the basin. However, other than along the tidal ravinement surface and for fine- to very fine-grained sublitharenite, intertidal to subtidal sand flat deposits (L3, 4, 5) within the inner estuary mudstone-dominated facies (FAm4), Great Falls member sandstone is highly quartzose. The quartzose sandstone also exhibits a

textural trend from coarse- and medium-grained in estuary mouth bar deposits to fine- and very fine-grained in basin-margin deposits in the upper reaches of the estuary. Associated with the quartz-sand trend, paleocurrent data for the estuary mouth bar and estuary axis channel bodies indicate flood dominance (fig. 9).

The combined compositional, textural, and paleocurrent data document the presence of two sediment-delivery systems that converge along the upper estuary margin and document that the texturally mature quartzose sand underwent net landward movement from outside the estuary mouth. Flood dominance and headward transport of marine sediment is a fundamental property of modern wide-mouth estuaries wherein tidal currents transport bed material through the lower estuary bar field and into more headward regions (Harris, 1988; Dalrymple and others, 2012). In tide-dominated estuaries, tidal currents redistribute the sediment supplied by both river and marine sources, explaining the increased lithic content in some of the Great Falls tidal deposits. Dalrymple and others (1992) also maintained that a net landward movement of sediment derived from outside the estuary mouth is one of the primary features that distinguishes estuaries from delta distributaries, where the net sediment transport is seaward. The fact that the Great Falls estuary was primarily filled with marine-derived sediment during both relative sea level rise and fall indicates that fluvial supply to the estuary system was minimal compared to marine supply.

Incised Valley

The incised valley outcrop is a cross-sectional view of a single paleovalley within the basin-scale estuary tract of the overall Great Falls member. The same exposure has previously served as a generalized example of an estuarine incised valley (Boyd and others, 2006; their fig. 23). The incised valley is part of a tributary network, the valleys of which contain different facies depending upon proximity to the sea (Boyd and others, 2006; their fig. 19). Here we provide a more detailed summary of the environmental succession and sequence properties at this site in order to document the history of paleovalley incision and filling. We also compare the paleogeographic location and depositional model with the main estuary basin.

Facies Succession and Sequence Stratigraphy of the Valley Fill

The base and walls of the incised valley as well as the lateral interfluve erosional surface constitute a lower boundary to an even higher order sequence within the upper part of the Great Falls member. The position of the upper boundary is uncertain, but most likely coincides with the Great Falls member–Kk4 contact. The duration and amount of fluvial incision during lowstand was sufficient to fully truncate preceding Great Falls shoreface deposits, resulting in the deposition of fluvial deposits (FAv1) upon, or nearly upon, Cutbank strata along the valley bottom during the early phase of subsequent sea level rise. The lithic-rich sand in FAv1 was most likely delivered by a northward-flowing stream, analogous in composition and paleoflow direction to fluvial deposits along the margin of the main estuary basin (L14). Tidal structures, wave ripples, and trace fossils of brackish to marine affinity within FAv1 document marine inundation and reworking, thus marking the beginning of a landward stacking pattern from the upper part of FAv1 to FAv2 (transgressive sandstone) and FAv3 (estuary-center mudstone). The upward fining succession represents deepening and the development of low-energy conditions, in what we interpret to be a restricted, mid-estuary setting. The maximum flooding surface is most likely located at the upper limit of transgressive FAv2 sandstone lapping upon the adjacent valley wall and near the base of the adjacent levee deposits that overlie the interfluve surface (fig. 34B). The succession from FAv4 to FAv5 and FAv6, with intermittent reoccurrences of FAv3, marks highstand filling of the paleovalley with an interplay of short-term estuarine mud deposition, fluvial sand influx, and paleosol development. Overall, this sequence is fundamentally similar in scale to incised valley sequences within the Mannville Group (fourth-order sequences of Cant, 1996, 1998).

Depositional Model

The paleovalley infill is most consistent with predicted incised valley lowstand to early highstand deposits for the middle part of a wave-dominated estuary (segment 2 of Boyd and others, 2006; their fig. 19), in particular one that contains a mud-dominated central basin (FAv3) and a prograding, typically lithic-rich, sand-dominated bay-head delta (FAv5, FAv6, and levee deposits).

Exposures for determining relative wave vs. tidal influence at the estuary mouth are missing; however, a lack of tidal current penetration into the headward zone is indicated by the absence of axial inner estuary, tidal channel bodies. Also, thin quartzose sandstone along the valley walls is consistent with a drowned-valley setting located behind a barrier mouth where limited amounts of marine sand are delivered by a combination of flood-tidal and wave transport. The incised valley is spatially associated with the tide-dominated shoreface facies, also suggesting location in part of the overall Great Falls member tract where wave influence was greatest.

DISCUSSION

Lower Kootenai Nonmarine Successions in Relation to the Great Falls Member Sequence

Juxtaposition of the estuarine Great Falls sequence and residual nonmarine deposits of the lower Kootenai Formation provides context for assessing the relationship between relative sea level and nonmarine deposition and for the application of nonmarine system tract concepts. Various associations between tidal deposition during short-term (e.g., fourth-order) late-stage transgressive to early highstand deposition and coeval nonmarine deposition in foreland settings have been demonstrated in several other studies (e.g., Shanley and McCabe, 1993, 1995; Hettinger and others, 1993; McLaurin and Steel, 2000; Plint and others, 2001). For the lower Kootenai, a direct case of coexisting marine and nonmarine deposits may be provided by a lacustrine limestone member that is present to the west and south of the study area and tentatively correlated with quartzose sandstone of the Great Falls member by Walker (1974) and with the Peterson Limestone of Wyoming and Idaho (fig. 2; McGookey and others, 1972; Holm and others, 1977). Using the lacustrine limestone–Great Falls association as a baseline, the remainder of the lower Kootenai sequence is summarized based upon reported facies and comparisons with other foreland successions (e.g., Shanley and McCabe, 1993, 1995; Hettinger and others, 1993; McLaurin and Steel, 2000; Plint and others, 2001).

Lacustrine late-stage transgressive to early highstand association

Although details of stratigraphic relationships are unobservable between the limestone member and the laterally equivalent Great Falls member, correlations and interpretations of Walker (1974) as well as clear evidence for the phenomenon of lake development at higher than maximum flooding levels during late-stage transgression and early highstand in a foreland basin (e.g., Hayes and others, 1994; Currie, 1997; Plint and others, 2001; Boyd and others, 2006, their fig. 21) suggest contemporaneity. In addition, other aspects of Peterson Limestone equivalent deposits, as well as similarity to the lacustrine upper Kootenai "gastropod limestone" (Draney Limestone in Wyoming and Idaho), suggest a causal link to marine encroachment.

Both the Peterson Limestone (lower calcareous member in southwestern Montana) and the Draney Limestone (upper calcareous limestone member or "gastropod limestone" in southwestern Montana; fig. 2; Holm and others, 1977; James, 1980) were deposited in a series of topographic lows along the foredeep to backbulge depozones in southwestern Montana, western Wyoming, and northeastern Idaho (McGookey and others, 1972; Glass and Wilkinson, 1980; Brown and Wilkinson, 1981; Schwartz and DeCelles, 1988). The topographic lows marked areas of differential subsidence (intraforeland basins) adjacent to basement-related positive features providing a paleogeographic scenario well suited for drainage impoundment and lake development (Schwartz and DeCelles, 1988). Immediately west and south of the Great Falls member, the Peterson Limestone equivalent was deposited in topographically irregular and basement-involved foredeep and forebulge regions as later described in this study. In all regions, both of the limestone members overlie and include paleosol-rich units and rare fine-grained isolated fluvial bodies (Glass and Wilkinson, 1980; DeCelles, 1986; Gresh and others, 2017) that signify preceding and concurrent widespread, low-relief floodplain and interfluve surfaces (with a reduced siliciclastic supply) that would be susceptible to lake development (Cohen and others, 2015). Paleocurrent and compositional data for sandstone bodies in the coarser grained Kootenai members (DeCelles, 1986; Schwartz and DeCelles, 1988; paleodrainage reinterpretation by Schwartz and Schwartz, 2013) and detrital zircon data (Laskowski and others, 2013; Quinn and others, 2018) indicate at least periodic through-going fluvial systems for the intraforeland basins, suggesting the likelihood of ex-orheism rather than isolation of individual basins. Of the two limestone members, a direct link to transgression and marine influence is only observable for the Draney and equivalents that contain capping tidal inlet facies and are overlain by a seemingly conformable transition into tidal and marine deposits of the Black-leaf Formation (Walker, 1974; Holm and others, 1977; James, 1980). Overall, Peterson lake-system development was also most likely contemporaneous with, and linked to, late-stage transgression and early highstand associated with the Great Falls member sequence. Strong supporting evidence that increased relative sea level can affect nonmarine systems, including base level and increased accommodation, with lake development during late-stage transgression to early highstand, is provided by Plint and others (2001) for Cenomanian deposits of the western Alberta foreland where lacustrine systems developed at least 200 km upgradient from the coastal margin. Aslan and Autin (1999) demonstrated that eustatic sea level affected changes in Holocene alluvial style, including lake development, up to 300 km from the current coast. Even so, the approximately 600 km length of the lower limestone member/Peterson Limestone cannot be solely explained in terms of sea level change. Other variables potentially influencing Peterson and Draney lake development, e.g., tectonism, climate change, limestone-rich source terrain, and siliciclastic sediment supply, are discussed by Drummond and others (1996) and Zaleha (2006).

Lower Kootenai higher frequency sequences

Stratigraphic properties of the entire lower Kootenai Formation and the relationship to system tracts are summarized in figure 40, and interpretive diagrams for evolution of the stratigraphic succession are shown in figure 41.

Study area

At least three sequences of higher order (possibly fourth-order), including the Great Falls member sequence and two underlying nonmarine sequences, make up the lower Kootenai Formation. Lowstand boundaries of the sequences are marked by a distinct to subtle lowstand erosional surface and incised valleys (fig. 40, disconformities 1, 2, and 3).
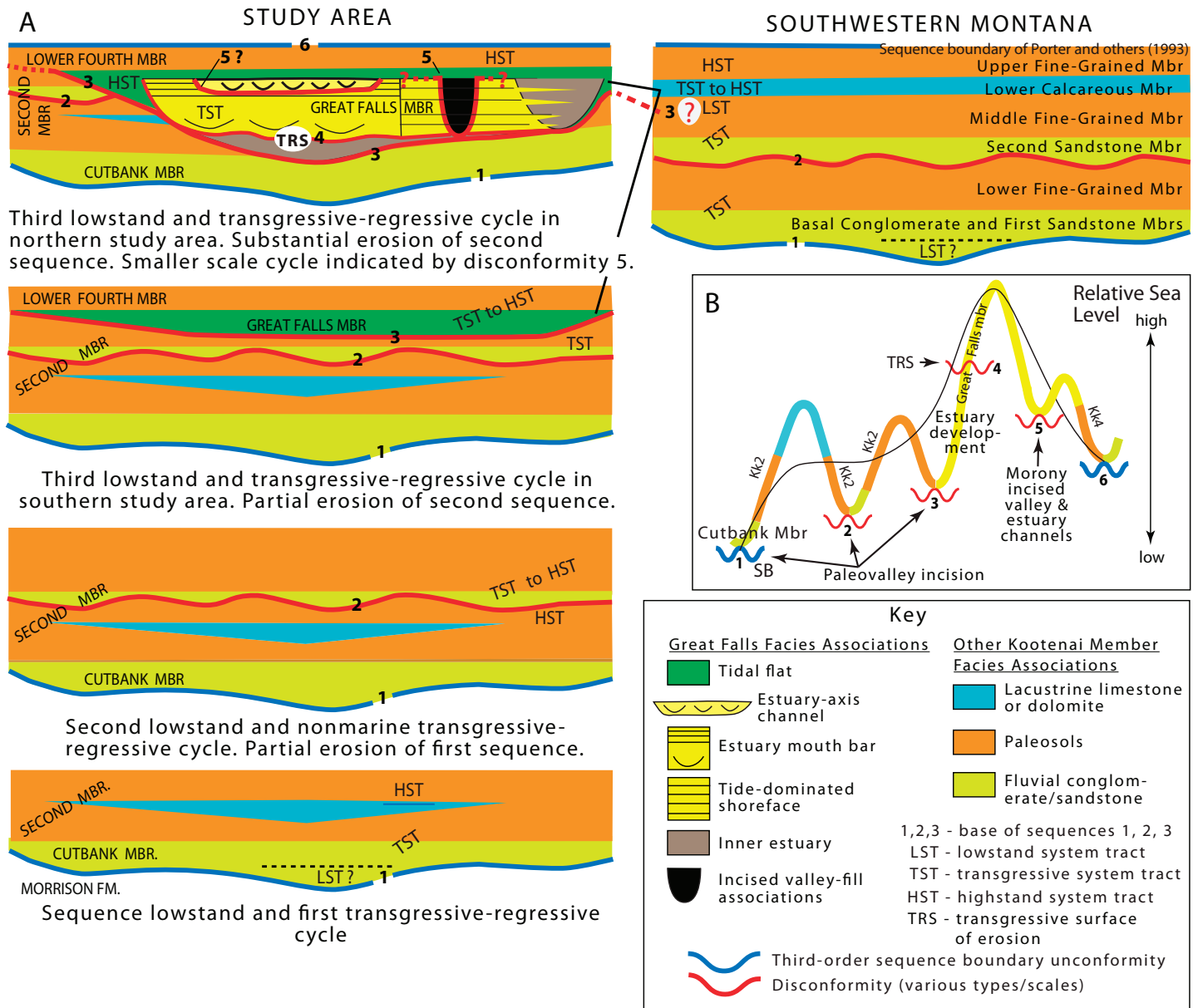
Figure 41. (A) Stratigraphic evolution of the lower Kootenai Formation in western Montana. The panels on the left depict several lowstand erosional events (disconformities 1–3, 5, and 6) and subsequent aggradation in the study area. The top two panels on the left illustrate transects across the estuary mouth (northern) and headward estuary (southern) areas. Disconformity 4 is due to tidal ravinement. The extent and correlation of disconformity 5 is uncertain and details of valley-fill and estuary channel aggradation are discussed in the text. The stratigraphic succession in the study area is tentatively correlated with the distal nonmarine lower Kootenai succession in southwestern Montana in the panel on the upper right. (B) Schematized third-order (thin black line) and fourth-order (thick colored lines) relative sea-level cycles based upon facies successions in the Great Falls area. Colored line segments indicate nonmarine facies associations (right side of key) and undifferentiated estuarine facies (yellow) of the Great Falls member. Disconformity 5 may represent a fifth-order cycle.

Sequence 1

The sub-Kootenai unconformity and an upward succession from basal braided-fluvial (Cutbank Member) deposits (fig. 40, unit 1) to a paleosol-dominated interval (unit 2) followed by limestone, dolomite, and siliciclastic lacustrine deposits (unit 3) and a subsequent paleosol interval (unit 4) mark lowstand erosion

followed by a primarily transgressive to highstand system tract. Lowermost coarse fluvial deposits of the Cutbank Member may, in part, represent lowstand aggradation in paleovalleys, but are more likely associated with base-level rise, (e.g., described by Shanley and McCabe, 1994), due to transgression of the Boreal Sea coupled with foreland subsidence. The paleosol-

dominated and lacustrine intervals indicate a diminished siliciclastic sedimentation rate and increased accommodation in the overall low-accommodation part of the foreland. Sea level rise was insufficient to inundate the study area; however, as established by the Great Falls member–lacustrine limestone correlation, a short-term highstand of the nearby Boreal Sea resulted in upgradient freshwater ponding and lake development during unit 3 deposition. Overall, sequence 1 reflects coastal plain onlap and lake development followed by coastal retreat during a short-term cycle of southward migration of the Boreal Sea, similar to the nonmarine sequence model of Boyd and others (2006; their fig. 21).

Sequence 2

A second erosional surface (disconformity 2) overlain by an upward succession from widespread, fine-grained fluvial sandstone bodies and a peculiar widespread, thin, debris-flow bed (unit 5) to a paleosol-dominated interval (unit 6) makes up part of a transgressive systems tract in a differentially truncated sequence. As shown in figure 40, disconformity 3 at the base of the Great Falls member sequence truncates all or part of Kk2 depending upon location in the basin.

Sequence 3 Great Falls member sequence

The Great Falls member and overlying delta plain deposits of Kk4 make up the final sequence, similar in scale to the previous two. Because of a lack of regional stratigraphic detail, we represent the incised valley succession at the Morony Dam site as an even higher-order sequence within sequence 3. Overall, sequence 3 represents a cycle of marine inundation and retreat that preceded the major Albian transgression and deposition of the Blackleaf Formation.

Regional Aspects

The lower Kootenai Formation of southwestern Montana is entirely nonmarine and contains lithofacies fundamentally similar to those of nonmarine units in the Great Falls area, including presence of the lower calcareous (or lower limestone) member (fig. 40, right side). Although sedimentologic detail is relatively sparse (Holm and others, 1977; DeCelles, 1986; Schwartz and DeCelles, 1988; Gresh and others, 2017), the vertical lithofacies trends appear to make up three higher-order sequences corresponding to those in

the Great Falls area. The southwestern Montana trends are consistent with findings for other studies where marine base level is interpreted to have controlled upgradient nonmarine deposition (e.g., Shanley and McCabe, 1993, 1994; Plint and others, 2001). Thus, it is most likely that sea level exerted at least partial control upon distal, longitudinal, upgradient (at least 220 km) deposition in the structurally and paleotopographically complex foredeep region to the south (fig. 41).

Paleolandscape Control upon Great Falls Estuary Location

Correspondence between sub-Kootenai drainage systems and the distribution of lower Kootenai fluvial and brackish marine deposits demonstrates paleotopographic control upon depositional environments. Basal Kootenai (Cutbank Member) and equivalent trunk-fluvial deposits lie within and between the Cutbank (*Taber–Cutbank* in southern Canada) and Whitlash drainage basins that extend from northern Montana into southern Alberta (figs. 3, 42; Dolson and Piombino, 1994; Zaitlin and others, 2002). Along the eastern side of the Kevin–Sunburst dome, subsurface Cutbank deposits are seemingly sparse or absent in the Whitlash drainage (Schulte, 1966). However, relatively thick trunk-fluvial Cutbank deposits are present within the paleo-upstream parts of the Whitlash drainage along the eastern side of and across the South Arch (this study area), as well as along the western side of the South Arch (Mudge and Rice, 1982; Berkhouse, 1985).

Similarly, the marine Great Falls member is present within the Whitlash and Cutbank paleovalley tracts along both sides of the Sweetgrass Arch, and it crops out across the South Arch. The Early Cretaceous sea flooded the Sweetgrass Arch area from the north, with bathymetric axes approximately north–south along the flanks of the Sweetgrass Arch in the Whitlash and Cutbank paleotopographic lows (fig. 42).

Overall, the topography during Great Falls member deposition was partially dependent upon pre-Kootenai valley incision and reoccupation of lower Kootenai valley tracts in a spatially persistent system. Similarly, an incisional valley landscape upon the sub-Cretaceous unconformity in the contiguous Sweetgrass–Bow Island Arch region of Alberta controlled subsequent Early Cretaceous fluvial incision and

Basal Kootenai Cutbank Member
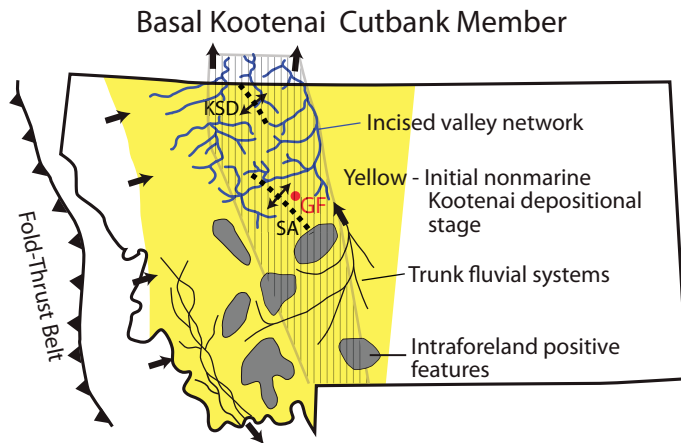
Axial, lithic-rich, coarse-grained sandstone and conglomerate fluvial systems dominate. The incised valley pattern (blue) on the sub-Kootenai unconformity reflects the forebulge and associated positive elements of the Sweetgrass Arch.

Sunburst/Great Falls Members and Associated Environments
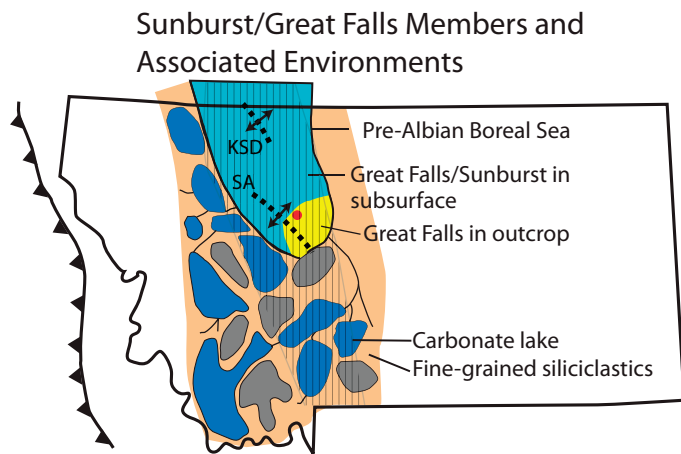
Maximum pre-Albian transgression along forebulge depozone. Tide-dominated Great Falls member sedimentation in study area; carbonate/dolomite lake, paleosol and localized low-gradient stream development to the west and in southwestern MT.

Location of forebulge based upon this study, DeCelles (2004) and Fuentes et al. (2011).

KSD - Kevin-Sunburst Dome of Sweetgrass Arch system
SA - South Arch of Sweetgrass Arch system
GF - Great Falls
Drainage synthesis based upon Walker (1974), Berkhouse (1985), DeCelles (1986), Dolson and Piombino (1994), Schwartz and Schwartz (2013).

Figure 42. Paleogeographic maps illustrating the pre-Kootenai fluvial-incision and initial fluvial-depositional stage (Cutbank Member) and subsequent marine stage of sedimentation (Great Falls member) in relation to the Early Cretaceous forebulge.

estuarine deposition within paleovalleys (e.g., Wood and Hopkins, 1989; Hayes and others, 1994; Arnott and others, 2000; Ardies and others, 2002; Lukie and others, 2002; Zaitlin and others, 2002; Stelck and others, 2007; Miles and others, 2012).

Foreland Depozones and Foreland Dynamics

Morrison Formation and lower Kootenai deposition took place during an early nonmarine-dominated phase (~155–110 Ma) of prolonged foreland basin development that lasted until ~55 Ma (Monger, 1989; DeCelles, 2004). Isopach and subsidence analysis place the timing of forebulge development along the Sweetgrass Arch prior to earliest Kootenai deposition (DeCelles, 2004; Fuentes and others, 2011). The marine Great Falls member was deposited in an elongate zone restricted to alongside and upon much of the Sweetgrass Arch (fig. 42). Thus, a spatial association exists between the ancestral Arch, the earliest Cretaceous forebulge, and the narrow highstand seaway. The spatial distribution of lower Kootenai depositional environments, in particular those of the Great Falls member and correlative strata, and the incised valley patterns on the sub-Kootenai unconformity, reflect paleotopographic patterns that bear a meaningful relationship to tectonic features and foreland dynamics. The paleotopography of the Kootenai foreland is considered on two scales: within the forebulge depozone and across the foredeep–forebulge–backbulge transect.

Forebulge Depozone Topography and Structural Control upon Fluvial Incision

In addition to the general pattern of axial trunk drainage along both sides of the forebulge, details of paleotopography within the forebulge and relationships to structural features are evident through the comparison of the sub-Kootenai incised valley pattern and components of the Sweetgrass Arch (fig. 3). Headwater drainages clearly show divergence away from, or routing around: (1) the Kevin–Sunburst dome, (2) a topographically positive feature bound by the Pendroy Fault and Scapegoat–Bannatyne trend, and (3) the South Arch. The transverse drainage that transects the northwestern end of South Arch and parallels the Scapegoat–Bannatyne trend is interpreted as a possible watergap that formed where the trunk system cut through South Arch, probably along zones of weakness related to the Scapegoat–Bannatyne trend. Maximum erosional relief on the sub-Kootenai

unconformity surface ranged from about 45 to 170 m (Dolson and Piombino, 1994; their fig. 13). Across the southern part of the South Arch, black shale and coal of the Neocomian upper part of the Morrison Formation (fig. 2) were preserved along another zone of structural weakness. Overall, the offset and orientation of the positive-relief paleogeographic zones (fig. 3) and the corresponding offset and orientation patterns of the divergent headwater drainage systems clearly demonstrate that both the antiformal components of the Sweetgrass Arch and major transverse structures influenced fluvial incision and deposition prior to and during Early Cretaceous time. Overall, the forebulge depozone consisted of elongate, centrally located, positive-relief landscape features flanked by fluvial systems with net-northward axial drainage.

The estuarine pathway during Great Falls deposition was inherited from pre-Cutbank incision through continued reoccupation of the original paleovalley tracts that were largely controlled by pre-Cutbank structures and associated differential erosion of folded strata within the Sweetgrass Arch. It is established that crustal inhomogeneity can affect the flexural profile, control location of the forebulge, and that flexure-caused reactivation of intraforeland structures can enhance control upon drainage patterns (Catuneanu, 2004; DeCelles, 2012). Similarly, the mid-Cenomanian forebulge of the western Canada foreland basin was positioned along the ancestral Peace River Arch and is interpreted to have had sufficient relief to deflect rivers and cause valleys to be axially oriented (Plint and Wadsworth, 2006).

Forebulge Elevation Relative to Foredeep and Backbulge Elevation

Paleocurrent, channel trend, and provenance data for lower Kootenai fluvial bodies (Oakes, 1966; Mudge and Sheppard, 1968; Mudge, 1972; Berkhouse, 1985; Fuentes and others, 2011), in combination with sub-Kootenai drainage patterns (fig. 3), document transverse drainage across the foredeep into the forebulge zone. Thus, the marginal zones of the forebulge were topographically lower than the foredeep. The distribution of marine Great Falls deposits compared to the depositional settings of laterally equivalent deposits provide further evidence of the relative elevation trend across the entire foredeep–forebulge–backbulge transect. Both east and west of the marine

lower Kootenai deposits, the lateral change to alluvial plain or alluvial fan deposits (Oakes, 1966; Walker, 1974; Mudge, 1972; Berkhouse, 1985; Dolson and Piombino, 1994) indicates that much of the forebulge depozone made up an area topographically lower in elevation than the adjacent foreland zones.

Forebulge Evolution—Interactive Static Flexure and Dynamic Subsidence

Several properties of the Kootenai foreland system, including paleolandscape, basin-fill status, and the distribution of sedimentary fill, place significant constraints upon interpretations of foreland evolution, especially with regard to forebulge development. Foremost among these is a topographic gradient in which the forebulge depozone was lower in elevation than adjacent depozones with axial trunk-fluvial systems marginal to a centralized higher zone above the Sweetgrass Arch. Basin-fill status, both prior to and following unconformity development, is important to the consideration of sediment distribution and topographic evolution. Widespread, nonmarine, Jurassic upper Morrison deposits beneath the sub-Kootenai unconformity are interpreted to represent an overfilled foreland system (DeCelles and Burden, 1992; Currie, 1997; DeCelles, 2004; Fuentes and others, 2011). Continued overfilled status of the foredeep during lower Kootenai time is evidenced by the widespread distribution of continental deposits with oblique to transverse (eastward) paleoflow across the foredeep (Oakes, 1966; Mudge, 1972; Walker, 1974; Berkhouse, 1985; Fuentes and others, 2011) into the forebulge-associated longitudinal drainage system rather than into a foredeep axial system as would be the case with an underfilled basin (Jordan, 1995; Catuneanu, 2004). With regard to the relative roles of static load-induced flexure and dynamic subsidence, the presence of widespread lower and upper Kootenai deposits above the foredeep–forebulge–backbulge flexural system requires system-wide accommodation driven by dynamic subsidence during that depositional period (DeCelles, 2012; Catuneanu, 2004, 2018). Sedimentary fill, including coarse fluvial bodies at the base of the lower Kootenai sequences, and fine-grained nonmarine highstand deposits, including paleosols and carbonates, bear implications regarding the relationship among sediment supply, sediment distribution, and base level effects upon gradient.

Two alternative explanations of foreland evolution are proposed based upon conventional concepts involving interactive static flexure and dynamic subsidence in a retroarc setting (DeCelles and Giles, 1996; DeCelles, 2012; Catuneanu, 2018). One model includes *orogenic loading and erosional unloading (quiescence)* as primary controls upon topographic low development across the forebulge depozone (fig. 43, stages B–C; modified from Catuneanu, 2018, his fig. 3, Case II). Alternatively, a simple *orogenic loading model* with differential erosion across the foredeep–forebulge–backbulge transect may have produced a similar topographic response (fig. 43, stage B').

Several stages of evolution are common to both models shown in figure 43. An initial stage shows early sub-Kootenai unconformity development upon an overfilled basin following post-Morrison deposition during a period when dynamic subsidence had greatly decreased (fig. 43, stage A; Currie, 1998; DeCelles, 2004; Fuentes and others, 2011). With subsequent orogenic loading and flexural uplift greater than dynamic subsidence, the flexural bulge migrated eastward, stabilizing along basement inhomogeneities (Sweetgrass Arch complex) and causing variable uplift and initial to full erosional incision of sub-Kootenai drainages in strata capping the reactivated basement blocks (fig. 43, stages B and B'). Also similar in both models are the stages for lower and upper Kootenai deposition, wherein widespread accommodation resulted from significantly increased dynamic subsidence such that flexural uplift was exceeded (fig. 43, stages D, C', and E). The lower and upper Kootenai stages differ in that a marked clastic-wedge geometry for upper Kootenai deposits (Walker, 1974), compared to a widespread, relatively thin, and irregular-tabular geometry for lower Kootenai deposits, reflects significant orogenic reloading with dynamic subsidence reinforcing increased flexural subsidence in the foredeep. Increased sediment input from the orogen during upper Kootenai time resulted in continued basin overfilling, nonmarine

sedimentation, and first-time igneous/metamorphic grain influx (Walker, 1974; Fuentes and others, 2011).

In the orogenic loading–erosional unloading model, topographic inversion is predicted to develop across the foreland under the conditions of erosional unloading (quiescence), flexural uplift > dynamic subsidence, and a full to nearly full foredeep (fig. 43, stage C; Catuneanu, 2004, 2018). Tectonic quiescence occurred prior to and during deposition of the Mannville (Kootenai equivalent; Paně and van der Pluijm, 2015; Tufano and Pietras, 2017). During unloading, the rates of isostatic rebound are highest in the proximal foredeep and gradually decrease toward the foredeep–forebulge hinge, beyond which slow flexural subsidence of the forebulge is reinforced by dynamic subsidence. Because of this differential, the topographic profile of an overfilled foreland does not follow the shape of the underlying flexural profile and the top of foredeep infill becomes more elevated than the forebulge depozone, which becomes a topographic low, or "foresag" of Catuneanu (2004, 2018). The topographic low is restricted to the forebulge zone (Catuneanu, 2018).

During the period of topographic low development in both models (fig. 43, stages C and B'), erosional processes would dominate during lowstands and result in a forebulge-centric drainage system with increasingly higher energy fluvial systems toward the forebulge depozone. This enhanced differential erosion along the unconformity surface and downstream concentration of coarser material (Catuneanu and others, 1999), as demonstrated by fluvial bodies at the base of the higher-order sequences. During highstands, increased base level would promote the deposition of fine sediment, and with increased dynamic subsidence (fig. 43, stages D and C'), proximal trapping of coarser sediment in the foredeep would promote reduced sediment influx in the more distal foreland area.

Additional models for development of a topographically higher, nonmarine, foredeep depozone and

Figure 43 (opposite page). Schematized alternative models for evolution of the overfilled Late Jurassic to Early Cretaceous foreland system as influenced by temporal variations in interactive static and dynamic loading. Succession A-B-C-D-E includes orogenic loading and erosional unloading events prior to lower Kootenai deposition whereas succession A-B'-C'-E simply involves orogenic loading and continued loading prior to and through lower Kootenai deposition. In both scenarios, orogenic loading increases at the time of upper Kootenai deposition. The red rectangle marks the vicinity of the study area. Static vs. dynamic loading history during Morrison deposition and early post-Morrison erosion based upon Currie (1998), DeCelles (2004), and Fuentes and others (2011).

E

upper Kootenai

Load (+)

INCREASED OROGENIC LOADING & UPPER KOOTENAI DEPOSITION

Dynamic subsidence > flexural uplift.
Early major loading of next tectonic cycle; dynamic subsidence counteracts flexural uplift in forebulge resulting in system-wide accommodation and upper Kootenai deposition/preservation. Greater dynamic subsidence and reinforcement of flexural subsidence in foredeep and increased sediment input from orogen results in continued foredeep overfilling, clastic-wedge foredeep geometry, and first-time igneous/metamorphic grain influx.

C'

lower Kootenai

Load (+)

CONTINUED OROGENIC LOADING, INCREASED DYNAMIC SUBSIDENCE, & LOWER KOOTENAI DEPOSITION

Dynamic subsidence > flexural uplift.
Increased dynamic subsidence results in system-wide accommodation, proximal coarse-sediment trapping, maintenance of topographic trend, and system-wide lower Kootenai deposition/preservation. Minor differential subsidence across foreland results in minor lower Kootenai thickening to west.
Regional drainage toward and axially along forebulge; marine inundation along forebulge topographic low with increase in sea level.

B'

?

Load (+)

Foredeep — Forebulge — Backbulge

OROGENIC LOADING - POST-MORRISON

Flexural uplift > continued negligible dynamic subsidence.
Assumes forebulge arrival at Sweetgrass Arch prior to Kk deposition. Proximal sediment trapping kept pace with proximal foredeep subsidence resulting in maintenance of low topographic gradient across foredeep.
Widespread erosion continues; variable uplift and maximum incision of sub-Kootenai drainages in strata capping flexurally reactivated basement blocks; erosion down to upper Paleozoic strata depending upon location; earliest and coarsest lower Kootenai deposition in incisional lows.
Regional drainage toward and axially along forebulge; topographic low with centralized high develops above flexural bulge.

Legend:

+ – Increase or decrease of orogenic load

Sector of lithospheric profile subject to static-flexure uplift

Direction of differential uplift - flexural vs. dynamic subsidence

Direction of differential subsidence - flexural vs. dynamic subsidence

- - - - sub-Kootenai unconformity

D

lower Kootenai

for positive load

for negative load

Load (+ or –)

UNLOADING or EARLY RENEWED LOADING - EARLY KOOTENAI

Dynamic subsidence > flexural uplift.
Dominance of dynamic subsidence with minor change in erosional unloading or early renewed orogenic loading results in maintenance of topographic trend, system-wide accommodation, coarse-sediment trapping in proximal foredeep, and widespread lower Kootenai deposition/preservation. Minor differential subsidence across foreland results in minor lower Kootenai thickening to west.
Regional drainage toward and axially along forebulge; marine inundation along forebulge topographic low during high sea level.

C

late-stage sub-Kootenai unconformity

Load (–)

EROSIONAL UNLOADING - PRE-KOOTENAI

Flexural uplift > dynamic subsidence.
Assumes erosional unloading of the orogen prior to Kootenai deposition. Reversed flexural motion coupled with dynamic subsidence promotes steepening of topographic gradient across foredeep and development of widespread low region across flexural forebulge.
Regional drainage toward and axially along forebulge; widespread erosion and sediment bypassing dominates; greater incision along axial drainages with maximum erosion down to upper Paleozoic strata; earliest and coarsest lower Kootenai deposition in incisional lows.

B

Load (+)

Foredeep — Forebulge — Backbulge

OROGENIC LOADING - POST-MORRISON

Flexural uplift > continued negligible dynamic subsidence.
Assumes forebulge arrival at Sweetgrass Arch prior to Kk deposition. Proximal sediment trapping kept pace with proximal foredeep subsidence resulting in maintenance of low topographic gradient across foredeep.
Widespread erosion continues; variable uplift and early incision of sub-Kootenai drainages in strata capping flexurally reactivated basement blocks.

A

topographic profile

Jurassic Morrison Fm and Ellis Group

lithospheric profile

Foredeep — Forebulge* — Backbulge*

Sweetgrass Arch

initiation of sub-Kootenai unconformity

EARLY SUB-KOOTENAI UNCONFORMITY DEVELOPMENT POST-MORRISON

Dynamic subsidence ceased or greatly decreased resulting in mild widespread uplift and unconformity initiation across much of Western Interior.**

* Flexural zone at time of Morrison deposition

** Currie (1998); DeCelles (2004); Fuentes et al. (2011)

a topographically lower cratonward foreland include foredeep overfilling with dynamic subsidence greater than flexural loading (Catuneanu, 2018) or situations where subsidence is interpreted to be driven mainly by sedimentary loading during a period of late-stage orogenic unloading (Yang, 2011). However, discrepant with the lower Kootenai, the low topographic zone in both of those cases is much wider (up to 800 km) than forebulge depozones (up to 300 km) and extends, typically beneath a wide shallow seaway, across the forebulge and backbulge flexural zones to the craton with bathymetric axes that lie within the backbulge flexural zone.

Other examples of topographic low development above a flexural forebulge have been reported for Late Cretaceous–Paleocene deposits in western Canada (Catuneanu and others, 1999, 2000) and late Albian deposits in Wyoming and Utah (Dolson and Muller, 1994; Currie, 1998; Uličný, 1999). In Wyoming and Utah, the forebulge also underwent axial-fluvial incision and controlled marine invasion from the north, facilitating estuarine filling of incised valley complexes. Catuneanu and others (1999, 2000) call upon orogenic unloading and interactive static flexure and dynamic subsidence for development of the western Canada forebulge low.

CONCLUSIONS

The stratigraphic succession in the lower Kootenai Formation provides a basis for reinterpreting Early Cretaceous foreland basin history in the study area and exemplifies the dependency of basin evolution and facies distribution upon tectonics, sea level, and incisional landscape development.

Tide-dominated deposits of the Great Falls member mark a short-lived Early Cretaceous transgression of the Boreal Sea into the nonmarine-dominated Cordilleran foreland of the northwestern United States. Paleocurrent data from fluvial bodies in nonmarine lower Kootenai members demonstrate northward axial drainage along this part of the foreland. The Great Falls member seaway opened toward the north, and paleocurrent data demonstrate that southwest-dominant tidal currents resulted in headward transport of marine quartzose sediment reworked from a northern cratonic source. In contrast, the lithic-rich composition of fluvial sandstone and conglomerate in adjacent Kootenai strata is consistent with an orogenic provenance to the south, southwest, and west.

Studied exposures were deposited in two end-member spaces: (1) a large-scale, or main, tide-dominated, estuary basin (~30 km maximum width) and (2) a small (~240 m wide), tidally influenced estuarine valley within the interior of the antecedent main estuary basin area. The main estuary basin resulted from maximum highstand during lower Kootenai deposition, whereas the small-scale estuary marks a lowstand to highstand cycle of smaller magnitude that occurred during final withdrawal of the Boreal Sea. The estuarine incised valley is analogous to estuarine paleovalleys that developed along the perimeter of the large-scale basin and reflects the presence of a wider main estuary system in the subsurface to the north.

The vertical succession of main estuary basin facies is consistent with tract development in a tide-dominated, estuarine, transgressive to highstand system. In the north, the transgressive system tract consists of a disconformable base, tidal flat and inner estuary basin facies, and an overlying ravinement-based estuary mouth bar sandstone body and laterally adjacent tide-dominated shoreface deposits. The highstand system tract contains facies of the moribund estuary mouth bar and overlying estuary axis channel bodies, tidal flat deposits, and delta plain facies of the Kk4 member. In the south, the thinner transgressive to highstand tract is marked by a disconformable base, tidal flat-and-channel deposits, and deltaic facies of the Kk4 member. In addition to the incised valley fill, high-frequency sea level cycles during Great Falls member deposition are also recorded by stacked upward coarsening tidal shoreface deposits, stacked estuary axis channel successions, reversing progradational-to-transgressive tidal flat cycles near the basin center, and stacked progradational, tidal flat successions along the basin margin. The Great Falls member is correlative with west-adjacent lacustrine carbonates, the lower Kootenai lacustrine limestone in southwestern Montana, and the Peterson Limestone of Idaho. Thus, a link between transgression, base-level rise, and marine to upgradient lake development is evident and may allow for correlation in the overall foreland basin as has been demonstrated for short-term, marine-incursion-related tidal deposits and correlative nonmarine strata in other foreland deposits.

Incised valley patterns upon the sub-Kootenai unconformity and the lateral distribution of estuarine Great Falls and bounding nonmarine facies document that the basement-involved Sweetgrass Arch, axial trunk-fluvial drainage systems, and Great Falls estuarine tract were within a longitudinally oriented topographic low situated atop the forebulge. The Late Jurassic and Early Cretaceous foreland basin was overfilled during and following forebulge migration into the area. Forebulge stasis during lower and upper Kootenai deposition most likely represents flexural anchoring along the basement heterogeneity. Topographic low development above the forebulge prior to lower Kootenai deposition may have resulted from a stage of orogenic unloading wherein isostatic adjustment of the filled foredeep resulted in an elevated foredeep surface and dynamic reinforcement of the subsiding flexural bulge resulted in a surficial topographic low. Alternatively, the low topographic zone may have been a result of continued orogenic loading with maximized differential erosion above the flexural forebulge. In either case, drainage from the foredeep and backbulge was toward the forebulge, where it was diverted to the north along two axial paleovalley tracts. This resulted in greater fluvial incision along the forebulge zone during lowstands, widespread nonmarine deposition during higher base levels, and marine invasion along the longitudinal paleovalley tracts during maximum sea level when the Great Falls member was deposited.

ACKNOWLEDGMENTS

REFERENCES CITED

Allen, J.R.L., 1980, Sandwaves: A model of origin and internal structure: Sedimentary Geology, v. 26, p. 281–328.

Allen, J.R.L., 1982, Sedimentary structures, their character and physical basis, volume II: Developments in Sedimentology, v. 30 B: Amsterdam, Netherlands, Elsevier, 663 p.

Allen, G.P., 1991, Sedimentary processes and facies in the Gironde estuary: A recent model for macrotidal systems, *in* Smith, D.G., Reinson, G.E., Zaitlin, B.A., and Rahmani, R.A., eds., Clastic tidal sedimentology: Canadian Society of Petroleum Geologists Memoir 19, p. 29–40.

Anderson, R., 1985, Clastic facies models and facies analysis: Geological Society of London Special Publications, v. 18, no. 1, p. 31–47.

Ardies, G.W., Dalrymple, R.W., and Zaitlin, B.A., 2002, Controls on the geometry of incised valleys in the Basal Quartz unit (Lower Cretaceous), Western Canada Sedimentary Basin: Journal of Sedimentary Research, v. 72, no. 5, p. 602–618, doi: https://doi.org/10.1306/032101720602

Arnott, R.W.C., Zaitlin, B.A., and Potocki, D.J., 2000, Geological controls on reservoir distribution in the Lower Cretaceous Basal Quartz, Chin Coulee–Horsefly Lake area, south-central Alberta: Bulletin of Canadian Petroleum Geology, v. 48, no. 3, p. 212–229, doi: https://doi.org/10.2113/48.3.212

Arnott, R.W.C., Zaitlin, B.A., and Potocki, D.J., 2002, Stratigraphic response to sedimentation in a net-accommodation-limited setting, Lower Cretaceous Basal Quartz, south-central Alberta: Bulletin of Canadian Petroleum Geology, v. 50, p. 92–104, doi: https://doi.org/10.2113/50.1.92

Aschoff, J.L., Olariu, C., and Steel, R.J., 2016, Recognition and significance of bayhead delta deposits in the rock record: A comparison of modern and ancient systems: Sedimentology, v. 65, p. 62–95, doi: https://doi.org/10.1111/sed.12351

Aslan, A., and Autin, W.J., 1999, Evolution of the Holocene Mississippi River floodplain, Ferriday, Louisiana: Insights on the origin of fine-grained floodplains: Journal of Sedimentary Research, v. 69, p. 800–815.

Babcock, L.E., Wegweiser, M.D., Wegweiser, A.E., Stanley, T.M., and McKenzie, S.C., 1995, Horseshoe crabs and their trace fossils from the Devonian of Pennsylvania: Pennsylvania Geology, v. 26, no. 2, p. 2–7.

Banerjee, I., and Kalkreuth, W., 2002, Sedimentology, sequence stratigraphy, organic petrology, geochemistry, and palynology of Mannville Group coals in south-central Alberta: Geological Survey of Canada Bulletin 571, 53 p., doi: https://doi.org/10.4095/213902

Bartram, J.G., and Erdmann, C.E., 1935, Natural gas in Montana, *in* Lay, G.A., ed., Geology of Natural Gas—A symposium: American Association of Petroleum Geologists Special Publication 7, p. 245–254.

Berkhouse, G.A., 1985, Sedimentology and diagenesis of the Lower Cretaceous Kootenai Formation in the Sun River Canyon area, northwestern Montana: Bloomington, Indiana University, M.S. thesis, 151 p.

Bjerstedt, Thomas W., 1987, Trace fossils indicating estuarine deposystems for the Devonian–Mississippian Cloyd Conglomerate Member, Price Formation, central Appalachians: PALAIOS, v. 2, p. 339–349.

Birkland, P.W., 1999, Soils and geomorphology: New York, Oxford University Press, 430 p.

Blakey, R.C., 2014, Paleogeography and paleotectonics of the Western Interior Seaway, Jurassic–Cretaceous of North America: AAPG Datapages, Search and Discovery Article #30392. http://www.searchanddiscovery.com/documents/2014/30392blakey/ndx_blakey.pdf [Accessed March 12, 2019].

Blakey, R.C., and Umhoefer, P.J., 2003, Jurassic–Cretaceous paleogeography, terrane accretion, and tectonic evolution of western North America: Geological Society of America Abstracts with Programs, v. 35, no. 6, p. 558; images modified from this poster session at http://plate-tectonic.narod.ru/terranesswamerphotoalbum.html [Accessed March 12, 2019].

Boyd, R., Dalrymple, R.W., and Zaitlin, B.A., 2006, Estuarine and incised-valley facies models, *in* Posamentier, H.W., and Walker, R.G., eds., Facies models revisited: SEPM, Society for Sedimentary Geology Special Publication 84, p. 171–235.

Brown, R.E., and Wilkinson, 1981, The Draney Limestone: Early Cretaceous lacustrine carbonate deposition in western Wyoming and southeastern Idaho:

Contributions to Geology, University of Wyoming, v. 20, no. 1, p. 23–31.

Buatois, L.A., Mángano, M.G., Maples, C.G., and Lanier, W.P., 1997, The paradox of nonmarine ichnofaunas in tidal rhythmites—Integrating sedimentologic and ichnologic data from the Late Carboniferous of eastern Kansas, U.S.A.: Palaios, v. 12, no. 5, p. 467–481, doi: https://doi.org/10.2307/3515384

Buck, S.G., 1985, Sand-flow cross strata in tidal sands of the Lower Greensand (Early Cretaceous), southern England: Journal of Sedimentary Petrology, v. 55, no. 6, p. 895–906.

Buck, S.G., and Goldring, R., 2003, Conical sedimentary structures, trace fossils or not? Observations, experiments, and review: Journal of Sedimentary Research, v. 73, no. 3, p. 338–353, doi: https://doi.org/10.1306/091602730338

Burden, E.T., 1984, Terrestrial palynomorph biostratigraphy of the lower part of the Mannville Group (Lower Cretaceous), Alberta and Montana, *in* Stott, D.F., and Glass, D.J., eds., Mesozoic of Middle North America: Canadian Society of Petroleum Geologists Memoir 9, p. 249–269.

Buso, J., Alvero, A., Pessenda, L.C.R., De Oliveira, P.E., Fonseca, G., Paulo, C., Cohen, L.M.C., Volkmer-Ribeiro, C., De Oliveira, S.M.B., Favaro, D.I.T., Rossetti, D.F., Lorente, F.L., and Filho, M.A.B., 2013, From an estuary to a freshwater lake: A paleo-estuary evolution in the context of Holocene sea-level fluctuations, SE Brazil: Radiocarbon, v. 55, no. 2, p. 1735–1746.

Cant, D.J., 1996, Sedimentological and sequence stratigraphic organization of a foreland clastic wedge, Mannville Group, Western Canada Basin: Journal of Sedimentary Research, v., 66, p. 1137–1147.

Cant, D.J., 1998, Sequence stratigraphy, subsidence rates, and alluvial facies, Mannville Group, Alberta foreland basin, *in* Shanley, K.W., and McCabe, P.J., eds., Relative role of eustasy, climate, and tectonism in continental rocks: SEPM, Society for Sedimentary Geology Special Publication 59, p. 49–63.

Carmona, N.B., Buatois, L.A., Ponce, J.J., and Mángano, M.G., 2009, Ichnology and sedimentology of a tide-influenced delta, Lower Miocene Chenque Formation, Patagonia, Argentina: Trace-fossil distribution and response to environmental stresses: Palaeogeography, Palaeoclimatology, Palaeoecology, v. 273, no. 1–2, p. 75–86.

Carmona, N.B., Mángano, M.G., Buatois, L.A., and Ponce, J.J., 2010, Taphonomy and paleoecology of the bivalve trace fossil Protovirgularia in deltaic heterolithic

facies of the Miocene Chenque Formation, Patagonia, Argentina: Animal-substrate interactions and the modern evolutionary fauna: Journal of Paleontology, v. 84, no. 4, p. 730–738.

Carstarphen, C.A., Smith, L.N., Mason, D.C., LaFave, J.I., and Richter, M.G., 2011, Data for water wells visited during the Cascade–Teton Groundwater Characterization Study: Montana Bureau of Mines and Geology Groundwater Assessment Atlas 7-01, scale 1:275,000.

Catuneanu, O., 2004, Retroarc foreland systems—Evolution through time: Journal of African Earth Sciences, v. 38, p. 225–242, doi: https://doi.org/10.1016/j.jafrearsci.2004.01.004

Catuneanu, O., 2018, First-order foreland cycles: Interplay of flexural tectonics, dynamic loading, and sedimentation: Journal of Geodynamics, doi: https://doi.org/10.1016/j.jog.2018.0300}

Catuneanu, O., Sweet, A.R., and Miall, A.D., 1999, Concept and styles of reciprocal stratigraphies: Western Canada Foreland System: Oxford, UK, Terra Nova, v. 11, p. 1–8, doi: https://doi.org/10.1046/j.1365-3121.1999.00222.x

Catuneanu, O., Sweet, A.R., and Miall, A.D., 2000, Reciprocal stratigraphy of the Campanian–Paleocene Western Interior of North America: Sedimentary Geology, v. 134, p. 235–255, doi: https://doi.org/10.1016/S0037-0738(00)00045-2

Clifton, H.E., 1982, Estuarine deposits, in Scholle, P.A., and Spearing, D., eds., Sandstone depositional environments: American Association of Petroleum Geologists Memoir 31, p. 179–189.

Clifton, H.E., 1983, Discrimination between subtidal and intertidal facies in Pleistocene deposits, Wilapa Bay, Washington: Journal of Sedimentary Petrology, v. 53, p. 353–369.

Clifton, H.E., 2006, A reexamination of clastic-shoreline facies models, in Posamentier, H.W., and Walker, R.G., eds., Facies models revisited: SEPM, Society for Sedimentary Geology Special Publication 84, p. 293–337, doi: https://doi.org/10.2110/pec.06.84.0293

Cobban, W.A., 1955, Cretaceous rocks of northwestern Montana, in Lewis, P.J., ed., Sweetgrass Arch-Disturbed Belt, Montana: Billings Geological Society, 6th Annual Field Conference, Guidebook, p. 107–119.

Cohen, A., McGlue, M.M., Ellis, G.S., Zani, H., Swarzenski, P.W., Assine, M.L., and Silva, A., 2015, Lake formation, characteristics, and evolution in retroarc deposystems: A synthesis of the modern Andean orogeny and its associated basins, in DeCelles, P.G., Ducea, M.N, Carrapa, B., and Kapp, P.A., eds., Geodynamics

of a Cordilleran orogenic system: The central Andes of Argentina and Northern Chile: Geological Society of America Memoir 212, p. 309–335, doi: https://doi.org/10.1130/2015.1212(16)

Collier, A.J., 1929, The Kevin–Sunburst oil field and other possibilities of oil and gas in the Sweetgrass Arch, Montana: U.S. Geological Survey Bulletin 812-B, p. 57–189.

Collinson, J.D., 1969, The sedimentology of Grindslow Shales and the Kinderscout Grit: A deltaic complex in the Namurian of northern England: Journal of Sedimentary Petrology, v. 39, p. 194–221.

Condon, S.M., 2000, Stratigraphic framework of Lower and Upper Cretaceous rocks in central and eastern Montana: U.S. Geological Survey Digital Data Series DDS-57, doi: https://doi.org/10.3133/ds57

Currie, B.S., 1997, Sequence stratigraphy of nonmarine Jurassic–Cretaceous rocks, central Cordilleran Foreland-Basin System: Geological Society of America Bulletin 109, p. 1206–1222, doi: https://doi.org/10.1130/0016-7606(1997)109%3C1206:SSONJC%3E2.3.CO;2

Currie, B.S., 1998, Upper Jurassic–Lower Cretaceous Morrison and Cedar Mountain Formations, NE Utah–NW Colorado: Relationships between nonmarine deposition and early Cordilleran foreland-basin development: Journal of Sedimentary Research, v. 68, no. 4, p. 632–652, doi: https://doi.org/10.2110/jsr.68.632

Daidu, F., Yuan, W., and Min, L., 2013, Classifications, sedimentary features, and facies associations of tidal flats: Journal of Palaeogeography, v. 2, p. 66–80, doi: https://doi.org/10.3724/SP.J.1261.2013.00018

Dalrymple, R.W., 1984, Morphology and internal structure of sand waves in the Bay of Fundy: Sedimentology, v. 31, p. 365–382, doi: https://doi.org/10.1111/j.1365-3091.1984.tb00865.x

Dalrymple, R.W., 2006, Incised valleys in time and space: an introduction to the volume and an examination of the controls on valley formation and filling, in Dalrymple, R.W., Leckie, D.A., and Tillman, R.W., eds., Incised valleys in time and space: SEPM, Society for Sedimentary Geology Special Publication 85, p. 5–12.

Dalrymple, R.W., 2010, Tidal depositional systems, in James, N.P., and Dalrymple, R.W., eds., Facies Models 4: Geotext 6: St. John's, Newfoundland, Geological Association of Canada, p. 201–231.

Dalrymple, R.W., and Rhodes, 1995, Estuarine dunes and bars, in Perillo, G.M.E., ed., Geomorphology and sedimentology of estuaries: Amsterdam, Netherlands, Elsevier, p. 359–422.

Dalrymple, R.W., Knight, R.J., and Lambiase, J.J., 1978, Bedforms and their hydraulic stability relationships in a tidal environment, Bay of Fundy, Canada: Nature, v. 275, p. 100–104, doi: https://doi.org/10.1111/j.1365-3091.1990.tb00624.x

Dalrymple, R.W., Knight, R.J., Zaitlin, B.A., and Middleton, G.V., 1990, Dynamics and facies model of a macrotidal sand-bar complex, Cobequid Bay–Salmon River estuary (Bay of Fundy): Sedimentology, v. 37, p. 577–612.

Dalrymple, R.W., Zaitlin, B.A., and Boyd, R., 1992, Estuarine facies models: Conceptual basis and stratigraphic implications: Journal of Sedimentary Petrology, v. 62, p. 1130–1146, doi: https://doi.org/10.1306/D4267A69-2B26-11D7-8648000102C1865D

Dalrymple, R.W., Mackay, D.A., Ichaso, A.A., and Choi, K.S., 2012, Processes, morphodynamics, and facies of tide-dominated estuaries, in Davis, R.A., Jr., and Dalrymple, R.W., eds., Principles of tidal sedimentology: Dordrecht, Netherlands, Springer, p. 79–107.

Dashtgard, S.E., Gingras, M.K., and MacEachern, J.A., 2009, Tidally modulated shorefaces: Journal of Sedimentary Research, v. 79, p. 793–807, doi: https://doi.org/10.2110/jsr.2009.084

Dashtgard, S.E., MacEachern, J.A., Frey, S.E., and Gingras, M.K., 2012, Tidal effects on the shoreface: Towards a conceptual framework: Sedimentary Geology, v. 279, p. 42–61, doi: https://doi.org/10.1016/j.sedgeo.2010.09.006

DeCelles, P.G., 1986, Sedimentation in a tectonically partitioned nonmarine foreland basin: The Lower Cretaceous Kootenai Formation, southwestern Montana: Geological Society of America Bulletin, v. 97, p. 911–931, doi: https://doi.org/10.1130/00167606(1986)97%3C911:SIATPN%3E2.0.CO;2

DeCelles, P.G., 2004, Late Jurassic to Eocene evolution of the Cordilleran thrust belt and foreland basin system, western U.S.A.: American Journal of Science, v. 304, p. 105–168, doi: https//doi.org/10.2475/ajs.304.2.105

DeCelles, P.G., 2012, Foreland basin systems revisited: Variations in response to tectonic settings, in Busby, C., and Pérez, A.A., eds., Tectonics of sedimentary basins: Recent advances: Hoboken, N.J., Wiley-Blackwell, p. 405–426, doi: https://doi.org/10.1002/9781444347166.ch20

DeCelles, P.G., and Burden, E.T., 1992, Non-marine sedimentation in the overfilled part of the Jurassic–Cretaceous Cordilleran foreland basin: Morrison and Cloverly Formations, central Wyoming, U.S.A.: Basin Research, v. 4, no. 3–4, p. 291–313, doi: https://doi.org/10.1111/j.1365-2117.1992.tb00050.x

DeCelles, P.G., and Giles, K.A., 1996, Foreland basin systems: Basin Research, v. 8, no. 2, p. 105–123, doi: https//doi.org: 10.1046/j.1365-2117.1996.01491.x

DeCelles, P.G., Langford, R.P., and Schwartz, R.K., 1983, Two new methods of paleocurrent determination from trough cross-stratification: Journal of Sedimentary Petrology, v. 53, p. 629–642, doi: https://doi.org/10.1306/212F824C-2B24-11D7-8648000102C1865D

Desjardins, P.R., Buatois, L.A., and Mángano, M.G., 2012, Tidal flats and subtidal sand bodies, in Knaust, D., and Bromley, R.G., eds., Trace fossils as indicators of sedimentary environments: Developments in Sedimentology, v. 64, p. 529–561, doi: https://doi.org/10.1016/B978-0-444-53813-0.00018-6

Devine, P.E., 1991, Transgressive origin of channeled estuarine deposits in the Point Lookout Sandstone, northwestern New Mexico: A model for Upper Cretaceous, cyclic regressive parasequences of the U.S. Western Interior: American Association of Petroleum Geologists Bulletin, v. 75, no. 6, p. 1039–1063, doi: https://doi.org/10.1306/0C9B28C1-1710-11D7-8645000102C1865D

Dolson, J.C., and Muller, D.S., 1994, Stratigraphic evolution of the Lower Cretaceous Dakota Group, Western Interior, U.S.A., in Caputo, M.V., Peterson, J.A., and Franczyk, K.J., eds., Mesozoic Systems of the Rocky Mountain Region, U.S.A.: Rocky Mountain Section, Society for Sedimentary Geology, p. 441–456.

Dolson, J.C., and Piombino, J., 1994, Giant proximal foreland basin non-marine wedge trap: Lower Cretaceous Cutbank Sandstone, Montana, in Dolson, J.C., Hendricks, M.L., and Wescott, W.A., Unconformity-related hydrocarbons in sedimentary sequences: Rocky Mountain Association of Geologists Guidebook, p. 135–148.

Drummond, C.N., Wilkinson, B.H., and Lohmann, K.C., 1996, Climatic control of fluvial-lacustrine cyclicity in the Cretaceous Cordilleran Foreland Basin, western United States: Sedimentology, v. 43, p. 677–689, doi: https://doi.org/10.1111/j.1365-3091.1996.tb02020.x

Durkin, P.R., Boyd, R.L., Hubbard, S.M., Shultz, A.W., and Blum, M.D., 2017, Three-dimensional reconstruction of meander-belt evolution, Cretaceous McMurray Formation, Alberta Foreland Basin, Canada: Journal of Sedimentary Research, v. 87, no. 10, p. 1075–1099, doi: https://doi.org/10.2110/jsr.2017.59

Elliott, T., and Gardiner, A.R., 2009, Ripple, megaripple and sandwave bedforms in the macrotidal Loughor Estuary, South Wales, U.K., *in* Nio, S.-D., Shüttenhelm, R.T.E., and Van Weering, T.C.E., eds., Holocene marine sedimentation in the North Sea Basin: Oxford, UK, Blackwell, p. 51–64, doi: http://doi.org/10.1002/9781444303759.ch4

Engelhardt, D.W., 1999, Palynologic analysis of Mesozoic samples from Wyoming and Montana for the University of Indiana: Columbia, University of South Carolina Earth Sciences and Resources Institute, 3 p.

Englemann, G., and Hasiotis, S.T., 1999, Deep dinosaur tracks in the Morrison Formation: Sole marks that are really sole marks, *in* Gillette, D.D., ed., Vertebrate paleontology in Utah: Utah Geological Survey Miscellaneous Publication 99-1, p. 179–184.

Farshori, M.Z., and Hopkins, J.C., 1989, Sedimentology and petroleum geology of fluvial and shoreline deposits of the Lower Cretaceous Sunburst Sandstone Member, Mannville Group, southern Alberta: Bulletin of Canadian Petroleum Geology, v. 37, no. 4, p. 371–388.

Fenies, H., and Tastet, J-P., 1998, Facies and architecture of an estuarine tidal bar (the Trompeloup bar, Gironde Estuary, SW France): Marine Geology, v. 150, p. 149–169, doi: https://doi.org/10.1016/S0025-3227(98)00059-0

Flemming, B.W., 2012, Siliciclastic back-barrier tidal flats, *in* Davis, R.A., Jr., and Dalrymple, R.W., eds., Principles of tidal sedimentology: Dordrecht, Netherlands, Springer, p. 231–267.

Frey, R.W., and Howard, J.D., 1986, Mesotidal estuarine sequences: A perspective from the Georgia Bight: Journal of Sedimentary Petrology, v. 56, no. 6, p. 911–924, doi: https://doi.org/10.1306/212F8A85-2B24-11D7-8648000102C1865D

Frey, S.E., and Dashtgard, S.E., 2012, Sedimentology, ichnology, and hydrodynamics of strait-margin, sand-and-gravel beaches and shorefaces: Juan de Fuca Strait, British Columbia, Canada: Sedimentology, v. 58, p. 1326–1346, doi: https://doi.org/10.1111/j.1365-3091.2010.01211.x

Fuentes, F., DeCelles, P.G., Constenius, K.N., and Gehrels, G.E., 2011, Evolution of the Cordilleran foreland basin system in northwestern Montana, U.S.A.: Geological Society of America Bulletin, v. 123, Issue 3–4, p. 507–533. https//doi.org/10.1130/B30204.1

Fuentes, F., DeCelles, P.G., and Constenius, K.N., 2012, Regional structure and kinematic history of the Cordilleran fold-thrust belt in northwestern Montana, U.S.A.: Geosphere, v. 8, p. 1104–1128, doi: https://doi.org/10.1130/GES00773.1

Gingras, M.K., and MacEachern, J.A., 2012, Tidal ichnology of shallow-water clastic settings, *in* Davis, R.A., Jr., and Dalrymple, R.W., eds., Principles of tidal sedimentology: Dordrecht, Netherlands, Springer, p. 57–77.

Gingras, M.K., MacEachern, J.A., Dashtgard, S.E., Zonneveld, J., Schoengut, J., Ranger, M., and Pemberton, S.G., 2012, Trace fossils as indicators of sedimentary environments, *in* Knaust, D., and Bromley, R.G., eds., Trace fossils: Developments in Sedimentology, v. 64, p. 463–497.

Glaister, R.P., 1959, Lower Cretaceous of southern Alberta and adjoining areas: American Association of Petroleum Geologists Bulletin, v. 43, p. 590–640.

Glass, S.W., and Wilkinson, B.H., 1980, The Peterson Limestone—Early Cretaceous lacustrine carbonate deposition in western Wyoming and southeastern Idaho: Sedimentary Geology, v. 27, p. 143–160.

Gresh, S., Landon Neumann, L., Yates, J., and Pope, M.C., 2017, Analysis of the paleoclimate and depositional environment of the Kootenai 2 Formation, southwestern Montana: American Association of Petroleum Geologists Search and Discovery Article #90291 [Accessed January 3, 2019]

Gussow, W.C., 1955, Oil and gas accumulation on the Sweetgrass Arch, *in* Lewis, P.J., Sweetgrass Arch-Disturbed Belt, Montana: Billings Geological Society, 6th Annual Field Conference Guidebook, p. 220–224.

Hager, D., 1923, The Sunburst oil and gas field, Montana: Transactions American Institute of Mining and Metallurgical Engineering, v. 69, p. 1101–1120.

Harleman, D.R.F., and Ippen, A.T., 1969, Salinity intrusion effects in estuary shoaling: Journal of the Hydraulics Division, Proceedings of the American Society of Civil Engineers, v. 95, p. 9–28.

Harris, P.T., 1988, Large-scale bedforms as indicators of mutually evasive sand transport and the sequential infilling of wide-mouthed estuaries: Sedimentary Geology, v. 57, no. 3–4, p. 273–298, doi: https://doi.org/10.1016/0037-0738(88)90034-6

Hayes, B.J.R., 1986, Stratigraphy of the basal Cretaceous Lower Mannville Formation, southern Alberta and north-central Montana: Bulletin of Canadian Petroleum Geology, v. 34, no. 1, p. 30–48.

Hayes, B.J.R., 1990, A perspective on the Sunburst Member of southern Alberta: Bulletin of Canadian Petroleum Geology, v. 38, no. 4, p. 483–484.

Hayes, B.J.R., Christopher, J.E., Rosenthal, L., Los, G., McKercher, B., Minken, D., Tremblay, R.M., and Fennell, J., 1994, Cretaceous Mannville Group of the Western Canada Sedimentary Basin, *in* Mossop, G.D., and Shetson, I., (compilers), Geological atlas of the Western Canada Sedimentary Basin: Canadian Society of Petroleum Geologists and Alberta Research Council, p. 317–334.

Heller, P.L., and Paola, C., 1989, The paradox of Lower Cretaceous gravels and the initiation of thrusting in the Sevier orogenic belt, United States Western Interior: Geological Society of America Bulletin, v. 1021, p. 864–875.

Herbaly, E.L., 1974, Petroleum geology of the Sweetgrass Arch, Alberta: American Association of Petroleum Geologists Bulletin, v. 58, no. 11, p. 2227–2244.

Hildred, G.V., Ratcliffe, K.T., Wright, A.M., Zaitlin, B.A., and Wray, D.S., 2010, Chemostratigraphic applications to low-accommodation fluvial incised valley settings: An example from the lower Mannville Formation of Alberta, Canada: SEPM, Society for Sedimentary Geology, v. 80, no. 11, p. 1032–1045, doi: https://doi.org/10.2110/jsr.2010.089

Hettinger, R.D., McCabe, P.J., and Shanley, K.W., 1993, Detailed facies anatomy of transgressive and high-stand systems tracts from the Upper Cretaceous of southern Utah, U.S.A., *in* Weimer, P., and Posamentier, H.W., eds., Siliclastic sequence stratigraphy: Recent developments and applications: American Association of Petroleum Geologists Memoir 58, p. 235–257.

Holm, M.R., James, W.C., and Suttner, L.J., 1977, Comparison of the Peterson and Draney Limestones, Idaho and Wyoming, and the calcareous members of the Kootenai Formation, western Montana: Wyoming Geological Association, 29th Annual Field Conference Guidebook, p. 259–270.

Hopkins, J.C., 1985, Channel-fill deposits formed by aggradation in deeply scoured, superimposed distributaries of the lower Kootenai Formation (Cretaceous): Journal of Sedimentary Petrology, v. 55, no. 1, p. 42–52, doi: https://doi.org/10.1306/212F85FD-2B24-11D7-8648000102C1865D

Hopkins, J.C., Lawton, D.C., and Gunn, J.D., 1987, Geological and seismic evaluation of a lower Mannville valley system: Alderson Prospect, Rolling Hills, southeastern Alberta: Bulletin of Canadian Petroleum Geology, v. 35, p. 296–315.

Howard, J.D., and Dorjes, J., 1972, Animal-sediment relationships in two beach-related tidal flats, Sapelo Island, Georgia: Journal of Sedimentary Petrology, v. 42, no. 3, p. 608–623.

Howard, J.D., and Reineck, H.-E., 1972, Georgia coastal region, Sapelo Island, U.S.A., *in* Sedimentology and biology, physical and biogenic sedimentary structures of the nearshore shelf: Senckenbergiana Maritima., v. 4, p. 81–123.

Howard, J.D., Mayou, T.V., and Heard, R.W., 1977, Biogenic sedimentary structures formed by rays: Journal of Sedimentary Petrology, v. 47, no. 1, p. 339–346, doi: https://doi.org/10.1306/212F7167-2B24-11D7-8648000102C1865D

Howard, J.D., and Reineck, H.-E., 1981, Depositional facies of high-energy beach-to-offshore sequence: Comparison with low-energy sequence: American Association of Petroleum Geologists Bulletin, v. 65, no. 5, p. 807–830.

Howard, J.D., and Scott, R.M., 1983, Comparison of Pleistocene and Holocene barrier island beach-to-offshore sequences, Georgia and northeast Florida coasts, U.S.A.: Sedimentary Geology, v. 34, no. 2–3, p. 167–183, doi: https://doi.org/10.1016/0037-0738(83)90085-4

Howard, J.D., Frey, R.W., and Reineck. H.-E., 1972, Georgia coastal region, Sapelo Island, U.S.A., *in* Sedimentology and biology, introduction: Senckenbergiana Maritima, v. 4, p. 3–14.

Hughes, Z.J., 2012, Tidal channels on tidal flats and marshes, *in* Davis, R.A., Jr., and Dalrymple, R.W., eds., Principles of tidal sedimentology: Dordrecht, Netherlands, Springer, p. 269–300.

Hunter, R.E., 1985, Subaqueous sand-flow cross-strata: Journal of Sedimentary Petrology, v. 55, no. 6, p. 886–894, doi: https://doi.org/10.1306/212F8832-2B24-11D7-8648000102C1865D

Jackson, S.J., Whyte, M.A., and Romano, M., 2009, Laboratory-controlled simulations of dinosaur footprints in sand: A key to understanding vertebrate track formation and preservation: PALAIOS, v. 24, no. 4, p. 222–238, doi: https://doi.org/10.2110/palo.2007.p07-070r

James, W.C., 1980, Limestone channel storm complex (Lower Cretaceous), Elkhorn Mountains, Montana: Journal of Sedimentary Petrology, v. 50, no. 2, p. 447–456.

Jennings, D.S., Platt, B.F., and Hasiotis, S.T., 2006, Distribution of vertebrate trace fossils, upper Morrison Formation, Bighorn Basin, Wyoming, U.S.A.: Im-

plications for differentiating paleoecological and preservational bias, *in* Foster, J.R., and Lucas, S.G., eds., Paleontology and geology of the Upper Jurassic Morrison Formation: New Mexico Museum of Natural History and Science Bulletin 36, p. 183–192.

Johnson, H.D., 1977, Shallow marine sand bar sequences: An example from the Late Precambrian of north Norway: Sedimentology, v. 24, p. 245–270.

Jordan, T.E., 1995, Retroarc foreland and related basins, *in* Busby, C., and Indersoll, R., eds., Tectonics of sedimentary basins: Cambridge, Mass., Blackwell Science, p. 331–391.

Kauffman, E.G., 1977, Geological and biological overview—Western Interior Cretaceous Basin, *in* Kauffman, E.G., ed., Cretaceous facies, faunas, and paleoenvironments across the Western Interior Basin: The Mountain Geologist, v. 14, p. 75–99.

Keighley, D.G., and Pickerill, R.K., 1994, The ichnogenus *Beaconites* and its distinction from *Ancorichnus* and *Taenidium*: Palaeontology, v. 37, no. 2, p. 305–338.

Land, C.B., 1972, Stratigraphy of Fox Hills Sandstone and associated formations: Rock Springs Uplift and Wamsutter Arch area, Sweetwater County, Wyoming: A shoreline-estuary sandstone model for the Late Cretaceous: Colorado School of Mines Quarterly, v. 67, p. 1–69.

Laporte, L.F., and Behrensmeyer, A.K., 1980, Tracks and substrate reworking by terrestrial vertebrates in Quaternary sediments of Kenya: Journal of Sedimentary Research, v. 50, no. 4, p. 1337–1346, doi: https://doi.org/10.1306/212F7BE9-2B24-11D7-8648000102C1865D

Laskowski, A.K., DeCelles, P.G., and Gehrels, G.E., 2013, Detrital zircon geochronology of Cordilleran retroarc foreland basin strata, western North America: Tectonics, v. 32, no. 5, p. 1027–1048, doi: https//doi.org/10.1002/tect.20065

Leckie, D.A., 2000, Stratigraphic complexity in the Cretaceous Mannville Group of southern Alberta and Saskatchewan: Montana Geological Society, Fiftieth Anniversary Symposium: Montana/Alberta Thrust Belt and Adjacent Foreland, v. II, p. 16.

Leckie, D.A., Vanbeselaere, N.A., and James, D.P., 1997, Regional sedimentology, sequence stratigraphy and petroleum geology of the Mannville Group: Southwestern Saskatchewan, *in* Pemberton, S.G., and James, D.P., eds., Petroleum geology of the Cretaceous Mannville Group, Western Canada: Canadian Society of Petroleum Geologists Memoir 18, p. 211–262.

Leckie, D.A., Wallace-Dudley, K.E., Vanbeselaere, N.A., and James, D.P., 2004, Sedimentation in a low-accommodation setting: Nonmarine (Cretaceous) Mannville and marine (Jurassic) Ellis Groups, Manyberries field, southeastern Alberta: American Association of Petroleum Geologists Bulletin 88, no. 10, p. 1391–1418, doi: https://doi.org/10.1306/05120403131

Leskela, W., 1955, Pondera field, in Lewis, P.J., Sweetgrass Arch-Disturbed Belt, Montana: Billings Geological Society, 6th Annual Field Conference Guidebook, p. 168–173.

Lorenz, J.C., 1982, Lithospheric flexure and history of the Sweetgrass Arch, northwestern Montana, *in* Powers, R.T., ed., Geologic studies of the Cordilleran Thrust Belt: Rocky Mountain Association of Geologists, Denver, Colorado, v. 1, p. 77–89.

Lukie, T.D., Ardies, G.W., Dalrymple, R.W., and Zaitlin, B.A., 2002, Alluvial architecture of the Horsefly unit (Basal Quartz) in southern Alberta and northern Montana: Influence of accommodation changes and contemporaneous faulting: Bulletin of Canadian Petroleum Geology, v. 50, no. 1, p. 73–91.

Lopez, D.A., 1995, Geology of the Sweet Grass Hills, north-central Montana: Montana Bureau of Mines and Geology Memoir 68, 35 p., 1 sheet.

Lynn, J.R., 1955, Cut Bank oil and gas field, Glacier County, Montana, *in* Lewis, P.J., Sweetgrass Arch-Disturbed Belt, Montana: Billings Geological Society, 6th Annual Field Conference Guidebook, p. 195–197.

MacEachern, J.A., and Gingras, M.K., 2007, Recognition of brackish-water trace fossil suites in the Cretaceous Western Interior Seaway of Alberta, Canada, *in* Bromley, R.G., Buatois, L.A., Mángano, M.G., Genise, J.F., and Melchor, R.N., eds., Sediment–organism interactions: A multifaceted ichnology: SEPM, Society for Sedimentary Geology Special Publication 88, p. 50–59.

Mángano, M.G., and Buatois, L.A., 2004, Ichnology of Carboniferous tide-influenced environments and tidal flat variability in the North American midcontinent: Geological Society of America Special Publication 228, no. 1, p. 157–178, doi: https//doi.org/10.1144/GSL.SP.2004.228.01.09

Mateer, N.J., 1987, The Dakota Group of northeastern New Mexico and southern Colorado: New Mexico Geological Society 38th Field Conference Guidebook, p. 223–236.

McGookey, D.P., Haun, J.D., Hale, L.A., Goodell, H.G., McCubbin, D.G., Weimer, R., and Wulf, G.R., 1972,

Cretaceous System, *in* Mallory, W.W., ed., Geologic Atlas of the Rocky Mountain Region: Rocky Mountain Association of Geologists, Denver, Colorado, p. 190–228.

McLaurin, B.T., and Steel, R.J., 2000, Fourth-order nonmarine to marine sequences, middle Castlegate Formation, Book Cliffs, Utah: Geology, v. 28, no. 4, p. 359–362, doi: https://doi.org/10.1130/0091-7613(2000)28%3C359:FNTMSM%3E2.0.CO;2

McMannis, W.J., 1965, Resumé of depositional and structural history of western Montana: American Association of Petroleum Geologists Bulletin, v. 49, no. 11, p. 1801–1823.

Meyers, J.H., and Schwartz, R.K., 1994, Summary of depositional environments, paleogeography, and structural control on sedimentation in the Late Jurassic (Oxfordian) Sundance foreland basin, western Montana, *in* Caputo, M.V., Peterson, J.A., and Franczyk, K.J., eds., Mesozoic Systems of the Rocky Mountain region, U.S.A.: Rocky Mountain Section, Society for Sedimentary Geology, p. 331–349.

Miall, A.D., 2016, Stratigraphy: The modern synthesis: New York, Springer, 370 p.

Miall, A.D., Catuneanu, O., Vakarelov, B., and Post, R., 2008, The Western Interior Basin, *in* Miall, A.D., ed., The sedimentary basins of the United States and Canada: Sedimentary basins of the world: Amsterdam, Netherlands, Elsevier, v. 5, p. 329–362.

Milàn, J., and Bromley, R.G., 2006, True tracks, undertracks and eroded tracks: Experimental work with tetrapod tracks in laboratory and field: Palaeogeography, Palaeoclimatology, and Palaeoecology, v. 231, no. 3–4, p. 253–264, doi: https://doi.org/10.1016/j.palaeo.2004.12.022

Miles, B.D., Kukulski, R.B., Raines, M.K., Zonneveld, J.P., Leier, A.L., and Hubbard, S.M., 2012, A stratigraphic framework for Late Jurassic–Early Cretaceous gas-bearing strata (Monteith Formation) in the subsurface of northwest Alberta: Bulletin of Canadian Petroleum Geology, v. 60, no. 1, p. 3–36, doi: https//doi.org/10.2113/gscpgbull.60

Miller, M.F., 1982, *Limulicubichnus*: A new ichnogenus of limulid resting traces: Journal of Paleontology, v. 56, p. 429–433.

Molenaar, C.M., and Cobban, W.A., 1991, Middle Cretaceous stratigraphy on the south and east sides of the Uinta Basin, northeastern Utah and northwestern Colorado: U.S. Geological Survey Bulletin 1787-P, 34 p.

Nio, S.-D., and Yang, C.-S., 1991, Diagnostic attributes of clastic tidal deposits: A review, *in* Smith, D.G.,

Reinson, G.E., Zaitlin, B.A., and Rahmani, R.A., eds., Clastic tidal sedimentology: Canadian Society of Petroleum Geologists Memoir 16, p. 3–27.

Oakes, M.H., 1966, North Cut Bank field and the Moulton sandstone, *in* Cox, J.E., Hunter, L.D., and Blair, J.E., eds., Jurassic and Cretaceous stratigraphic traps, Sweetgrass Arch: Billings Geological Society, 17th Annual Field Conference Guidebook, p. 191–201.

O'Neill, J.M., and Lopez, D.A., 1985, Character and regional significance of the Great Falls Tectonic Zone, east-central Idaho and west-central Montana: American Association of Petroleum Geologists Bulletin 69, no. 3, p. 437–447.

Pană, D.I., and van der Pluijm, B.A., 2015, Orogenic pulses in the Alberta Rocky Mountains: Radiometric dating of major faults and comparison with the regional tectono-stratigraphic record: Geological Society of America Bulletin, v. 127, no. 3/4, p. 480–502, doi: https//doi.org/10.1130/B31069.1

Pankowski, K.P., 2007, Interpretations of the lithostratigraphic sequence in the Early Cretaceous second Kootenai member in west-central Montana: Meadville, Penn., Allegheny College, Senior Comprehensive Project, 66 p.

Peterson, J.A., 1966, Sedimentary history of the Sweetgrass Arch: Billings Geological Society, 17th Annual Field Conference Guidebook, p. 112–134.

Peterson, J.A., 1981, General stratigraphy and regional paleostructure of the western Montana overthrust belt: *in* Tucker, T.E., ed., Southwest Montana: Montana Geological Society, Field Conference and Symposium Guidebook, p. 5–35.

Platt, B.F., and Hasiotis, S.T., 2006, Newly discovered sauropod dinosaur tracks with skin and foot-pad impressions from the Upper Jurassic Morrison Formation, Bighorn Basin, Wyoming, U.S.A.: PALAIOS, v. 21, no. 3, p. 249–261, doi: https://doi.org/10.2110/palo.2004.p04-69

Plink-Björklund, P.I.R.E.T., 2005, Stacked fluvial and tide-dominated estuarine deposits in high-frequency (fourth-order) sequences of the Eocene Central Basin, Spitsbergen: Sedimentology, v. 52, no. 2, p. 391–428.

Plint, A.G., and Wadsworth, J.A., 2006, Delta-plain paleodrainage patterns reflect small-scale fault movement and subtle forebulge uplift: Upper Cretaceous Dunvegan Formation, western Canada Foreland Basin, *in* Dalrymple, R.W., Leckie, D.A., and Tillman, R.W., eds., Incised valley systems in time and space: SEPM, Society for Sedimentary Geology Special Publication 85, p. 219–237.

Plint, A.G., McCarthy, P.J., and Faccini, U.F., 2001, Nonmarine sequence stratigraphy: Updip expression of sequence boundaries and systems tracts in a high-resolution framework, Cenomanian Dunvegan Formation, Alberta foreland basin, Canada: American Association of Petroleum Geologists, v. 85, no. 11, p. 1967–2001.

Porter, K.W., Dyman, T.S., and Tysdal, R.G., 1993, Sequence boundaries and other surfaces in Lower and lower Upper Cretaceous rocks of central and southwest Montana–A preliminary report, in Hunter, L.D.V., ed., Energy and mineral resources of central Montana: Montana Geological Society, Field Conference Guidebook, p. 45–59.

Posamentier, H.W., and Vail, P.R., 1988, Eustatic controls on clastic sedimentation II—Sequence and systems tract models, in Wilgus, C.K., Hastings, B.S., Ross, C.A., Posamentier, H.W., Van Wagoner, J., and Kendall, C.G.St.C., eds., Sea level changes: An integrated approach: SEPM, Society for Sedimentary Geology Special Publication 42, p. 125–154.

Quinn, G.M., Hubbard, S.M., Putnam, P.E., Matthews, W.A., Daniels, B.G., and Guest, B., 2018, A Late Jurassic to Early Cretaceous record of orogenic wedge evolution in the Western Interior basin, U.S.A. and Canada: Geosphere, v. 14, no. 3, p. 1187–1206, doi: https://doi.org/10.1130/GES01606.1

Ranger, M.J., and Pemberton, S.G., 1988, Marine influence on the McMurray Formation in the Primrose area, Alberta, in James, D.P., and Lecke, D.A., eds., Sequences, stratigraphy, sedimentology: Surface and subsurface: Canadian Society of Petroleum Geologists Memoir 15, p. 439–449.

Rahmani, R.A., 1988, Estuarine tidal channel and nearshore sedimentation of a Late Cretaceous epicontinental sea, Drumheller, Alberta Canada, in de Boer, P.L., van Gelder, A., and Nio, S.-D., eds., Tide-influenced sedimentary environments and facies: Dordrecht, Netherlands, D. Reidel, p. 433–471.

Ratcliffe, K.T., Wright, A.M., Hallsworth, C., Morton, A., Zaitlin, B.A., Potocki, D., and Wray, D.S., 2004, An example of alternative correlation techniques in a low-accommodation setting, nonmarine hydrocarbon system: The (Lower Cretaceous) Mannville Basal Quartz succession of southern Alberta: American Association of Petroleum Geologists Bulletin, v. 88, no. 10, p. 1419–1432, doi: https://doi.org/10.1306/05100402035

Reid, C.R., 2015, Incised valley-fill system development and stratigraphic analysis of the Lower Cretaceous Kootenai Formation, northwest Montana: Bozeman, Montana State University, M.S. thesis, 142 p.

Reid, E.L., 1955, The Darling area, Glacier and Toole Counties, Montana, in Lewis, P.J., Sweetgrass Arch-Disturbed Belt, Montana: Billings Geological Society, 6th Annual Field Conference Guidebook, p. 174–176.

Reineck, H.-E., and Singh, I.B., 1980, Depositional sedimentary environments: New York, Springer-Verlag, 549 p.

Reineck, H.-E., and Wunderlich, F., 1968, Classification and origin of flaser and lenticular bedding: Sedimentology, v. 11, no. 1–2, p. 99–104.

Reynolds, M.W., and Brandt, T.R., 2005, Geologic map of the Canyon Ferry Dam 30' x 60' quadrangle, west-central Montana: U.S. Geological Survey Scientific Investigations Map 2860, 32 p., scale 1:100,000.

Rhodes, R.B., 1955, The Pakowki Lake-Sweetgrass Hills area, southeastern Alberta and north central Montana, in Lewis, P.J., Sweetgrass Arch-Disturbed Belt, Montana: Billings Geological Society, 6th Annual Field Conference Guidebook, p. 195–197.

Rice, D.D., 1976, Revision of Cretaceous nomenclature of the northern Great Plains in Montana, North Dakota, and South Dakota, in Cohee, G.V., and Wright, W.B., Changes in Stratigraphic Nomenclature by the U.S. Geological Survey: U.S. Geological Survey Bulletin 1422-A, p. 66–67.

Rudkin, D.M., and Young, G.A., 2009, Horseshoe crabs—An ancient ancestry revealed, in Tanacredi, J., Botton, M., and Smith, D., eds., Biology and conservation of Horseshoe crabs: Boston, Mass., Springer, p. 25–44, doi: https://doi.org/10.1007/978-0-387-89959-6_2

Santos, A.E.A., Jr., and Rossetti, D.F., 2006, Depositional model of the Ipixuna Formation (Late Cretaceous-?Early Tertiary, Rio Capim area, northern Brazil: Latin American Journal of Sedimentology and Basin Analysis, v. 13, no. 2, p. 101–117.

Savrda, C.E., and Nanson, L.L., 2003, Ichnology of fair-weather and storm deposits in an Upper Cretaceous estuary (Eutaw Formation, western Georgia, U.S.A.): Palaeogeography, Palaeoclimatology, Palaeoecology, v. 202, no. 1, p. 67–83, doi: https://doi.org/10.1016/S0031-0182(03)00628-X

Schnurrenberger, D., Russell, J., and Kelts, K., 2003, Classification of lacustrine sediments based on sedimentary components: Journal of Paleolimnology, v. 29, no. 2, p. 141–154.

Schulte, J.J., 1966, Correlation of the Sunburst zone with the Second Cat Creek zone in northwestern and central Montana: Billings Geological Society 17th Annual Field Conference Guidebook, p. 220–224.

Schwartz, R.K., 1982, Broken Early Cretaceous foreland basin in southwestern Montana: Sedimentation related to tectonism, *in* Powers, R.B., ed., Geologic studies of the Cordilleran Thrust Belt: Denver, Colo., Rocky Mountain Association of Geologists, p. 159–184.

Schwartz, R.K., and DeCelles, P.G., 1988, Cordilleran foreland-basin evolution and synorogenic sedimentation in response to interactive Cretaceous thrusting and reactivated foreland partitioning, southwestern Montana, *in* Schmidt, C.J., and Perry, W.J., eds., Interaction of the Rocky Mountain Foreland and Cordilleran Thrust Belt: Geological Society of America Memoir 171, p. 489–513, doi: https//doi,org/10.1130/MEM171-p489

Schwartz, T.M., and Schwartz, R.K., 2013, Paleogene post-contractile intermontane basin evolution along the frontal Cordilleran fold-thrust belt of southwestern Montana: Geological Society of America Bulletin, v. 125, no. 5/6, p. 961–984, doi: https//doi.org/10.1130/B30766.1

Schwartz, R.K., and Vuke, S.M., 2006, Tide-dominated facies complex at southern terminus of Sunburst Sea, Cretaceous Kootenai Formation, Great Falls, Montana: American Association of Petroleum Geologists Search and Discovery Article #50045, http://www.searchanddiscovery.com/documents/2007/07036schwartz/ [Accessed February 22, 2015].

Schwartz, R.K., Pankowski, K., and Thompson, J., 2006, Re-interpretation of Kootenai Formation in western Montana on the basis of new tidal evidence for Early Cretaceous (Neocomian) transgression: Geological Society of America Abstracts with Program, v. 38, no. 7, p. 147.

Shanley, K.W., and McCabe, P.J., 1993, Alluvial architecture in a sequence stratigraphic framework: A case history from the Upper Cretaceous of southern Utah, U.S.A., *in* Flint, S.S., and Bryant, I.D., eds., Quantitative modeling of clastic hydrocarbon reservoirs and outcrop analogues: International Association of Sedimentologists Special Publication 15, p. 21–56.

Shanley, K.W., and McCabe, P.J., 1994, Perspectives on the sequence stratigraphy of continental strata: American Association of Petroleum Geologists Bulletin 78, no. 4, p. 544–568.

Shanley, K.W., and McCabe, P.J., 1995, Sequence stratigraphy of Turonian–Santonian strata, Kaiparowits Plateau, southern Utah, U.S.A.: Implications for regional correlation and foreland basin evolution, *in* VanWagoner, J.C., and Bertram, G.T., eds., American Association of Petroleum Geologists Memoir 64, p. 103–136.

Slattery, J.S., Cobban, W.A., McKinney, K.C., Harries, P.J., and Sandness, A.L., 2015, Early Cretaceous to Paleocene paleogeography of the Western Interior Seaway: The interaction of eustasy and tectonism, *in* Bingle-Davis, M., ed., Cretaceous Conference: Evolution and revolution: Wyoming Geological Association 68th Annual Field Conference Guidebook, p. 22–60, doi: https://doi.org/10.13140/RG.2.1.4439.8801

Smith, J.J., Hasiotis, S.T., Kraus, M.J., and Woody, D.T., 2008, *Naktodemasis bowni:* New ichnogenus and ichnospecies for adhesive meniscate burrows (AMB), and paleoenvironmental implications, Paleogene Willwood Formation, Bighorn Basin, Wyoming: Journal of Paleontology, v. 82, no. 2, p. 267–278, doi: https://doi.org/10.1666/06-023.1

Steel, R.J., Plink-Bjorklund, P., and Aschoff, J., 2012, Tidal deposits of the Campanian Western Interior Seaway, Wyoming, Utah, and Colorado, U.S.A., *in* Davis, R.A., Jr., and Dalrymple, R.W., eds., Principles of tidal sedimentology: New York, Springer, p. 437–471, doi: https://doi.org/10.1007/978-94-007-0123-6_17

Stelck, C.R., Trollope, F.H., Norris, A.W., and Pemberton, S.G., 2007, McMurray Formation foraminifera within the lower Albian (Lower Cretaceous) Loon River shales of northern Alberta: Canadian Journal of Earth Sciences, v. 44, no. 11, p. 1627–1651, doi: https://doi.org/10.1139/e07-033

Stride, A.H., 1982, Offshore tidal sands, processes and deposits: New York, Chapman and Hall, p. 95–125.

Suttner, L.J., Schwartz, R.K., and James, W.C., 1981, Late Mesozoic to Early Cenozoic foreland sedimentation in southwest Montana, *in* Tucker, T.E., Southwest Montana: Montana Geological Society Field Conference and Symposium Guidebook, p. 93–103.

Tessier, B., 2012, Stratigraphy of tide-dominated estuaries, *in* Davis, R.A., Jr., and Dalrymple, R.W., eds., Principles of tidal sedimentology: Dordrecht, Netherlands, Springer, p. 109–128, doi: https://doi.org/10.1007/978-94-007-0123-6_6

Thompson, J.C., 1966, Fred and George Creek field, Toole County, Montana, *in* Cox, J.E., Hunter, L.D., and Blair, J.E., eds., Jurassic and Cretaceous stratigraphic traps, Sweetgrass Arch: Billings Geological Society, 17th Annual Field Conference Guidebook, p. 179–190.

Tschudy, R.H., Tschudy, B.D., and Craig, L.C., 1984, Palynological evaluation of Cedar Mountain and Burro Canyon Formations, Colorado Plateau: U.S. Geological Society Professional Paper 1281, 24 p.

Tufano, B.C., and Pietras, J.T., 2017, Coupled flexural-dynamic subsidence modeling approach for retro-foreland basins: Example from the Western Canada Sedimentary Basin: Geological Society of America Bulletin 129, no. 11/12, p. 1622–1635, doi: https://doi.org/10.1130/B31646.1

Uličný, D., 1999, Sequence stratigraphy of the Dakota Formation (Cenomanian), southern Utah: Interplay of eustasy and tectonics in a foreland basin: Sedimentology, v. 46, no. 5, p. 807–836, doi: https://doi.org/10.1046/j.1365-3091.1999.00252.x

Vakarelov, B.K., Ainsworth, R.B., and MacEachern, J.A., 2012, Recognition of wave-dominated, tide-influenced shoreline systems in the rock record: Variations from a microtidal shoreline model: Sedimentary Geology, v. 279, p. 23–41, doi: https://doi.org/10.1016/j.sedgeo.2011.03.004

van Straaten, L.M.J.U., 1954, Composition and structure of recent marine sediments in the Netherlands: Leidse Geologische Mededelingen, v. 19, no. 1, p. 1–108.

Van Wagoner, J.C., Posamentier, H.W., Mitchum, R.M., Vail, P.R., Sarg, J.F., Louitt, T.S., and Hardenbol, J., 1988, An overview of the fundamentals of sequence stratigraphy and key definitions, in Wilgus, C.K., Hastings, B.S., Ross, C.A., Posamentier, H.W., Van Wagoner, J., and Kendall, C.G.St.C., eds., Sea level changes: An integrated approach: SEPM, Society for Sedimentary Geology Special Publication 42, p. 39–45, doi: http://dx.doi.org/10.2110/pec.88.01.0039

Visser, M.J., 1980, Neap-spring cycles reflected in Holocene subtidal large-scale bedform deposits: A preliminary note: Geology, v. 8, no. 11, p. 543–546.

Vuke, S.M., 1987, Marine tongue in the middle Kootenai Formation north of Helena, central Montana, in Berg, R.B., and Breuninger, R., eds., Guidebook of the Helena area, west-central Montana, Tobacco Root Geological Society, Twelfth Annual Field Conference: Montana Bureau of Mines and Geology Special Publication 95, p. 63–64.

Vuke, S.M., 2000, Geologic map of the Great Falls South 30' x 60' quadrangle, central Montana: Montana Bureau of Mines and Geology Open-File Report 407, 18 p., scale 1:100,000.

Vuke, S.M., Berg, R.B., Colton, R.B., and O'Brien, H.E., 2002a, Geologic map of the Belt 30' x 60' quadrangle, central Montana: Montana Bureau of Mines and Geology Open-File Report 450, 18 p., scale 1:100,000.

Vuke, S.M., Colton, R.B., and Fullerton, D.S., 2002b, Geologic map of the Great Falls North 30' x 60' quadrangle, central Montana: Montana Bureau of

Mines and Geology Open-File Report 459, 10 p., scale 1:100,000.

Walker, R.G., 2006, Facies models revisited, introduction, in Posamentier, H.W., and Walker, R.G., Facies models revisited: SEPM, Society for Sedimentary Geology Special Publication 84, p. 1–17, doi: https://doi.org/10.2110/pec.06.84.0001

Walker, T.F., 1974, Stratigraphy and depositional environments of the Morrison and Kootenai Formations in the Great Falls area, central Montana: Missoula, University of Montana, Ph.D. dissertation, 195 p.

Weimer, R.J., Howard, J.D., and Lindsay, D.R., 1982, Tidal flats and associated tidal channels, in Scholle, P.A., and Spearing, D., eds., Sandstone depositional environments: American Association of Petroleum Geologists Memoir 31, p. 191–245.

Williams, G.D., and Stelck, C.R., 1975, Speculations on the Cretaceous paleogeography of North America: Geological Association of Canada Special Paper 13, 20 p.

Winslow, N.S., and Heller, P.L., 1987, Evaluation of unconformities in Upper Jurassic and Lower Cretaceous nonmarine deposits, Bighorn Basin, Wyoming and Montana, U.S.A.: Sedimentary Geology, v. 53, no. 3–4, p. 181–202.

Wood, J.M., and Hopkins, J.C., 1989, Reservoir sandstone bodies in estuarine valley fill: Lower Cretaceous Glauconitic member, Little Bow Field, Alberta, Canada: American Association of Petroleum Geologists Bulletin 73, no. 11, p. 1361–1382, doi: https://doi.org/10.1306/44B4AA50-170A-11D7-8645000102C1865D

Woodroffe, C.D., Chappell, J., Thom, B.G., and Wallensky, E., 1989, Depositional model of a macrotidal estuary and floodplain, South Alligator River, Northern Australia: Sedimentology, v. 36, no. 5, p. 737–756, doi: https://doi.org/10.1111/j.1365-3091.1989.tb01743.x

Wunderlich, F., 1972, Georgia coastal region, Sapelo Island, U.S.A., in Sedimentology and biology III, beach dynamics and beach development: Senckenbergiana Maritima, v. 4, p. 47–79.

Yang, Y., 2011, Tectonically-driven underfilled-overfilled cycles, the middle Cretaceous in the northern Cordilleran foreland basin: Sedimentary Geology, v. 233, p. 15–27, doi: https://doi.org/ 10.1016/j.sedgeo.2010.10.002

Zaleha, M.J., 2006, Sevier orogenesis and nonmarine basin filling: Implications of new stratigraphic correlations of Lower Cretaceous strata throughout Wyoming,

U.S.A.: Geological Society of America Bulletin, v. 118, no. 7/8, p. 886–896, doi: https://doi.org/10.1130/B25715.1

Zaitlin, B.A., Dalrymple, R.W., and Boyd, R., 1994, The stratigraphic organization of incised-valley systems, *in* Dalrymple, R.W., Boyd, R., and Zaitlin, B.A., eds., Incised-valley systems: Origin and sedimentary sequences: SEPM, Society for Sedimentary Geology Special Publication 51, p. 45–60, doi: https://doi.org/10.2110/pec.94.12.0045

Zaitlin, B.A., Potocki, W.D., Rosenthal, L., and Boyd, R., 2002, Depositional styles in a low accommodation foreland basin setting: An example from the Basal Quartz (Lower Cretaceous) southern Alberta: Bulletin of Canadian Petroleum Geology, v. 50, no. 1, p. 31–72, doi: https://doi.org/10.2113/50.1.31

Zonneveld, J.-P., and Gingras, M.K., 2013, The ichno-taxonomy of vertically oriented, bivalve-generated *Equilibrichnia*: Journal of Paleontology, v. 87, no. 2, p. 243–253, doi: https://doi.org/10.1666/11-064R1.1

APPENDIX

Appendix Table 1. Location of studied outcrops.

Symbol	Outcrop Location	Latitude	Longitude	Observed Facies Association and Lithofacies*	Figure No.
A	Armington	47.364379°	-110.896809°	FAm2: L2, L10	
AJn	Armington Junction north	47.352542°	-110.892542°	FAm2: L2, L10	
AJs	Armington Junction south	47.337754°	-110.896758°	FAm1: L1	13
AM	Ace Missile	47.285794°	-110.785398°	FAm2: L2	21
As1	Armington south 1	47.286964°	-110.911533°	FAm1: L1	
As2	Armington south 2	47.281566°	-110.888866°	FAm1: L1	
BB1	Big Bend 1	47.410833°	-111.314313°	FAm5: L11	
BB2	Big Bend 2	47.412336°	-111.317903°	FAm1: L1	
BC	Belt Creek	47.597958°	-111.043622°	FAm4: L3, L5, L17, L19	29
BrCo	Brigman Coulee	47.252599°	-110.831892°	FAm1: L1	
BCR	Boston Coulee Road	47.245290	-111.359920	FAm1: L1	
BE	Box Elder	47.566416°	-111.091334°	FAm3: L7a, L7b FAm4: L3, L5, L17, nonspecified tabular units	
BEC	Box Elder Coulee	47.418079°	-111.004396°	FAm2: L2	
BEe	Box Elder east	47.571381°	-111.083451°	FAm2: L2 FAm3: L7a, L7b	24
BEw	Box Elder west	47.565974°	-111.098935°	FAm1:L1 FAm3: L7a, L7b FAm4: L12, L17, nonspecified tabular units	30
Bl	Blythe	47.286903°	-110.849307°	FAm1: L1	
BR	Belt road cut	47.384128°	-110.942667°	FAm1: L1, L8, L9	7, 11, 12, 13, 14 16, 18, 21
BRR	Belt railroad cut	47.423204°	-110.929807°	FAm2: L2	
CC1	Cottonwood Coulee Road 1	47.284490	-111.103260	FAm1: L1	
CC2	Cottonwood Coulee Road 2	47.315260	-111.139430	FAm1: L1	
CDn	Cochran Dam north	47.554308°	-111.148347°	FAm1: L1 FAm3 FAm5	25
CDs	Cochran Dam south	47.552519°	-111.147452°	FAm3: 7a	
CM	Centerville Mine	47.400758°	-111.140837°	FAm3: L7a, L7b	24, 27
CR	Centerville road cut	47.385546°	-111.124061°	FAm1: L1, L14 FAm3: L7b	15
ERn	Eden Road north	47.274846°	-111.253060°	FAm1: L1	
Ers	Eden Road south	47.232660	-111.283060	FAm1: L1	
FF	Fisher–Fields road intersection	47.452284°	-111.266058°	FAm3: L7a, L7b	8, 10, 11, 12, 27
FR	Fields Road	47.445520°	-111.194185°	FAm1: L1	
FS	Fields Station	47.451624°	-111.239187°	FAm3: L7a, L7b	8, 24
GCR	Goodwyn Coulee Road	47.387981°	-111.318958°	FAm3: L7a FAm4: L17	25
GF	Gibson Flats	47.461775°	-111.216201°	FAm3: L7a, L7b	25
HC	Hound Creek	47.138967°	-111.484484°	FAm1: L1	
LBC	Little Belt Creek	47.434980°	-110.910850°	FAm4: L4, L17	29
MC	Ming Coulee	47.278835°	-111.424457°	FAm1: L1, L8	10
MDs1	Morony Dam south 1	47.582678°	47.582678°	FAm2: L2	16, 18, 19, 20, 21, 22
MDs2	Morony Dam south 2	47.586640°	-111.057702°	FAm2: L10	

Symbol	Outcrop Location	Latitude	Longitude	Observed Facies Association and Lithofacies*	Figure No.
MDn	Morony Dam north	47.586246°	-111.060502°	FAm2: L2, L10	17
MR	Millegan Road	47.205750	-111.422040	FAm1: L1	
NC	Neill Creek	47.337950°	-110.927876°	FAm1: L1	
R	Raynesford	47.277733°	-110.721665°	FAm1: L14	12, 15
Re1	Raynesford east 1	47.273484°	-110.685761°	FAm1: L1, L20	7
Re2	Raynesford east 2	47.274950°	-110.682394°	FAm1: L1, L20	7
RaD	Rainbow Dam	47.541611°	-111.191631°	FAm1: L1	
RDp	Ryan Dam power plant cliff	47.569790°	-111.120377°	FAm5: L11	13, 31, 32, 33
RDs	Ryan Dam spillway	47.568572°	-111.123791°	FAm3 FAm5: L11	31, 32
RDse	Ryan Dam southeast	47.564897°	-111.109744°	FAm3 FAm5: L11	
REt	River Edge Trail	47.568248°	-111.100242°	FAm1: L1 FAm3: L7a, L7b FAm4:L17, nonspecified tabular units	28
RI	Ryan Island	47.568430°	-111.120549°	FAm3: 7a	12, 26, 29
RQ	Ryan Quarry	47.566712°	-111.112393°	FAm3: L7a, L7b	28
RR1	River Road 1	47.418963°	-111.282766°	FAm3: L7a, L7b	
RR2	River Road 2	47.407479°	-111.290905°	FAm3: L7a, L7b	25
SR	Smith River	47.265396°	-111.425977°	FAm1: L1, L8, L9, L13	10, 14
SCC	Spring Creek Coulee	47.386133°	-111.074984°	FAm1: L1, L8	10, 11
STR	Stockett road cut	47.445069°	-111.147467°	FAm1: L1, L8	
TBR	Tiger Butte Road	47.269680°	-111.047802°	FAm1: L1	
UMRn	Upper Millegan Road north	47.166510	-111.412180	FAm1: L1	
UMRs	Upper Millegan Road south	47.140880	-111.411810	FAm1: L1	

*Facies Assemblage (FA) and Lithofacies (L) defined in tables 2 and 3.

Appendix Table 2. Facies associations (Fam, main estuary basin; Fav, paleovalley) and interpretations.

	FA	Interpreted Environmental Setting	Lithofacies	Facies (Lithofacies Interpretation)
Main estuary basin	FAm1	Tidal flat complex (tidal flats and channels)	L1 Quartzose tabular sandstone and heterolithic units	Supratidal to subtidal flat
			L8 Quartzose channel-shaped body within L1 unit	Run-off channel in sandy tidal flat
			L9 Quartzose channel-shaped heterolithic body transecting multiple L1 units	Deep tidal channels in mud- or mixed mud-and-sand tidal flat
			L13 Ms-filled channel-shaped body transecting multiple L1 units	Deep tidal channels in mud- or mixed mud-and-sand tidal flat
			L14 Lithic-rich channel-shaped, bioturbated ss body transitional into L1	Tidally influenced fluvial channel along tidal-basin margin
			L20 Tabular limestone	Low-energy, restricted, carbonate tidal flat
	FAm2	Tide-dominated shoreface	L2 Quartzose tabular sandstone and heterolithic beds	Tide-dominated, low wave energy shoreface
			L10 Quartzose channel-shaped heterolithic bodies within L2	Cross-shoreface tidal channels
	FAm3	Estuary mouth bar	L7a Upward fining quartzose– lower channel-bearing sandstone body	Large-scale, elongate bar-and-channel complex: high energy part
			L7b Upward fining quartzose–upper tabular-bedded sandstone body	Large-scale, elongate bar-and-channel complex: low energy part
	FAm4	Inner estuary basin	L3 Lithic-rich laminated tabular ss	Intertidal/subtidal sand flat and localized bar
			L4 Lithic-rich cross-stratified tabular ss	Tide-dominated subtidal sand flat
			L5 Lithic-rich tabular heterolithic units	Intertidal to subtidal sand flat
			L12 Quartzose composite-channel unit within L17	Axial inner-estuary channel
			L17 Widespread gray mudstone	Mud flat to mud-dominated subaqueous basin
			L19 Maroon mudstone	Subaerially exposed estuarine/muddy alluvial plain with pedogenesis.
	FAm5	Estuary-axis channel system	L11 Quartzose stacked channel-shaped heterolithic bodies	Axial inner-estuary channel system
Incised valley	FAv1	Tidally reworked fluvial channel (base of incised valley)	L15 Lithic-rich, ripple-bundled, channel-shaped ss body	Tidally reworked fluvial body
	FAv2	Transgressive shorezone	L6 Quartzose concavo-convex ss body	Transgressive brackish or marine sand
	FAv3	Estuary-center mudstone	L18 Localized gray mudstone	Low energy brackish or marine, mud-dominated setting
	FAv4	Carbonate lake or pond	L21 Deformed lenticular limestone	Low energy, carbonate-producing pond or lake
	FAv5	Fluvial channel	L16 Lenticular deformed bioturbated lithic ss	Dinosaur-trampled fluvial body
	FAv6	Floodplain soil	L19 Maroon mudstone	Subaerially exposed estuarine/muddy alluvial plain with pedogenesis

Appendix Table 3. Lithofacies (L) and interpretations.

Lithofacies	General Description	Textural Properties	Sedimentary Structures	Biogenic Properties	Facies (Lithofacies Interpretation) and Processes
Quartzose tabular units					
L1 — Upward fining ss and heterolithic beds	Widespread single or stacked tabular-shaped ss- and ms-dominated units (generally 1–3 m thick) with horizontal to very low-angle beds. Planar to slightly undulating erosional base of ss beds typical. Ss-dominated units: Amalgamated ss or upward transition from amalgamated ss to finer-grained and thinner ss interbedded with subordinate sts and ms. Ms-dominated units: Heterolithic. Tabular ms-enclosed ss beds. Ms color typically gray, although maroonish where in contact with reddish non-marine ms (L19). Basal ss units that overlie non-marine facies contain about 5–25% lithic clasts. Higher ss units become increasingly quartz rich upward. Black specks of organic debris and small wood fragments within ss increase in abundance adjacent to overlying non-marine Kk4 strata.	Upward fining or, rarely, upward coarsening units. Heterolithic units may not show an upward textural trend. Normal graded ss beds common. Discontinuous rip-up clast cgl, including reworked freshwater ls and dol clasts.	Linguoid ripples, sharp- and flat-crested wave ripples, wave-ripple cross-lamination with internal mud drapes, flaser and wavy bedding with bimodal-bipolar foreset orientations and internal mud drapes, parallel-laminated ss, and rare well-developed. Local occurrences of small- to medium-scale trough and tabular cross-stratification less common. Where not bioturbated, thinner ss beds are typically ripple cross-laminated with subordinate parallel laminations. Paleocurrent distributions bimodal.	Bioturbation fabric abundant in ms-dominated intervals, less common in ss-rich intervals. Trace fossils include *Cylindrichnus*, *Psammichnites*, small *Planolites*, *Spongliomorpha*, possible *Teichichnus*, *Skolithos*, small *Diplocraterion*, *Lingulichnus*, horseshoe crab-like crawling and resting traces, and arthropod burrows. Rare occurrences of terrestrial trace fossils *Fuersichnus*, *Nakdodemais*, *Steinichnus*, small *Taenidium*, earthworm tunnels and pellets, probable beetle larvae burrows and dinosaur tracks in ss beds that contain reddish mud matrix, located adjacent to reddish ms beds.	**Supratidal to subtidal flat.** Physical structures indicate dominant mixed tractive current and suspension fall-out tidal conditions coupled with minor wave influence. Ss-dominated units: relatively high energy, subtidal to intertidal sand-flat to intertidal mixed-flat settings. Ms-dominated units: middle intertidal to supratidal zone. Upward fining units: progradation of laterally adjacent subtidal (sand), intertidal (mixed sand/mud), and supratidal (mud) settings. Upward coarsening units: most likely transgression of subtidal, intertidal, and supratidal zones, or possible progradation of seaward sand-to-mud trend from subtidal zone. Trace fossils indicate physiologically stressed environmental conditions.
L2 — Upward coarsening ss and heterolithic beds	Tabular-shaped, rhythmically bedded, ss-dominated units, typically 2-4 meters thick. Internal bedding usually tabular and subhorizontal to very low angle; less commonly, convex-up on a bar scale (dm) wave length. Widespread erosional surfaces separate the units as well as occur internally. Discordances between units are distinct where erosional surfaces truncate underlying low-angle or convex bedding. Units may occur singly or stacked.	Upward coarsening units characteristic; most commonly upward from a thin basal ms and/or 0.5- to 2 m-thick heterolithic interval of interbedded, thin (cm to dm scale), very fine-grained ss, sts, and ms to an amalgamated, thicker ss bed (~0.3–1 m), fine- to rarely medium-grained ss. Ms thickness and relative abundance in heterolithic intervals decreases upward. Tabular ss units may also be similar sand size throughout with upward coarsening only due to an upward decrease in interstitial mud. Rarely, upward coarsening is sequentially followed by upward fining into thin, ms-rich, heterolithic bedding.	Flaser bedding, amalgamated ripple bedding separated by slightly undulatory reactivation surfaces, and rhythmically alternating ripple- and parallel-laminations. Mm-scale clay drapes commonly between parallel laminations, within current- and wave-ripple cross-lamination sets, and within lateral sequences of small-scale ripple bundles. Wave-ripple bedforms common. Possible swaley cross-stratification very rare. Scattered, small channel-shaped lenses are present within ss units marked by an erosional base and wide (1–5 m), low-amplitude, trough cross-stratified fill. Diagnostic: vertical successions of sedimentary structures are present on two scales. Single bed or couplet scale: upward fining from ripple bedding with clay drapes, or from stacked bundles of parallel laminations, into more thinly laminated and more heavily bioturbated muddy ss or ms. Upward coarsening unit scale: commonly a distinct upward trend from lenticular to wavy to flaser to amalgamated ripple bedding and/or small-scale (<10 cm thick) trough cross-stratification at the top. Sedimentary structures in some exposures not apparent either due to weathering and/or biogenic overprinting. Current-ripple foresets may be locally unimodal, although bimodal-bipolar on the outcrop scale.	Trace fossils abundant. *Arenicolites*, arthropod burrows, *Ophiomorpha* (very rare), *Macaronichnus*, *Piscichnus*, *Planolites*, and *Protovirgulari*, *Thalassinoides*, possible *Treptichnus,* and possible shore-crab burrows. Unidentified feeding traces are especially common along bedding planes. Rare local occurrences of *Taenidium*.	**Tide-dominated, low wave energy shoreface.** Planar depositional surfaces, low-relief barforms, and localized scour channels or depressions. Abundant tidal structures reflect tidal dominance. Rip-up clasts and increased lithic sand along the basal disconformity mark the reworking of underlying nonmarine Kootenai lithologies due to ravinement. Trace fossils indicative o a marginal marine setting, most likely brackish-dominated; possible freshwater influence from adjacent nonmarine setting. Upward coarsening units and stacking pattern due to net shallowing through multiple progradational events.
Lithic-rich tabular units					
L3 — Laminated ss units within L17	Widespread tabular units (1–4 m thick) of amalgamated ss beds (0.3–1.0 m thick). Unit lower contact sharp, commonly erosional; erosional surfaces between beds or bed sets within unit. Bedding typically horizontal although locally convex upward. Commonly overlie L5 units.	Fine-grained ss. Upward fining in upper 10-50 cm.	Trough and very low-angle foresets common in base of unit; overlain by subhorizontal parallel laminations. Ripple bedding and pervasive bioturbation associated with fining in upper 10-50 cm.	*Skolithos*, bioturbation fabric, and scattered unidentified trace fossils.	**Intertidal/subtidal sand flat and localized bar.** Deposition of units and beds/bed sets associated with initial relatively strong current activity and scour followed by energy decrease.
L4 — Cross-stratified ss units within L17	Widespread tabular units (1-6 m thick) of amalgamated ss beds (0.3–1 m thick). Unit lower contact sharp; typically erosional.	Fine-grained ss; slight upward fining in upper part of unit.	Medium- to large-scale trough cross-stratification in lower part overlain by very low-angle to horizontal ripple bedding or ripple bedded medium- to large-scale foresets. Rhythmically alternating bundles of parallel laminations and ripple bedding. Mud rip-up clasts along erosional surfaces. Wave ripple bedforms. Cross-strata foresets unimodal to bimodal-bipolar.	Vertical escape traces and *Taenidium*. Bioturbation fabric.	**Tide-dominated subtidal sand flat.** Structures indicate current dominated sandy area with relatively large, three-dimensional ripples commonly mantled by small-scale current ripples; intermittent strong current and scour events. Rhythmic bedding and foreset orientations indicate tidal control. Minor wave influence.
L5 — Heterolithic units within L17	Widespread tabular units (about 1-3 m thick) of heterolithic beds; typically underlie L3 units. Beds within units 5–50 cm thick.	Units typically coarsen/thicken upward into L3. Ss beds: fine- to very fine-grained; clay matrix.	Flaser bedding and mud-draped trough cross-stratification. Rhythmically alternating ripple-bedded and parallel laminated zones. Very low-angle truncation surfaces between amalgamated units. Some ss beds are oxidized brownish and structureless; associated with 100% bioturbation.	Bioturbation fabric common.	Intertidal to subtidal sand flat. Widespread, with mixed supply of sand and mud. Sand/mud deposition dependent upon tidal-current strength and periodicity. Association with L3 demonstrates a genetic link. Rhythmic bedding, flaser bedding, and mud drapes reflect tidal control.

Appendix Table 3. Lithofacies (L) and interpretations.

Lithofacies	General Description	Textural Properties	Sedimentary Structures	Biogenic Properties	Facies (Lithofacies Interpretation) and Processes
Quartzose concavo-convex ss body					
L6	Concavo-convex ss lens (confined by incised valley)	Lensoidal body with erosional base and tapered margins lapping upward onto paleovalley wall. Upward transition from amalgamated quartzose ss beds to rhythmic heterolithic beds with rapid change into overlying gray ms (L18). Maximum thickness 2 m.	Medium- to fine-grained, upward fining succession.	Parallel laminations dominant in lower, thicker beds; ripple bedding dominant in upper, thinner beds.	Small *Thalassinoides*; rare unidentified vertical burrows; general bioturbation fabric; heavily bioturbated in thin heterolithic beds.	Transgressive brackish or marine sand.
Quartzose upward fining ss body					
L7a	Lower channel-bearing unit	Ss body (7–11 m thick) with disconformable lower contact marked by a sharp, planar to undulating, erosional surface with local meter-scale relief. Contains channel-shaped bodies and upward fining and thinning tabular/lenticular bed successions (several m scale) with an erosional base. Abundant lithic clasts (up to about 20%) mixed with mature quartz sand near base. Lithic constituents include ms rip-up clasts, some of which are small, angular, whitish-gray ms flakes (several mm diameter), light gray to black chert sand and pebbles, and quartz pebbles that occur as thin (4–8 cm thick) conglomerate lenses or scattered grains. Light gray mud matrix is typical of the lowermost ss beds.	Entire lower body: upward fining and thinning from very coarse-grained to fine-grained ss. Channel bodies: upward fining. Tabular/lenticular bed successions: upward fining.	Lower part of channel-bearing unit: Large- to very large-scale trough cross-stratified tabular to lenticular beds and bed sets with planar to undulating erosional base. Upper-flow regime parallel-laminated beds (about 5–20 cm thick) near base of the body. Other structures include two-dimensional dune-form sets, lateral successions of large- and small-scale ripple bundles with rare and partially developed reactivation surfaces, very rare small-scale bipolar ripple foresets, and very rare mud drapes. Distinct erosional surfaces within lower body are common and frequently lined with imbricated pebbles or ms rip-up clasts. Sedimentary structures in the channel-shaped bodies are similar to those in the tabular/lenticular bodies, suggesting dependency upon outcrop orientation relative to channel orientation. Upper part of channel-bearing unit and upper part of channel fills within lower part of channel-bearing unit: Thinner strata containing large- to medium-scale, locally unimodal planar and trough cross-stratified tabular beds with planar to slightly undulatory erosional lower contacts. Widespread surfaces appear to be slightly erosional to non-erosional and are mantled by linguoid, interference, or nearly symmetrical straight-crested wave ripples. Overall, cross-stratification locally unimodal to multimodal and	Trace fossils relatively rare; include *Skolithos*, *Planolites*, relatively large *Diplocraterion*, and very rare *Ophiomorpha*.	**Large-scale, elongate bar-and-channel complex.** Evolved from a high-energy, elongate channel-and-bar system (a) to a shallower and lower energy system with large two- and three-dimensional dunes and subsequent smaller-scale dunes that migrated along sloping erosional surface. Final low-energy stage in bar evolution (b) marked by decreased grain size and small-scale current and wave-ripple bedding. Tidal current dominance indicated by channels, ripple-bundle successions, reactivation surfaces, and bipolar current-ripple foresets. Strong time-velocity asymmetry resulted in stacked unimodal-foreset beds. Ripple bundle thickening and thinning reflects neap-spring cyclicity whereas rhythmic thin-thick foreset laminations within ripple bundles document semidiurnal cyclicity. Tidal ravinement and lithic enrichment at base of ss body resulted from channel-associated scour. Ichnogenera consistent with relatively high-energy estuarine conditions.
L7b	Upper part of ss body–tabular-bedded unit	Transitional from lower part of ss body. An upward thinning, typically two-part unit (<5–8 m thick) containing a lower zone of stacked upward thinning successions (½–1½ m thick) of tabular to slightly wedge shaped, two-part bedsets and an upper zone of ripple bedding.	Entire upper body: upward fining, becoming finer grained than in the lower ss body. Internal bed-set successions: upward fining.	Lower part of unit: Two-part bedsets consist of a basal, 2- to 5-cm-thick, ripple-bedded toeset layer and a conformable thicker and coarser foreset layer locally containing scattered shale rip-up clasts. Subhorizontal planar to gently sloping (<10°) curviplanar erosional surfaces mark the base of bedsets; (1) upward sloping erosional surfaces are inclined in the direction of foreset dips, indicating upslope bedform migration, (2) less common, erosional surfaces are sloping downward relative to foreset orientation, indicating downslope bedform migration. Lateral successions of thickening and thinning ripple bundles are sometimes distinct within a bedset, although separate bundles are commonly unrecognizable due to a lack of structural or textural discordance. Rhythmic thin-thick foreset laminations separated by clay drapes are present within ripple bundles. Rare simple and compound avalanche sand-tongue structures present within tabular-planar foresets. Upper part of unit: Current ripple bedding including scattered wave-ripple cross-lamination.		

Appendix Table 3. Lithofacies (L) and interpretations.

Lithofacies	General Description	Textural Properties	Sedimentary Structures	Biogenic Properties	Facies (Lithofacies Interpretation) and Processes
Quartzose plano-convex (channel-shaped) ss bodies					
L8 — Ss body within tabular L1 ss units	Lithologically similar to the tabular L1 host unit. Relatively small (several to 10 m wide, to several m thick), isolated and locally coalesced, channel-shaped bodies with erosional base. Very low-angle channel margins.	Texturally similar to the host unit (L1 ss). Thin basal cgl. Slight upward fining of ss.	Horizontal tabular to slightly inclined internal bedding; some cross-bedding with mud drapes.	None observed.	Run-off channel in sandy tidal flat. Lithologic association with, and similarity to, L1 and mud drapes indicate tidal flat setting.
L9 — Heterolithic bodies transecting multiple tabular L1 units	Larger scale (10s of m wide, several m thick) heterolithic body of ms and bioturbated quartzose ss. Concave to undulating erosional base transects multiple, surrounding ms-dominant or heterolithic tabular units. Bedding includes inclined heterolithic strata and symmetrically horizontal beds that become slightly concave-up and tangential along the channel margin.	Textural grading: (1) Symmetrically filled channel bodies fine upward from a thicker bedded (about 0.5–1 m) basal zone of bioturbated, fine-grained ss to finer and thinner ss interbedded with increased amounts of ms. (2) Channel units with inclined heterolithic strata coarsen upward from ms and thinly bedded ss above an erosional base to thicker bedded and commonly amalgamated ss at the top.	Inclined heterolithic strata may be highly deformed including small-scale folding, offset, and segmentation due to dinosaur trampling.	Various amounts of bioturbation fabric. Dinosaur tracks and undertracks.	Deep tidal channels in mud- or mixed mud-and-sand tidal flat. Alternating tractive and non-tractive (suspension fallout) tidal flow. Upward fining, symmetric-heterolithic units reflect filling of symmetric, straight channel segments. Upward coarsening, inclined-heterolithic successions represent point bar accretion in a sinuous mud-dominated channel tract. Lithologic association with L1 as well as mud drapes further indicate tidal setting.
L10 — Heterolithic bodies transecting tabular L2 units	Ss-dominated heterolithic channel bodies 50–100s of m wide and 5–10 m thick, scattered within L2. Erosional margins transect one or more tabular L2 units. Channel fill concave and subparallel to erosional boundary; top of fill slightly convex where it overlaps lateral margins before pinching out beneath overlying tabular L2 unit. Ss beds similar in thickness and composition to those of encasing tabular L2 ss. Multiple channel bodies may be vertically stacked.	Upward fining and thinning from thicker basal ss beds with upward transition into a ms-dominated zone.	Sedimentary structures similar to those of the encasing tabular L2 units.	General bioturbation fabric in upper part of some ss beds; bioturbation more pervasive in finer, thinner upper parts of channel fill. Trace fossils rare compared to L2.	**Cross-shoreface tidal channels.** Incision and relatively energetic channelized flow across regionally planar shoreface setting (L2). Upward fining due to channel shifting and/or sea level change. No evidence for emergence at top of channel bodies or between confining tabular L2 units. Geographically persistent location indicated by vertical stacking.
L11 — Stacked heterolithic bodies above FAm3 (table 2)	Vertical succession of stacked channel bodies. Channel body complex up to 40 m thick, >5 km wide. Concave erosional bases, cross-channel widths several to >20 m scale, thicknesses 1 m to 10 m scale. Erosional boundary pattern indicates lateral and vertical truncation of multiple channels.

Bed geometry in ss-dominated bodies includes (1) symmetric-concave at base up to horizontal, (2) epsilon cross-stratified (inclined heterolithic), (3) rare convex-up cross-channel bedding.

Bed geometry in heterolithic- and ms-dominated channels is generally concave and symmetric throughout or asymmetrically inclined. Beds commonly extend beyond low-relief channel margins over wider area. | Upward fining within channel bodies. Overall upward fining of channel-body succession: coarse-to-medium or medium-to-fine sand within basal channels; fine and very fine sand in upper channels. Ss very clayey to clean. Ss rhythmically interbedded with mm- to dm-scale ms layers. Strong textural variability between laterally adjacent channel bodies. | Basal channels show at least several meters of scour into the underlying L7a/b. Medium- to large-scale trough cross-stratification with widths up to 8 m. Small-scale current-ripple bedding abundant, mud drapes, wave ripples, vertically accreted rhythmic bundles of parallel lamination, gutter casts and flute casts. Paleocurrent data locally unimodal, but regionally bipolar, or rarely locally bimodal-bipolar. Over-steepened beds within large (m to several m scale) dinosaur-trampled slump block. | Trace fossils are locally abundant.*Siphonichnus*. Abundant small-sized, mixed horizontal and vertical trace fossils as well as localized very high degrees of general bioturbation fabric. Bioturbation increases upward through a fining succession, dinosaur tracks. | **Axial inner-estuary channel system.** Sinuous tidal-channel network within estuary basin. Physical structures indicate: tidal currents with strong time-velocity asymmetry as well as local transport-efficient bipolar flow; channels contained large three-dimensional dunes to small three-dimensional ripples, point bars, longitudinal bars, and wave reworked deposits. Ichnogenera consistent with estuarine conditions. |
L12 — Widespread, upward-fining composite-channel unit within L17 and FAm4 (table 2)	Lensoidal unit (100s of m wide, maximum thickness about 4 m) that contains up to several stacked, widespread, ss-dominated, channel bodies. Subhorizontal to slightly concave scour surface along base of channel bodies overlain by dominantly subhorizontal bedded ss and rhythmic (heterolithic) ss-ms beds. Erosional base of uppermost body may fully truncate underlying bodies.	Upward fining and thinning ss. Ss rhythmically bedded with mm- to dm-scale ms layers.	Trough cross-stratification along base of channel bodies. Small-scale ripple bedding within thin ss beds. Unit geometry and trough cross-stratifications indicate a general basin-axial orientation.	None observed.	**Axial inner-estuary channel.** Channelized scour and fill overlain by wider, but channel-associated, sand-flat fill. Subhorizontal heterolithic beds indicate rhythmic fluctuation in tidal current instensity, perhaps on the seasonal scale (Gingras and MacEachern, 2012).
Mudstone Plano-Convex (Channel-Shaped) Bodies					
L13 — Ms-filled channel transecting multiple tabular quartzose L1 units	Lensoidal ms-filled channel-shaped body of intermediate dimension (10s of m wide, less than several m thick). Subhorizontal to slightly concave erosional base. Truncates multiple ms-dominated tabular units of L1.	Not applicable	Not applicable	Variable amounts of bioturbation fabric.	Deep tidal channels in mud- or mixed mud-and-sand tidal flat. Deeper channelized flow across mud-flat or mixed mud-and-sand flat areas. Lithologic association with L1 and ms dominance indicates low-energy tidal setting with negligible sand supply.

Appendix Table 3. Lithofacies (L) and interpretations.

Lithofacies		General Description	Textural Properties	Sedimentary Structures	Biogenic Properties	Facies (Lithofacies Interpretation) and Processes
Lithic-Rich Plano-Convex (Channel-Shaped) Bodies						
L14	Upward fining bioturbated; transitional into quartzose L1	Isolated (1–2 m thick) to stacked ('3 m total thickness) lithic-rich channel-shaped bodies with erosional base overlain by transition into quartzose, bioturbated and rippled L1 tabular beds.	Ss upward fining, angular, coarse- to medium-grained with exceptionally abundant gray mud matrix. Mud matrix is similar in appearance to kaolinitic mud in L17. Scattered Paleozoic cobbles/boulders along base.	Relict (biogenically overprinted) large-scale unidirectional cross stratification; possible epsilon cross strata. Load casts, most likely penetrative dinosaur undertracks as in L1, L9, L12, and L16.	Ss body can be 100% bioturbated with complete overprinting of physical structures.	**Tidally influenced fluvial channel along tidal basin margin**. Upward transition into L1 reflects transgressive inundation. Dinosaur trampled.
L15	Upward fining ripple bundled ss (confined by incised valley)	Lithic-rich channel-shaped ss body (2–3 m thick) along the axial base of an incised paleovalley.	Coarse- to medium-grained, angular.	Stacked lateral sequences of medium- to large-scale ripple bundles with ms drapes, stacked two-part ss-ms parallel laminations, wave ripples. Ripple-bundle foresets are oriented SSW, opposite regional fluvial paleoflow and in the flood-current direction for the basin.	*Cochlichnus* and medium- to very small-sized *Thalassinoides*; small, unidentified, tubular to cylindrical traces along clayey bedding planes; some beds 100% bioturbated.	**Tidally reworked fluvial body**. Composition of ss due to fluvial delivery. Physical structures reflect rhythmic tidal processes, and biogenic structures indicate a brackish to marine setting. Foresets reflect southward flood-current reworking up the paleovalley, similar to flood-current directions in the main estuar basin.
L16	Deformed and bioturbated ss (confined by incised valley)	Thin ss lens (10–50 cm thick).	Homogeneous coarse- to medium-grained, angular ss. Abundant clay matrix.	Bed and internal fabric strongly deformed. Bulbous load casts associated with penetrative dinosaur tracks. Fluidized-flow deformation pits on upper surface capping penetrative dinosaur tracks.	Rhizoliths and 100% small-scale bioturbation. Penetrative dinosaur tracks.	Dinosaur-trampled fluvial body.
Mudstone						
L17	Widespread gray ms	Gray ms (<0.1–11 m thick). Typically ranges from massive, nearly pure, light gray kaolinite (Walker, 1974) to nondescript medium gray ms. Rarely, dark gray carbonaceous ms and interbedded thin coal (Walker, 1974). Interbedded thin, bioturbated ss.	Not applicable	Ms - Not applicable Interbedded ss - flaser bedding.	Bioturbation fabric.	**Mud flat to mud-dominated subaqueous basin**. Low-energy brackish/marine setting ranging from well to poorly oxygenated. Adjacent marginal areas of poor drainage and localized mire development
L18	Localized gray ms (confined by incised valley)	Medium gray, organic-rich mudstone. Thickness 16–18 m.	Not applicable	Not applicable	Palynomorphs, dinoflagellates, and acritarchs indicating brackish to marine conditions (Burden, 1984).	**Low-energy brackish or marine, mud-dominated setting**. Ranges from from well to poorly oxygenated.
L19	Maroon ms	Thin maroon to mottled maroon and gray ms.	Not applicable	Varying amounts/combinations of blocky ped fabric, small-scale slickensides, gray rhizomorphs, and drab haloes	Plant bioturbation fabric.	**Subaerially exposed estuarine/muddy alluvial plain with pedogenesis**. Possible wet-and-dry seasonality in a sub-humid to arid climate.
Limestone						
L20	Tabular ls	Biomicrite beds 10–40 cm thick.	Floating quartz sand grains.	Not applicable	Ostracods relatively abundant.	**Low-energy, restricted, carbonate tidal flat**. Adjacent to siliciclastic setting.
L21	Deformed lenticular ls (confined by incised valley)	Biomicrite 30–60 cm thick.	Abundant disarticulated and fractured mollusk shells.	Bed strongly deformed. Includes dinosaur-foot penetration columns, shear zones, and under-track load casts.	Disarticulated and fractured mollusk shells. Penetrative dinosaur tracks, undertracks, and a pervasive bioturbation fabric.	Low-energy, carbonate-producing pond or lake. Post-depositional trampling by dinosaurs.

Note. cgl, conglomerate; ss, sandstone; sts, siltstone; ms, mudstone; ls, limestone; dol, dolomite.

Appendix Table 4. Summary of environmental and sedimentologic properties of the Sapelo Island beach-shoreface and Nordergründe intertidal-subtidal zones, both of which are considered to be tide-dominated shoreface in this study. Sapelo Island data are from Howard and Dörjes (1972), Howard and Reineck (1972), Wunderlich (1972), Reineck and Singh (1980), and Howard and Scott (1983). Nordergründe data are from Reineck and Singh (1980).

	Beach	Shoreface	Transition Zone	Offshore
Geomorphic Setting	**Sapelo (S):** Located between large estuaries. Profile gradient: very low to inner shelf. Beach is exceptionally wide (100–200 m scale), generally planar other than in ridge-and-runnel locales; grades seaward into sandy tidal flat in some locales (Howard and Dörjes, 1972). Transected by tidal creeks and associated ebb-tidal shoals; tidal channels extend across the shoreface. **Nordergründe (N):** Located between large estuaries. Dominated by intertidal sand flats (originally referred to as sand tongues) that extend subtidally seaward as very low-relief, planar-topped areas. Profile gradient: very low to inner shelf; subtidal depths similar to shoreface and transition zones of open-coast "beach shores" (Reineck and Singh, 1980). Tidal channels* transect the subtidal sand flat.			
Tidal Range	**S:** average 2.4 m mean; spring tide up to 3.4 m (mesotidal) **N:** average 3.18 m mean; spring tide up to 4.90 m (macrotidal)			
Wave Height	**S:** average 0.25 m; storm typically <2 m **N:** average less than 1.2 m			
Terminology for Tide-Dominated Shoreface-Associated Zones				
Original Terminology for Depositional Zone	**S:** Beach (supratidal to Intertidal) **N:** Sand flat (supratidal to intertidal)	**S:** Upper Shoreface (low water line to 1 m depth) **N:** Subtidal sand tongue or flat (low water line to 6 m depth; estimated wave base)	**S:** Lower Shoreface (1–2 m depth) **N:** Subtidal sand tongue or flat (6–20 m depth)	**S:** Upper Part of Upper Offshore (2–5 m depth) **N:** Transition zone (20–? m depth)	**S:** Lower Part of Upper Offshore (5–16 m depth) **N:** Inner Shelf or Offshore
Texture	Medium to upper-fine sand; some slightly coarser	Medium-fine sand	Fine sand	Muddy fine sand	Mud and fine sand. Relict clean, medium to coarse Pleistocene sand beyond 16 m at Sapelo.
Primary Sedimentary Structures Sapelo Island	Parallel laminations typical. Wave ripples, small-scale current ripples, and thin mud layers in nearly flat intertidal areas; some flaser and wavy bedding. Other: Antidune cross-stratification. Localized ridge-and-runnel systems produce large- to small-scale landward-oriented foresets and runnel-associated wave-ripple cross-lamination, small-scale current-ripple lamination, megaripple (trough) cross-stratification, and mud lenses (<10 cm thick). Overall, nearly impossible to establish a facies boundary between the foreshore and shoreface (Howard and Reineck, 1981).	Parallel laminations abundant. Some ripple laminations. Some mud lenses in outer part of zone.	Small-scale ripple bedding most abundant. Interbedded parallel laminations decrease and ripple bedding increase seaward; both structural types merge and interbed with bioturbated sand.	Alternating sand and mud layers dominant. Includes wavy bedding as well as parallel-laminated, rippled or rare hummocky beds (Howard and Scott, 1983) that are burrowed/bioturbated upward.	Highly bioturbated muddy sand.
	Megaripple (trough) cross-stratification is scattered and present in the intertidal zone to below wave base as well as near estuary bars or channels, wherever stronger tidal currents or wave activity may occur.			
Primary Sedimentary Structures Nordergründe	Mix of small-scale ripple bedding (~30%), parallel laminations (~15%), and megaripple (trough) cross-stratification (<50%).	**P**arallel laminations (<40%) and small-scale ripple bedding (<40%). Parallel laminations decrease and ripple bedding with flaser structures increase seaward. Scattered megaripple (trough) cross-stratification (~15%).	Small-scale ripple bedding (~50%), parallel laminations (15–20%), mud or alternating thin sand and mud layers (5–20%). Megaripple (trough) cross-stratification (<30%).	Abundant ripple bedding (~80%; incl. wavy and lenticular structures), parallel laminations (<10%); muddy beds and alternating thin sand and mud layers (~10%).	Relatively thick mud layers with storm layers of sand and silt.
Degree of bioturbation	Low bioturbation	Zero to very low bioturbation	Bioturbation very low to 20%	Bioturbation 75% to very high	Very high bioturbation (>90%)

*The channels that transect the Nordergründe shoreface generally range from 1 – 3 kilometers wide and 6 – 13 meters deep, becoming wider and deeper in the seaward direction. There is no significant difference in grain size or bedding types between channels and adjacent areas. As the channels migrate, channel fill is capped by subhorizontal sand sheets.